Strangeness in nuclear physics

A. Gal*

Racah Institute of Physics, The Hebrew University, Jerusalem 91904, Israel

E. V. Hungerford†

University of Houston, Houston, TX 77204, USA

D. J. Millener‡

Brookhaven National Laboratory, Upton, NY 11973, USA

(Dated: February 2016)

Extensions of nuclear physics to the strange sector are reviewed, covering data and models of Λ and other hypernuclei, multi-strange matter, and anti-kaon bound states and condensation. Past achievements are highlighted, present unresolved problems discussed, and future directions outlined.

PACS numbers: 13.75.Ev, 13.75.Jz, 21.80.+a, 25.80.-e, 26.60.+c, 97.60.Jd

Contents

I. Introduction 1
A. Brief historical overview 1
B. General features of Λ hypernuclear formation 2
1. The $(K^-_{\rm stop},\pi^-)$ reaction 3
2. The in-flight (K^-,π^-) reaction 3
3. The (π^+,K^+) reaction 4
4. The $(e,e'K^+)$ reaction 5
5. Addendum: hypernuclear lifetime measurements 6

II. Λ Hypernuclear Structure Calculations 8
A. The effective YN interaction and s-shell hypernuclei 8
B. p-shell hypernuclei, γ-ray measurements, and spin dependence of the ΛN interaction 8

III. Weak Decays of Λ Hypernuclei 14
A. Mesonic decays 14
B. Nonmesonic decays 16

IV. Ξ Hypernuclei 20

V. Λ − Λ Hypernuclei 21

VI. Strange Dense Matter 24
A. Strange hadronic matter 24
B. Neutron stars 25

VII. $\bar{K}$-Nuclear Interactions and Bound States 27

VIII. Future Experiments and Directions 31
A. Spectroscopy using meson beams 31
1. Hyperon production and hyperon-nucleon interactions 31
2. Reaction spectroscopy with mesons 32
3. Experiments using emulsion detectors 32
4. Spectroscopy using electromagnetic transitions 32
B. Spectroscopy with electron accelerators 33
1. Electroproduction at Mainz (MAMI) 33
2. Electroproduction at Jlab 34
C. Experiments at PANDA 34
D. Weak decay of hypernuclei 35
1. mesonic decays 35
2. nonmesonic decays 35
3. Λ hypernuclear lifetimes 36
E. Multi-strange systems 36
F. Experiments at heavy-ion facilities 37
G. $\overline{K}$-nucleus bound-state searches 38

IX. Summary 38

Acknowledgments 39

References 39

I. INTRODUCTION

A. Brief historical overview

In the early 1950s a quantum number, conserved under the strong interaction, was introduced (Gell-Mann, 1953) in order to explain the behavior of the "strange" particles which had been observed in emulsions exposed to cosmic rays. Almost simultaneously, the first hypernucleus, formed by a Λ hyperon bound to a nuclear fragment, was observed in an emulsion exposed to cosmic rays (Danysz and Pniewski, 1953). For the next 20 years or so, hypernuclei were explored using emulsion detectors, first with cosmic rays, and then with beams from existing accelerators. Within the last 40 years, modern particle accelerators and electronic instrumentation has increased the rate and breadth of the experimental investigation of strangeness in nuclei. As always, theoretical interest has closely followed the experimental development.

The behavior of a Λ in a nuclear system is a nuclear many-body problem, since the forces between the baryons are predominantly hadronic and the time scale of the strong interaction is about 10^{-23} s compared to the

*Electronic address: avragal@vms.huji.ac.il
†Electronic address: hunger@uh.edu
‡Electronic address: millener@bnl.gov

weak-interaction lifetime of a Λ lifetime in the nuclear medium (Bhang *et al.*, 1998; Park *et al.*, 2000) of approximately 10^{-10} s. Therefore, the combined hypernuclear system can be treated using well developed nuclear-theory models such as the shell or mean-field models with an effective Λ-nucleus interaction. New dynamical symmetries may also arise in hypernuclei, *e.g.* by treating the Λ hyperon shell-model orbitals on par with those of nucleons within the Sakata version of SU(3) symmetry (Sakata, 1956). This approach was found useful in hypernuclear spectroscopic studies (Auerbach *et al.*, 1981, 1983). Furthermore, by coupling SU(3)-Sakata with SU(2)-spin, the resulting SU(6) symmetry group presents a natural extension of Wigner's SU(4) spin-isospin symmetry group in light nuclei (Dalitz and Gal, 1981).

Λ hypernuclei also offer a test-ground for microscopic approaches to the baryon-baryon interaction. Thus, since one-pion exchange (OPE) between a Λ hyperon and a nucleon is forbidden by isospin conservation, the ΛN interaction has shorter range, and is dominated by higher mass (and multiple) meson exchanges when compared to the NN interaction. For example, two-pion exchange between a Λ hyperon and a nucleon proceeds through intermediate ΣN states ($\Lambda N \to \Sigma N \to \Lambda N$), potentially leading to non-negligible three-body ΛNN forces (Gibson and Lehman, 1988). The analogous mechanism of intermediate ΔN states ($NN \to \Delta N \to NN$) in generating three-body NNN forces in two-pion exchange seems to be less important in nuclear physics, not only because the NN interaction is dominated by OPE, but also because of the considerably higher mass of the Δ resonance with respect to that of the Σ hyperon. Such theoretical expectations may be explored in hypernuclear few-body and spectroscopic calculations.

Finally, the Λ can be used as a selective probe of the nuclear medium, providing insight into nuclear properties that cannot be easily addressed by other techniques. Thus, since from a hadronic as opposed to a quark perspective, the Λ remains a distinguishable baryon within the nucleus, and samples the nuclear interior where there is little direct information on the single-particle structure of nuclei. Because of this, various aspects of hypernuclear studies such as Λ decay, or the spectra of heavy hypernuclear systems, can illuminate nuclear features which would be more obscured in conventional nuclei.

Useful material on the subject of this review can be found in the proceedings of the recent triennial conferences on Hypernuclear and Strange Particle Physics (**????**), recent special volumes (**???**), schools (**?**), and several review articles (Botta *et al.*, 2012; Hashimoto and Tamura, 2006; **?**).

B. General features of Λ hypernuclear formation

A hypernucleus is characterized by its spin, isospin, and in the case of Λ hypernuclei, a strangeness of −1. If the Λ is injected into the nuclear system, the resulting hypernucleus will normally de-excite by a nuclear Auger process, or by γ emission. The resulting ground state then decays by the weak interaction, emitting π mesons as in the free Λ decay, and also nucleons in a four-fermion in-medium interaction $\Lambda N \to NN$. Therefore, observation of the energetics of hypernuclear formation and decay can provide information on binding energies and spins of hypernuclear ground states. To conserve baryon number, a reaction producing a hypernucleus commonly replaces a nucleon with a Λ.

TABLE I Experimental Λ separation energies, B_Λ, of light hypernuclei from emulsion studies. These are taken from a compilation (Davis and Pniewski, 1986) of results from (Cantwell *et al.*, 1974; Jurič *et al.*, 1973), omitting ${}^{15}_{\Lambda}$N (Davis, 1991). A reanalysis for ${}^{12}_{\Lambda}$C (Dłuzewski *et al.*, 1988) gives 10.80(18) MeV.

Hypernucleus	Number of events	$B_\Lambda \pm \Delta B_\Lambda$ (MeV)
${}^{3}_{\Lambda}$H	204	0.13 ± 0.05
${}^{4}_{\Lambda}$H	155	2.04 ± 0.04
${}^{4}_{\Lambda}$He	279	2.39 ± 0.03
${}^{5}_{\Lambda}$He	1784	3.12 ± 0.02
${}^{6}_{\Lambda}$He	31	4.18 ± 0.10
${}^{7}_{\Lambda}$He	16	not averaged
${}^{7}_{\Lambda}$Li	226	5.58 ± 0.03
${}^{7}_{\Lambda}$Be	35	5.16 ± 0.08
${}^{8}_{\Lambda}$He	6	7.16 ± 0.70
${}^{8}_{\Lambda}$Li	787	6.80 ± 0.03
${}^{8}_{\Lambda}$Be	68	6.84 ± 0.05
${}^{9}_{\Lambda}$Li	8	8.50 ± 0.12
${}^{9}_{\Lambda}$Be	222	6.71 ± 0.04
${}^{9}_{\Lambda}$B	4	8.29 ± 0.18
${}^{10}_{\Lambda}$Be	3	9.11 ± 0.22
${}^{10}_{\Lambda}$B	10	8.89 ± 0.12
${}^{11}_{\Lambda}$B	73	10.24 ± 0.05
${}^{12}_{\Lambda}$B	87	11.37 ± 0.06
${}^{12}_{\Lambda}$C	6	10.76 ± 0.19
${}^{13}_{\Lambda}$C	6	11.69 ± 0.12
${}^{14}_{\Lambda}$C	3	12.17 ± 0.33

The acquisition of hypernuclear binding energies, well-depths, and positions of the hypernuclear levels began in the 1960s. Early work included K^- absorption in emulsions and bubble chambers, where hyperfragments were identified by their mesonic decays. These efforts successfully established the binding energies of a number of light hypernuclei in their ground states (g.s.) where the Λ is in the lowest $s_{1/2}$ orbit, as summarized in Table I. In 1972, the existence of a ${}^{12}_{\Lambda}$C particle-unstable state with a Λ in the p orbit was confirmed (Jurič *et al.*, 1972), and the reaction $K^- + {}^{12}\mathrm{C} \to \pi^- + p + {}^{11}_{\Lambda}\mathrm{B}$ in emulsion was used to study excited states of ${}^{12}_{\Lambda}$C decaying by proton emission to ${}^{11}_{\Lambda}$B. In this case, the emitted proton energy was measured in the emulsion, and the level structure interpreted in terms of three p-shell Λ states located at about 11 MeV excitation energy (Dalitz *et al.*, 1986).

1. The $(K^-_{\rm stop}, \pi^-)$ reaction

The $(K^-_{\rm stop}, \pi^-)$ reaction was the first reaction used for hypernuclear production, as kaon beams, particularly those produced in early accelerator experiments, were weak and the intensity of pions in the beams obscured the production reaction pions. Thus, it was easier to identify a stopped K^-, and stopping the K^- assured that essentially all the kaons interacted with the target. A recent example from the FINUDA Collaboration at DAΦNE, Frascati (Agnello *et al.*, 2011a) is shown in Fig. 1. Two particle-stable excited states, in addition to the g.s. of ${}^{7}_{\Lambda}$Li, were observed and formation rates determined for this and for several other p-shell hypernuclei. These formation rates were used then in a theoretical study of the in-medium modification of the $\bar{K}N$ interaction, as derived within a coupled-channel chiral model, concluding that the $(K^-_{\rm stop}, \pi^-)$ reaction can be used to better determine the K^--nuclear optical potential depth (Cieplý *et al.*, 2011). FINUDA's special niche in hypernuclear physics was its remarkable performance connecting together production and decay of light Λ hypernuclei. This will become clear in the Weak Decay subsection further down this Review.

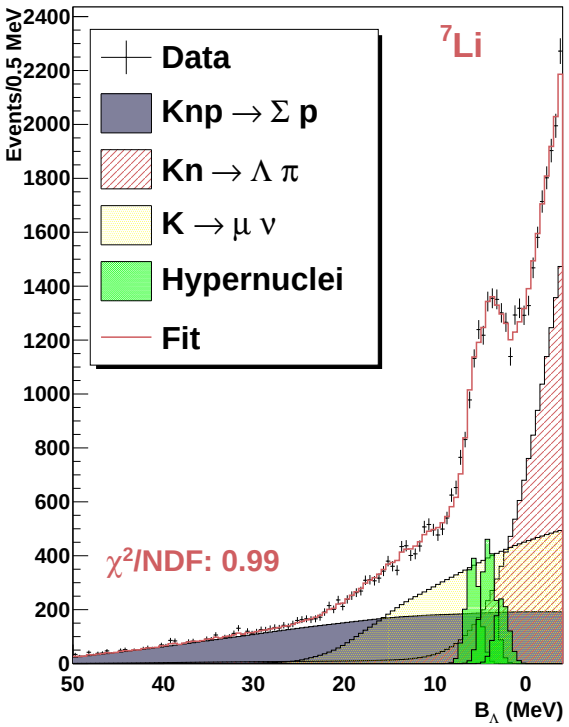

FIG. 1 ${}^{7}_{\Lambda}$Li bound-state spectrum, consisting of three levels (in green), obtained in $(K^-_{\rm stop}, \pi^-)$ on a ^{7}Li target by the FINUDA Collaboration at DAΦNE, Frascati (Agnello *et al.*, 2011a). The experimental resolution was about 400 keV and the formation rate of these $1s_\Lambda$ states was about $1 \times 10^{-3}/K^-_{\rm stop}$

2. The in-flight (K^-, π^-) reaction

Beginning in the mid 1970's, the structure of p-shell hypernuclei was further explored using accelerated beams of kaons and magnetic spectrometers. It was recognized that the incident momentum of the in-flight ${}^{A}Z(K^-, \pi^-){}^{A}_{\Lambda}Z$ reaction could be chosen so that the momentum transferred to the hypernucleus is close to zero, favoring no transfer of orbital (or spin) angular momentum. In this case, the spectra of light hypernuclei exhibit peaks when a Λ replaces a neutron without changing the quantum numbers of the single-particle orbit. This is illustrated in Fig. 2 for pure single-particle transitions on ^{16}O at $p_K = 800$ MeV/c, near where a maximum in the elementary cross section occurs. Another important feature of the elementary reaction around these momenta is that the spin-flip amplitudes are small. The resulting Λ hypernuclear states are called 'substitutional states' (populated via 'recoilless' transitions). The strong nuclear absorption of the incident K^- and exiting π^- limits penetration into the nucleusand favors transitions with surface-peaked transition densities (generally between nodeless orbits).

Thus, using this reaction, a series of experiments were initiated at CERN (Povh, 1980) and then at BNL (May *et al.*, 1981). The spectra produced by the (K^-, π^-) experiments show peaks for substitutional states near the nuclear surface (*i.e.*, a neutron replaced by a Λ with the same quantum numbers).

One of the early investigations used the spin splitting of states in ${}^{16}_{\Lambda}$O to obtain a value for the Λ-nucleus spin orbit interaction. Figure 3 shows that the split-

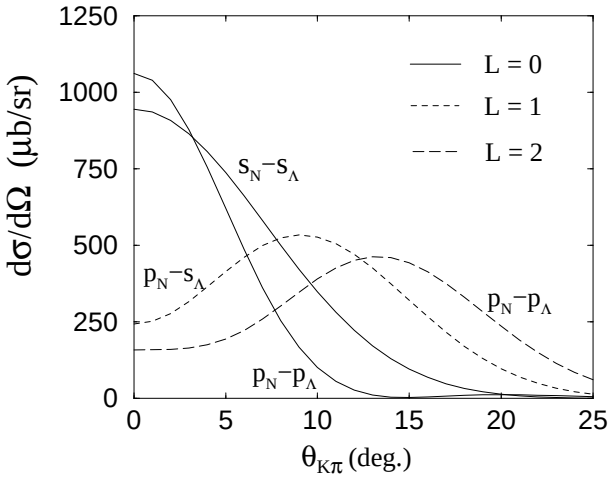

FIG. 2 Angular distributions for the (K^-, π^-) reaction for pure single-particle transitions on ^{16}O at $p_K = 800$ MeV/c.

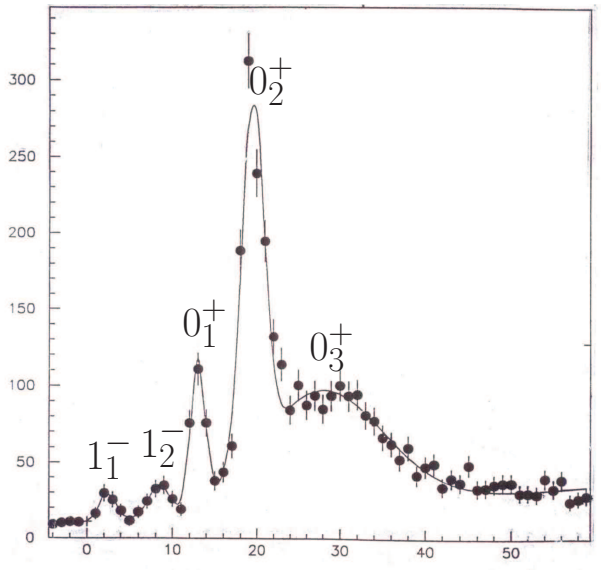

FIG. 3 Spectrum for the (K^-, π^-) reaction on ^{16}O at $p_K =$ 715 MeV/c near 0° (**?**). The 1^- states are s_Λ states based on the $p_{1/2}^{-1}$ and $p_{3/2}^{-1}$ hole states of ^{15}O. The $0^+_{1,2}$ states are p_Λ substitutional states based on the same core states, while the 0_3^+ state is based on the broad $0s$-hole strength in ^{15}O.

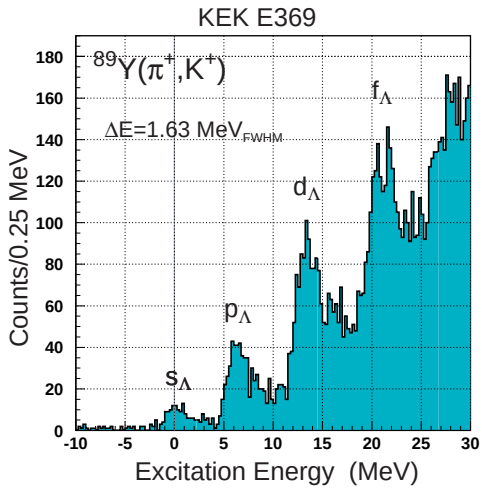

FIG. 4 (color online). The hypernuclear spectrum of $^{89}_{\Lambda}$Y showing the major Λ shell structure. (Hotchi *et al.*, 2001)

ting of the two p_Λ states (0_1^+ and 0_2^+) observed in the ^{16}O$(K^-, \pi^-)^{16}_\Lambda$O reaction spectrum shows that the energy difference between the states obtained when replacing a $p_{1/2}$ or $p_{3/2}$ neutron by a Λ is essentially the same as the energy splitting of the hole states in ^{15}O (6.18 MeV). This indicates that the effective ΛN spin-orbit splitting is small (Povh, 1980), a conclusion that remains valid when the residual ΛN interaction is taken into account (**?**). A small effective ΛN spin-orbit potential was also confirmed in the analysis of the angular distribution of the p_Λ substitutional peak based on the ^{12}C ground state observed in the ^{13}C$(K^-, \pi^-)^{13}_\Lambda$C reaction spectrum. In this experiment (May *et al.*, 1981), the $p_{1/2\Lambda}$ state is formed via a $\Delta L = 0$ transition near 0° while the $p_{3/2\Lambda}$ state is formed via a $\Delta L = 2$ transition near 15° (see Fig. 2). Therefore, by measuring a shift of 0.36 ± 0.3 MeV in the excitation of the substitutional peak between 0° and 15°, the Λ spin-orbit coupling was shown to be small (Auerbach *et al.*, 1981, 1983). Finally, the Λ spin-orbit splitting in $^{13}_\Lambda$C was found to be very small by observing two γ rays, correlated with the two constituent states of this substitutional peak and split by 152±54(stat)±36(syst) keV, interpreted essentially as $p_{j\Lambda} \rightarrow s_{1/2\Lambda}$ $E1$ γ transitions of energy ≈11 MeV (Ajimura *et al.*, 2001; **?**).

3. The (π^+, K^+) reaction

Binding energies of heavier hypernuclear systems were extracted from spectra obtained using the (π^+, K^+) reaction. This reaction has greater probability to populate interior states (Dover *et al.*, 1980; Thiessen *et al.*, 1980). It was first explored at the BNL-AGS in a series of investigations providing spectra across a wide range of hypernuclei. Typical energy resolution of 3–4 MeV was obtained (Milner *et al.*, 1985; Pile *et al.*, 1991). The reaction was then explored in detail at KEK with a dedicated beamline and a high resolution spectrometer, SKS (Fukuda *et al.*, 1995), specifically built to detect the reaction kaons. Using this system, the resolution improved to about 2 MeV (Nagae, 2001). Unfortunately, the mass (or binding energy) scale for most of the data was normalized to the emulsion B_Λ value (Table I) for $^{12}_\Lambda$C that is determined by only a few events. This, coupled with resolution issues in the reaction spectra, lead to some uncertainties in binding energies. Some of the binding-energy uncertainties have been sorted out in recent years by comparing with $(e, e'K^+)$ electroproduction measurements.

The elementary reaction $n(\pi^+, K^+)\Lambda$ peaks at an incident pion momentum near 1.05 GeV/c, and all (π^+, K^+) experiments have been performed at this incident momentum. The outgoing K^+ has a momentum of ≈0.7 GeV/c and the momentum and angular-momentum transfer to the Λ is substantial. The (π^+, K^+) reaction then preferentially populates spin-stretched states with an angular-momentum transfer $\Delta L = l_n + l_\Lambda$. For nodeless orbitals, the momentum dependence (form factor) of the transition density is given by $y^{\Delta L/2} e^{-y}$ with $y = (bq/2)^2$, where q is the 3-momentum transfer and b is the harmonic oscillator parameter ($b^2 = 41.5/\hbar\omega$, $\hbar\omega = 45A^{-1/3} - 25A^{-2/3}$). The maximum of the form factoroccurs for $y = \Delta L/2$. For light hypernuclei and transitions to inner Λ orbitals in heavier nuclei, the momentum transfer q is generally over 300 MeV/c which is well past the peak in the form factor and cross sections are small, falling rapidly with angle. However, the

(π^+, K^+) reaction becomes more effective in producing sates with large l_Λ in heavier hypernuclei due to the increasing spin of the valence neutron orbital involved in the reaction. Indeed, in Fig. 4, the full spectrum of nodeless, bound Λ orbitals is clearly evident for the ${}^{89}_{\Lambda}$Y hypernucleus (Hotchi *et al.*, 2001). The main part of the cross section arises from associated production on a $g_{9/2}$ neutron, while the origin of possible fine structure in the peaks is open to interpretation (Motoba *et al.*, 2008). The $\Delta L = 7$ transition dominating the f_Λ peak is well matched in the sense that the peak of the form factor occurs for $q \sim 345$ MeV/c and closely matches the momentum transfer to the hypernucleus. In general, (π^+, K^+) cross sections are found to be roughly a factor of 100 below those in the (K^-, π^-) reactions (different final states are populated) but, in terms of running time, the decrease in cross section can be more than compensated by the increased intensity of pion beams.

The (π^+, K^+) reaction provides a textbook example of the single-particle shell structure of hypernuclei, with Fig. 4 showing the prime example. In Section **??**, we collect together the Λ single-particle energies (B_Λ values) extracted from (π^+, K^+), $(e, e'K^+)$, (K^-, π^-), and emulsion studies. Most of the values come from three (π^+, K^+) experiments at KEK, namely E140a (Hasegawa *et al.*, 1996) (targets ^{10}B, ^{12}C, ^{28}Si, ^{89}Y, ^{139}La, ^{208}Pb), E336 (Hashimoto and Tamura, 2006; **?**) (targets ^{7}Li, ^{9}Be, ^{12}C, ^{13}C, ^{16}O), and E369 (Hotchi *et al.*, 2001) (targets ^{12}C, ^{51}V, ^{89}Y). All the targets are largely a single isotope, either because the natural target is a monotope, or nearly so, or because an enriched target was used (^{7}Li, ^{10}B, ^{13}C, ^{208}Pb). For the heavier targets (^{51}V, ^{89}Y, ^{139}La, ^{208}Pb), the aim is to identify peaks due to a series of Λ orbitals based on holes in the nodeless $f_{7/2}$, $g_{9/2}$, $h_{11/2}$, and $i_{13/2}$ neutron shells. For the odd-mass targets there is fragmentation of the neutron pickup strength due to the presence of an odd proton, and this must be accounted for in the analysis. In addition, other filled neutron orbits can make substantial contributions to the cross sections, as can be seen from attempts to analyze the data for ${}^{139}_{\Lambda}$La and ${}^{208}_{\Lambda}$Pb in Fig. 27 of (Hashimoto and Tamura, 2006). We note that DWIA calculations generally give reliable estimates for the cross sections of states populated in the (π^+, K^+) reation (Motoba *et al.*, 1988; **?**; **?**).

4. The $(e, e'K^+)$ reaction

Neither of the (K^-, π^-) or (π^+, K^+) reactions has significant spin-flip amplitude at forward angles, and consequently all spectra are dominated by transitions to non spin-flip states. Also, aside from early emulsion experiments, meson-beam spectroscopy has generally provided hypernuclear spectra with energy resolutions ≈2 MeV. This is due to the intrinsic resolutions of secondary mesonic beamlines, and the target thicknesses required to obtain sufficient counting rates. However, one study did achieve a spectrum resolution of approximately 1.5 MeV for the ${}^{12}_{\Lambda}$C hypernucleus, using a thin target and devoting substantial time to data collection (Hotchi *et al.*, 2001).

Electron beams, in comparison, have excellent spatial and energy resolutions, and the exchange of a photon can be accurately described by a first order perturbation calculation. In addition, electroproduction has been used for precision studies of nuclear structure so many experimental techniques are well established. Although previous electron accelerators had poor duty factors significantly impairing high singles-rate coincidence experiments, continuous-beam accelerators have now overcome this limitation. The cross section for nuclear kaon electroproduction is smaller than that for hypernuclear production by the (π, K) reaction for example, but reaction rates can be compensated by increased beam intensity. Targets can be physically small and thin (10-100 mg cm^{-2}), allowing studies of almost any isotope. However, the great advantage of the $(e, e'K^+)$ reaction is the potential to reach energy resolutions of a few hundred keV with reasonable counting rates at least up to medium-weight hypernuclei (Hungerford, 1994). Resolutions of a few hundred keV are sufficient for many studies where reactions can be used to selectively extract the spectroscopic factors to specific states (Rosenthal *et al.*, 1988).

Furthermore, the $(e, e'K^+)$ reaction proceeds by the absorption of a spin–1 virtual photon which carries high spin-flip probability even at forward angles. The 3-momentum transfer to a quasi-free Λ is high (approximately 300 MeV/c at zero degrees for 1500 MeV incident photons), so the resulting reaction is expected to predominantly excite spin-flip transitions to spin-stretched states (Motoba *et al.*, 1994). Recall that spin-flip states are not strongly excited in hadronic production, and the $(e, e'K^+)$ reaction acts on a proton rather than a neutron, creating proton-hole Λ-particle states which are charge symmetric to those studied with meson beams.

The ${}^{12}_{\Lambda}$B spectrum obtained in these experiments on a ^{12}C target is shown in Fig. 5, demonstrating the improved resolution in the more recent, E05-115, experiment with respect to that in the older one, E01-011, and also with respect to Hall A experiment E94-107 (Iodice *et al.*, 2007). In the upper panel of the figure, peaks 1,2,3,4 result from the $p_N \to s_\Lambda$ transition strength, with peak 1 standing for the ${}^{12}_{\Lambda}$B g.s. doublet which to a very good approximation is based on the ^{11}B g.s. core state. The other 3 peaks correspond to coupling the s_Λ hyperon to known excited levels in ^{11}B. Peaks 5,6,7,8 result from the $p_N \to p_\Lambda$ transition strength which extends further up into the continuum. Similar spectra were reported for the charge-symmetric hypernucleus ${}^{12}_{\Lambda}$C in (π^+, K^+) and $(K^-_{\rm stop}, \pi^-)$ experiments at KEK (Hotchi *et al.*, 2001) and at DAΦNE (Agnello *et al.*, 2005b), respectively. Yet, the JLab $(e, e'K^+)$ experiment provides by far the most refined $A = 12$ Λ hypernuclear excitation spectrum. Data were taken using targets of ^{12}C (Iodice *et al.*, 2007), ^{16}O (**?**), and ^{9}Be (**?**). In particular, $B_\Lambda = 13.76 \pm 0.16$

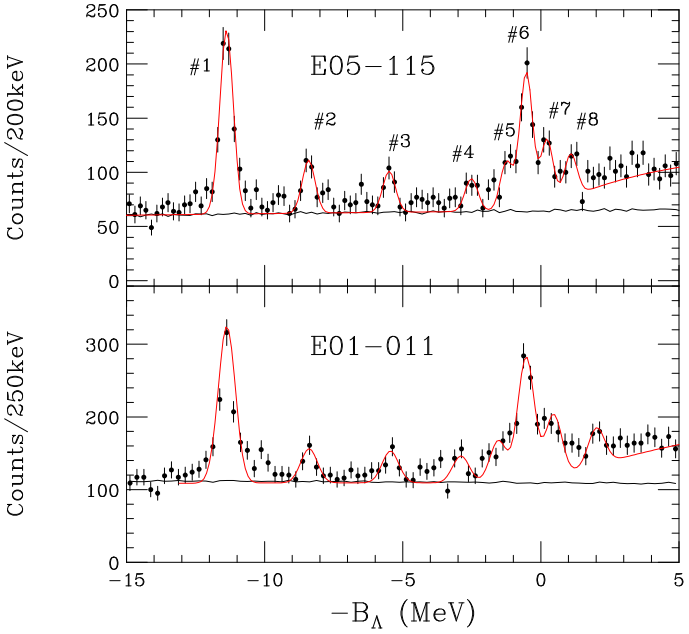

FIG. 5 (color online). Spectroscopy of ${}^{12}_{\Lambda}$B from the E05-115 and E01-011 experiments. The area below the black line is the accidental background. Figure adapted from (Tang *et al.*, 2014).

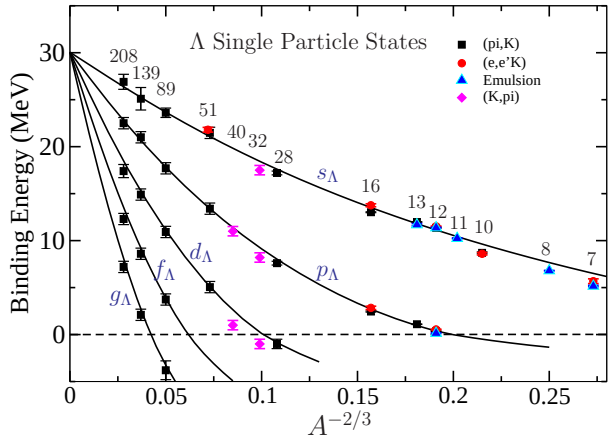

FIG. 6 (color online). Energy levels of the Λ single-particle major shells in ${}^{A}_{\Lambda}$Z hypernuclei as a function of $A^{-2/3}$. The curves are obtained from a standard Woods-Saxon potential $V_{\rm WS}$ representing the Λ-nucleus interaction (Millener *et al.*, 1988) with depth V_0=−30.05 MeV, radius R=$r_0A^{1/3}$, where r_0=1.165 fm, and diffusivity a = 0.6 fm.

MeV was determined for ${}^{16}_{\Lambda}$N by using the Λ and Σ^0 peaks from the elementary $(e,e'K^+)$ reaction on the hyprogen in a waterfall target.

Taking the positions of the Λ major shells as observed in the (π^+,K^+) and other reactions, the Λ single-particle energies show a very smooth A-dependence, which can be reproduced by a simple Woods-Saxon potential $V_{\rm WS}$, as shown in Fig. 6 for a data set that includes information up to ${}^{208}_{\Lambda}$Pb (Hasegawa *et al.*, 1996). The data used in the construction of Fig. 6 differ in several respects from the values given in the original papers and reviews (e.g., (Hashimoto and Tamura, 2006)). A full discussion of these differences is given elsewhere. The data in Fig. 6 are quite well fit by a simple Woods-Saxon potential. However, when replacing $V_{\rm WS}$ by the low-density limit form $\tilde{V}_0\rho_N(r)$, with ρ_N the nuclear density, the fit to the data requires adding a repulsive potential with a higher power of ρ_N and, obviously, a depth $\tilde{V}_0$ of the attractive potential much larger than $V_{\rm WS}(r=0)$ (Millener *et al.*, 1988). The resulting density-dependent Λ-nucleus potential can be traced back within a Skyrme-Hartree-Fock approach to a combination of two-body attractive ΛN and a three-body repulsive ΛNN interaction terms. Similar conclusions were also reached by (Yamamoto *et al.*, 1988). These early papers were based on a (π^+,K^+) experiment performed at BNL in 1987 (Pile *et al.*, 1991). Since that time, there have been a large number of both non-relativistic and relativistic mean-field calculations that reproduce the Λ single-particle energies (Lonardoni *et al.*, 2014; **?**; **?**; **?**; **?**; **?**). The smooth behavior of the B_Λ values is such that it should be possible to fit the updated data set very well in almostany model with small adjustments in the parameters.

5. Addendum: hypernuclear lifetime measurements

If the velocity of a hypernucleus recoiling from a production reaction is known, its lifetime can be measured by the distance it travels before decaying. This recoil-distance technique was used to observe and measure the lifetime of many short lived particles. In particular the lifetime of a free, unbound Λ, (263 ± 2) ps (Olive *et al.*, 2014), was determined by observing its mesonic decay in a beam of neutrally charged hyperons (Clayton *et al.*, 1975; Poulard *et al.*, 1973; Zech *et al.*, 1977).

Lifetimes of ${}^{3}_{\Lambda}$H, ${}^{4}_{\Lambda}$H and ${}^{5}_{\Lambda}$He measured in emulsion were published as early as in 1964 (Prem and Steinberg, 1964), but since hypernuclei are generally produced in emulsion with low kinetic energies, only very few decayed in flight, incurring relatively large experimental uncertainties on the deduced lifetimes. The more precise ${}^{3}_{\Lambda}$H lifetime deduced in a subsequent emulsion measurement, $\tau({}^{3}_{\Lambda}{\rm H})=128^{+35}_{-26}$ ps (Bohm *et al.*, 1970a), is considerably shorter than the one deduced from a helium bubble-chamber measurement, $\tau({}^{3}_{\Lambda}{\rm H})=246^{+62}_{-41}$ ps (Keyes *et al.*, 1973), the latter is equal to the free Λ lifetime within the experimental uncertainties. This was explained by (Bohm and Wysotzki, 1970) by a possible Coulomb dissociation of the very weakly bound ${}^{3}_{\Lambda}$H when traversing the high-Z emulsion. Finally, the ${}^{5}_{\Lambda}$He lifetime deduced in that emulsion study (Bohm *et al.*, 1970b) agrees perfectly within its larger uncertainties with the lifetime deduced 35 years later in a KEK experiment in which ${}^{5}_{\Lambda}$He was produced in a (π^+,K^+) reaction (Kameoka *et al.*, 2005). This and other lifetimes measured similarly at KEK are listed in Table II, with ${}_{\Lambda}$Fe the heaviest Λ hypernucleus

TABLE II Λ hypernuclear lifetimes (in ps) measured at KEK, using (π^+, K^+) production reactions.

Λ	${}^{5}_{\Lambda}$He	${}^{12}_{\Lambda}$C	${}^{28}_{\Lambda}$Si	${}_{\Lambda}$Fe
263 ± 2^a	276 ± 11^b	212 ± 6^b	206 ± 11^c	215 ± 14^c

[a](Olive *et al.*, 2014)
[b](Kameoka *et al.*, 2005)
[c](Bhang *et al.*, 1998; Park *et al.*, 2000)

for which this information is available. It is clear from the table that beginning with ${}^{12}_{\Lambda}$C the Λ hypernuclear lifetimes saturate at a value about 80% of the free Λ lifetime.

The first accelerator experiment to apply the recoil-distance method in a hypernuclear experiment used the LBL Bevatron to produce a hypernuclear beam by bombarding a polyethylene target with a 2.1 GeV/nucleon ^{16}O beam (Nield *et al.*, 1976). Spark chamber detectors with photographic readout were positioned behind the target and scanned for tracks with a decay vertex. The readout trigger required that an interaction occurred in the target and a potential decay was observed within a given time delay. These events were analyzed in a fit to the form $N(x) = A\exp(-x/\lambda) + B$ by varying A, B and λ, where B is a constant background, λ the mean lifetime of the hypernucleus, and x the mesured distance between the vertex and the target. Although the actual system which decayed was not directly identified, the most likely hypernuclear production reactions were assumed to be

$$^{16}\mathrm{O} + p \rightarrow {}^{16}_{\Lambda}\mathrm{O} + n + K^+ , \quad (1)$$

$$^{16}\mathrm{O} + n \rightarrow {}^{16}_{\Lambda}\mathrm{N} + n + K^+ . \quad (2)$$

The measured mean life was found to be 86^{+33}_{-26} ps, which is twice to three times shorter than lifetimes measured in this hypernuclear mass range in more recent, better controlled (π^+, K^+) experiments at KEK (Bhang *et al.*, 1998; Park *et al.*, 2000), as demonstrated in Table II.

More recently, the HypHI Collaboration at GSI reported lifetimes of ${}^{3}_{\Lambda}$H and ${}^{4}_{\Lambda}$H produced by bombarding a carbon target with a 2 GeV/nucleon ^{6}Li beam (Rappold *et al.*, 2013). The lifetime of ${}^{3}_{\Lambda}$H has also been measured in heavy ion central collisions, by the STAR Collaboration at the BNL-RHIC collider (Abelev *et al.*, 2010) and by the ALICE Collaboration at CERN-LHC (Adam *et al.*, 2016a). These measurements use the time dilation of a Lorentz boost to the recoiling hypernucleus produced in the collision, as shown in Fig. 7 from the ALICE determination of $\tau({}^{3}_{\Lambda}\mathrm{H})$. The values deduced from these measurements for the ${}^{3}_{\Lambda}$H lifetime are about 25% shorter than the free Λ lifetime, see the latest compilation by (Rappold *et al.*, 2014). This poses a serious theoretical challenge as discussed later in this Review.

Several programs have attempted to obtain the lifetime of heavy hypernuclei using the recoil-distance method by stopping antiprotons (Armstrong *et al.*, 1993; Bocquet *et al.*, 1987) in, or by electron production (Noga, 1986) on Bi and U targets. These use back-to-back fission fragments from the presumed decay of a recoiling hypernucleus to obtain the position of the decay relative to the target. As previously, the recoil velocity and decay position provide the hypernuclear lifetime.

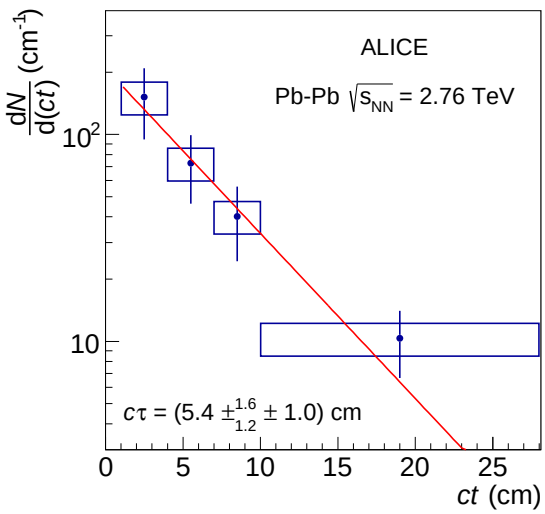

FIG. 7 Measured $\mathrm{d}N/\mathrm{d}(ct)$ distribution and exponential fit used by the ALICE Collaboration to determine the lifetime of ${}^{3}_{\Lambda}$H produced in Pb–Pb central collisions at $\sqrt{s_{NN}} = 2.76$ TeV at the CERN-LHC. The bars and boxes are statistical and systematic uncertainties, respectively. Figure adapted from (Adam *et al.*, 2016a).

As an example, this technique was used by the COSY-13 Collaboration to obtain the lifetime of hypernuclei averaged over hypernuclear masses from A=160–190, 170–200, and 200–230. The data were obtained from the fission of nuclear systems recoiling from an approximately 1.9 GeV proton beam incident on Au, Bi, and U targets, respectively (Cassing *et al.*, 2003; Pysz *et al.*, 1999). Obviously the specific recoiling system was unknown, so the masses and momenta of the recoils were obtained from coupled channel transport and statistical evaporation models. In both the COSY-13 and $\bar{p}$ experiments, fragments and particles emitted directly from the target were blocked from entering the amplitude-sensitive fission detectors – the recoil shadow method. The result of the COSY-13 experiment was a lifetime of (145 ± 11) ps. This is significantly shorter than the lifetime expected by extrapolating the measured lifetimes listed in Table II which indicate that saturation of hypernuclear lifetimes is achieved already for $A \geq 12$. The authors of (Cassing *et al.*, 2003) argue that the result shows significant violation of the $\Delta I = 1/2$ rule. However, it was pointed out by (Bauer and Garbarino, 2010) that no known mechanism could account for this significant decrease in the lifetime compared to (215±14) ps measured for ${}_{\Lambda}$Fe (Bhang *et al.*, 1998; Park *et al.*, 2000; Sato *et al.*, 2005). Therefore, ad-

ditional, more constrained measurements are needed to resolve this controversy.

II. Λ HYPERNUCLEAR STRUCTURE CALCULATIONS

A. The effective YN interaction and s-shell hypernuclei

The hyperon-nucleon interaction involves the coupled ΛN and ΣN channels, as illustrated in Fig. 8. The diagrams in the figure make the point that the direct $\Lambda N - \Lambda N$ interaction does not contain a one-pion exchange contribution because of isospin conservation (except for electromagnetic violations via $\Lambda - \Sigma^0$ mixing) while the coupling between the ΛN and ΣN channels does. For this reason alone, the ΛN interaction is considerably weaker than the NN interaction, and there is reason to believe that the three-body ΛNN interaction in a hypernucleus could be relatively important.

The free-space interactions are obtained as extensions of meson-exchange models for the NN interaction by invoking, e.g., a broken flavor, $SU(3)_f$, symmetry. The most widely used model is the Nijmegen soft-core, one-boson-exchange potential model known as NSC97 (Rijken *et al.*, 1999). The six versions of this model, labeled NSC97a..f, cover a wide range of possibilities for the strength of the central spin-spin interaction ranging from a triplet interaction that is stronger than the singlet interaction to the opposite situation. More recently, extended soft-core versions, ESC04 (Rijken and Yamamoto, 2006a) and ESC08 (Nagels *et al.*, 2015b), have become available. Effective interactions for use in a nuclear medium are then derived through a G-matrix procedure (Rijken *et al.*, 1999; Rijken and Yamamoto, 2006a; Yamamoto *et al.*, 2010).

The ΛN effective interaction can be written (neglecting a quadratic spin-orbit component) in the form

$$\begin{aligned} V_{\Lambda N}(r) &= V_0(r) + V_\sigma(r)\ \vec{s}_N \cdot \vec{s}_\Lambda + V_\Lambda(r)\ \vec{l}_{N\Lambda} \cdot \vec{s}_\Lambda \\ &+ V_N(r)\ \vec{l}_{N\Lambda} \cdot \vec{s}_N + V_T(r)\ S_{12}\ , \end{aligned} \tag{3}$$

where V_0 is the spin-averaged central interaction, V_σ is the difference between the triplet and singlet central interactions, V_Λ and V_N are the sum and difference of the strengths of the symmetric spin-orbit (LS) interaction $\vec{l}_{N\Lambda} \cdot (\vec{s}_\Lambda + \vec{s}_N)$ and antisymmetric spin-orbit (ALS) interaction $\vec{l}_{N\Lambda} \cdot (\vec{s}_\Lambda - \vec{s}_N)$, and V_T is the tensor interaction with

$$S_{12} = 3(\vec{\sigma}_N \cdot \hat{\vec{r}})(\vec{\sigma}_\Lambda \cdot \hat{\vec{r}}) - \vec{\sigma}_N \cdot \vec{\sigma}_\Lambda\ . \tag{4}$$

For the Λ in an s orbit, $\vec{l}_{N\Lambda}$ is proportional to $\vec{l}_N$ (Gal *et al.*, 1971). The effective $\Lambda N - \Sigma N$ and $\Sigma N - \Sigma N$ interactions can be written in the same way.

Effective interactions in common use are the YNG interactions (Yamamoto *et al.*, 1994a, 2010) in which each term is represented by an expansion in terms of a limited number of Gaussians with different ranges,

$$V(r) = \sum_i v_i\, e^{-r^2/\beta_i^2} \tag{5}$$

for the central and spin-orbit components, and

$$V_T(r) = \sum_i v_i\, r^2\, e^{-r^2/\beta_i^2} \tag{6}$$

for the tensor component. When based on nuclear-matter calculations, the YNG matrix elements are made density dependent by parametrizing the coefficients v_i through the Fermi momentum k_F.

Effective interactions for finite nuclei, specifically for p-shell hypernuclei, have been generated using a Brueckner-Hartree procedure (Halderson, 2008). These use Yukawa forms in place of the Gaussians above, are density-independent, and are available for most of the Nijmegen interactions (D. Halderson, private communications). Ab-initio calculations of s-shell Λ hypernuclei have been done using free-space as well as effective YN interactions. In such calculations the ΛN interaction is weaker than the NN interaction, in part because one-pion exchange between a Λ and a nucleon is forbidden by isospin. The inclusion of two-pion exchange introduces coupling of Λs and Σs in hypernuclei, in analogy to the coupling of Δs with nucleons in nuclei. However, $\Lambda - \Sigma$ coupling is much more important because of the suppression of the long-range OPE, the smaller mass difference between the Λ and Σ, and the narrower Σ-nuclear conversion width. $\Lambda - \Sigma$ coupling naturally induces 3-body forces as generated by the last diagram in Fig. 8 (Nemura *et al.*, 2002), and electromagnetic $\Lambda - \Sigma^0$ mixing generates charge-symmetry breaking (Gal, 2015). Thus the use of a ΛN potential in a many-body calculation must include in-medium effects, as these are not included in any 2-body "elementary" potential (Nemura *et al.*, 2002; Nogga *et al.*, 2002). We note that the variational calculation (Nemura *et al.*, 2002) attempted to explicitly include 3-body forces within a coupled-channel approach. This study claims to have obtained reasonable agreement with the separation energies for all the s-shell hypernuclei, including the excited states, by using a NSC97e-simulated potential. However, The genuine NSC97e potential in Nogga's calculation (Nogga, 2013; Nogga *et al.*, 2002) significantly underbinds ${}^{3}_{\Lambda}$H. Therefore, there appears sufficient discrepancy between the results of theoretical calculations, and also when compared to the data, to warrant a more conservative view that all calculations are still missing something.

B. p-shell hypernuclei, γ-ray measurements, and spin dependence of the ΛN interaction

The results from various production reactions for hypernuclei have establishd that the Λ moves in a well about 30 MeV deep and that the $\vec{l}_{N\Lambda} \cdot \vec{s}_\Lambda$ spin-orbit term

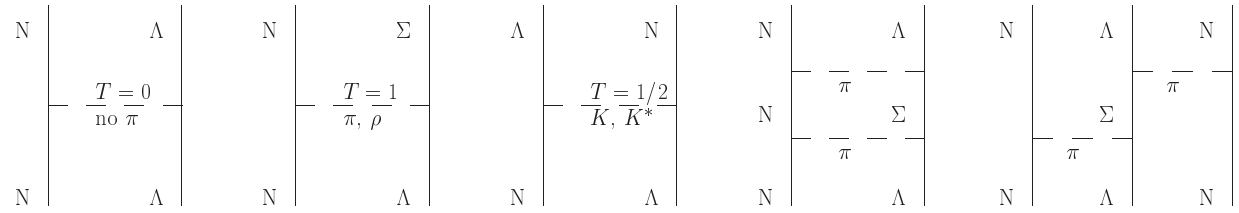

FIG. 8 Diagrams showing the important features of the coupled $\Lambda N - \Sigma N$ strangeness -1 interaction for isospin 1/2. The last diagram shows the two-pion exchange three-body interaction.

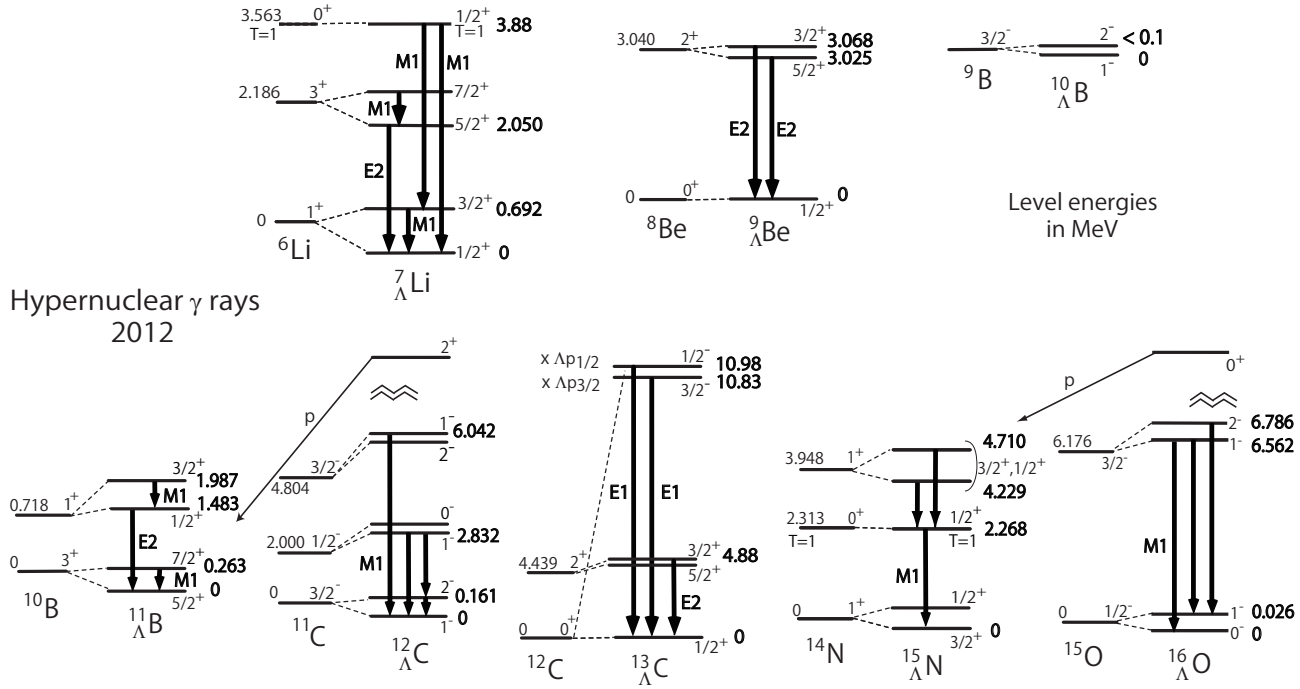

FIG. 9 Spectra of p-shell hypernuclei showing observed γ-ray transitions, all with the Hyperball detector except for the transitions in ${}^{13}_{\Lambda}$C (Ajimura *et al.*, 2001; **?**) and ${}^{12}_{\Lambda}$C, for which the Hyperball2 detector was used (**?**). All energies are in MeV. From Tamura *et al.*, 2013.

is quite small. However, multiplets based on particular core levels cannot be resolved. The splitting of a multiplet is governed by terms in Eq. (3) that depend on the spin of the Λ. In the p shell, the five $p_N s_\Lambda$ two-body matrix elements depend on the radial integrals associated with each component in Eq. (3), are conventionally denoted by the parameters $\overline{V}$, Δ, S_Λ, S_N and T (Gal *et al.*, 1971)

$$V_{\Lambda N} = \overline{V} + \Delta\ \vec{s}_N \cdot \vec{s}_\Lambda + S_\Lambda\ \vec{l}_N \cdot \vec{s}_\Lambda + S_N\ \vec{l}_N \cdot \vec{s}_N + T\ S_{12}\ . \quad (7)$$

Note that the operators associated with Δ and S_Λ are $\vec{S}_N \cdot \vec{s}_\Lambda$ and $\vec{L}_N \cdot \vec{s}_\Lambda$. This enables simple estimates for the contributions of Δ and S_Λ to be made from the known LS structure of the nuclear core state.

The only way to measure the doublet spacings, and hence determine Δ, S_Λ, and T, is to perform γ-ray spectroscopy with high-resolution γ-ray detectors (usually germanium). Figure 9 shows 20 γ-ray transitions observed in p-shell hypernuclei via $(\pi^+, K^+\gamma)$ experiments at KEK and $(K^-, \pi^-\gamma)$ experiments at BNL between 1998 and 2005 using the Hyperball array of 14 large-volume Ge detectors (Hashimoto and Tamura, 2006). It can be seen that the data set includes the measurement of nine doublet spacings. As will be discussed, the data for ${}^{7}_{\Lambda}$Li, ${}^{9}_{\Lambda}$Be, and ${}^{16}_{\Lambda}$O play an important role in determining Δ, S_Λ, and T, respectively. Also looking ahead, Table III shows that all nine doublet spacings can be well described in terms of the contributions of these three parameters and contributions arising from Λ-Σ mixing.

The motivation for including both Λ and Σ hypernuclear states in the shell-model basis is provided in the previous subsection where it is noted that the coupling between these configurations is necessary to solve the

TABLE III Doublet spacings in p-shell hypernuclei. E_c identifies the core state upon which the doublet is built. Energies are given in keV. The entries in the top (bottom) half of the table are calculated using the parameters in Eq. (12) (Eq. (13)). The individual contributions do not sum to exactly ΔE^{th}, which comes from the diagonalization, because small contributions from the energies of admixed core states are not included.

	J_u^π	J_l^π	E_c	$\Lambda\Sigma$	Δ	S_Λ	S_N	T	ΔE^{th}	ΔE^{exp}
${}^{7}_{\Lambda}$Li	$3/2^+$	$1/2^+$	0	72	628	-1	-4	-9	693	692
${}^{7}_{\Lambda}$Li	$7/2^+$	$5/2^+$	2186	74	557	-32	-8	-71	494	471
${}^{8}_{\Lambda}$Li	2^-	1^-	0	149	393	-14	-15	-23	445	(442)
${}^{9}_{\Lambda}$Li	$5/2^+$	$3/2^+$	0	116	531	-18	-18	-10	590	
${}^{9}_{\Lambda}$Li	$3/2^+_2$	$1/2^+$	981	-79	229	-13	-11	-91	-13	
${}^{9}_{\Lambda}$Be	$3/2^+$	$5/2^+$	3030	-8	-14	37	0	28	44	43
${}^{10}_{\Lambda}$Be	2^-	1^-	0	-10	180	-22	-4	-33	110	< 100
${}^{10}_{\Lambda}$Be	3^-	2^-	2429	-19	172	-37	-5	-10	103	
${}^{11}_{\Lambda}$B	$7/2^+$	$5/2^+$	0	56	339	-37	-10	-80	267	264
${}^{11}_{\Lambda}$B	$3/2^+$	$1/2^+$	718	61	424	-3	-44	-10	475	505
${}^{12}_{\Lambda}$C	2^-	1^-	0	65	167	-22	-12	-42	158	161
${}^{15}_{\Lambda}$N	$3/2^+_2$	$1/2^+_2$	3948	65	451	-2	-16	-10	507	481
${}^{15}_{\Lambda}$N	$1/2^+_1$	$3/2^+_1$	0	45	244	34	-8	-214	99	
${}^{16}_{\Lambda}$O	1^-	0^-	0	-33	-123	-20	1	188	23	26
${}^{16}_{\Lambda}$O	2^-	1^-_2	6176	92	207	-21	1	-41	248	224

'overbinding' problem in the s-shell hypernuclei by providing considerable extra binding energy for the ${}^{4}_{\Lambda}$H and ${}^{4}_{\Lambda}$He 0^+ ground states. This means that the ΛN spin-spin interaction and Λ-Σ coupling both contribute strongly to the spacing of the 0^+ and 1^+ states.

The $s_N s_Y$ matrix elements are purely from relative s states while the central $p_N s_Y$ matrix are roughly half relative s state and half relative p state. Because the p-state matrix elements are much smaller than s-state matrix elements, the scale for energy shifts from Λ-Σ coupling goes down a factor of four in p-shell hypernuclei. This can be seen from Fig. 9 and Table III but the effects are still significant.

The parametrization of Eq. (7) applies to the direct ΛN interaction, the ΛN-ΣN coupling interaction, and the direct ΣN interaction for both isospin 1/2 and 3/2. Values for the parameters based on various Nijmegen models of the YN interactions are given in Section 3 of (**?**); see also (Yamamoto *et al.*, 2010). Formally, one could include an overall factor $\sqrt{4/3}\, t_N \cdot t_{\Lambda\Sigma}$ in the analog of Eq. (3) that defines the interaction, where $t_{\Lambda\Sigma}$ is the operator that converts a Λ into a Σ. Then, the core operator associated with $\overline{V}'$ is $T_N = \sum_i t_{Ni}$. This leads to a non-zero matrix element only between Λ and Σ states that have the same core, with the value

$$\langle (J_c T, s_\Sigma) JT | V_{\Lambda\Sigma} | (J_c T, s_\Lambda) JT \rangle = \sqrt{\frac{4}{3}}\, \sqrt{T(T+1)}\, \overline{V}' \ , \tag{8}$$

in analogy to Fermi β decay of the core nucleus. Similarly, the spin-spin term involves $\sum_i s_{Ni} t_{Ni}$ for the core and connects core states that have large Gamow-Teller (GT) matrix elements between them. This can be the case when the core states are the same (this has been called coherent Λ-Σ coupling (Akaishi *et al.*, 2000)) but, because Δ' is large, there can be large coupling matrix elements for other states, often with different isospin. Not surprisingly then, energy shifts due to Λ-Σ coupling grow with the isospin of the core nucleus and are predicted to be more than 250 keV for the ground states of ${}^{9}_{\Lambda}$He and ${}^{10}_{\Lambda}$Li that could be reached by double-charge-exchange reactions from stable targets (Gal and Garcilazo, 2013).

Shell-model calculations for p-shell hypernuclei start with the Hamiltonian

$$H = H_N + H_Y + V_{NY} \ , \tag{9}$$

where H_N is an empirical Hamiltonian for the p-shell core, the single-particle H_Y supplies the $\sim 80\,\mathrm{MeV}$ mass difference between Λ and Σ, and V_{NY} is the YN interaction. The shell-model basis states are chosen to be of the form $|(p^n \alpha_c J_c T_c, j_Y t_Y) JT\rangle$, where the hyperon is coupled in angular momentum and isospin to eigenstates of the p-shell Hamiltonian for the core, with up to three values of T_c contributing for Σ-hypernuclear states. This is known as a weak-coupling basis and, indeed, the mixing of basis states in the hypernuclear eigenstates is generally very small. In this basis, the core energies can be taken from experiment where possible and from the p-shell calculation otherwise.

The technical details of such calculations are quite simple (Auerbach *et al.*, 1983; Millener, 2007). Because the product of creation and annilation operators for a two-body YN interaction can written in terms $a^\dagger a$ pairs for the nucleons and hyperons, we simply need a complete set of one-body density-matrix elements (OBDME) between p-shell eigenstates (the maximum dimension for a

TABLE IV Root-mean-square charge radii and dominant wave function components for the ground states of stable p-shell nuclei (par4 interaction). The L decomposition of states with good K are given in Eqs. (10) and (11).

Nucleus	$\langle r^2\rangle_{ch}^{1/2}$ fm	[f]	% [f]	wfn.
^{6}Li	2.57	[2]	98.2	$L=0, S=1$
^{7}Li	2.41	[3]	96.6	$L=1, S=1/2$
^{9}Be	2.52	[41]	94.7	$K=3/2, J=3/2$
^{10}B	2.45	[42]	94.0	$K=3, J=3$
^{11}B	2.42	[43]	81.0	$K=3/2, J=3/2$
^{12}C	2.47	[44]	79.3	$L=0, S=0$
^{13}C	2.44	[441]	66.5	$L=1, S=1/2$
^{14}C	2.56	[442]	59.7	$L=0, S=0$
^{14}N	2.52	[442]	94.2	$L=2, S=1$
^{15}N	2.59	[443]	100.0	$L=1, S=1/2$

given JT in the p shell is only 14) to compute matrix elements of the hypernuclear Hamiltonian. Only isoscalar OBDME are needed in the Λ space and isovector OBDME are needed for the Λ-Σ coupling matrix elements.

Many hypernuclear calculations have used the venerable Cohen and Kurath interactions (**?**). Here, the p-shell interaction has been refined using the following strategy. The one-body spin-orbit splitting between the $p_{3/2}$ and $p_{1/2}$ orbits is fixed to give a good description of the light p-shell nuclei (say for $A \leq 9$). The overall strength of the tensor interaction is also fixed, ultimately to produce the cancellation in ^{14}C β decay. The well-determined linear combinations of the central and vector p-shell interactions are then chosen by fitting the energies of a large number of states that are known to be dominantly p shell in character, including the large spin-orbit splitting at $A=15$. Some properties of stable p-shell nuclei are shown in Table IV for this interaction. A detailed discussion of p-shell nuclei, including spectra, is given in Section 5 of (Millener, 2007). In Table IV

$$|K=3/2, J=3/2\rangle = \sqrt{\frac{21}{26}}L=1 - \sqrt{\frac{5}{26}}L=2\,, \qquad (10)$$

with $S=1/2$, while

$$|K=3, J=3\rangle = \sqrt{\frac{6}{7}}L=2 - \sqrt{\frac{3}{22}}L=3 + \sqrt{\frac{1}{154}}L=4\,, \qquad (11)$$

with $S=1$.

In the LS basis for the core, the matrix elements of $\vec{S}_N\cdot\vec{s}_\Lambda$ are diagonal (similarly for $\vec{L}_N\cdot\vec{s}_\Lambda = (\vec{J}_N - \vec{S}_N)\cdot\vec{s}_\Lambda$) and depend just on the intensities of the total L and S for the hypernucleus. Because supermultiplet symmetry $[f_c]K_cL_cS_cJ_cT_c$ is generally a good symmetry for p-shell core states (Table IV and Eqs. (10) and (11)), only one or two values of L and S are important. The mixing of different $[f_c]L_cS_c$ is primarily due to the one-body LS and two-body SLS and ALS terms in the effective p-shell Hamiltonian; the central interaction is essentially SU(4) conserving. Of the remaining ΛN parameters, $\overline{V}$ contributes only to the overall binding energy; S_N does not contribute to doublet splittings in the weak-coupling limit but a negative S_N augments the nuclear spin-orbit interaction and contributes to the spacings between states based on different core states; in general, there are no simple expressions for the coefficients of T.

With reference to Table III, the set of ΛN parameters used up to $^{9}_{\Lambda}$Be (chosen to fit the energy spacings in $^{7}_{\Lambda}$Li perfectly) is (parameters in MeV)

$$\Delta = 0.430 \quad S_\Lambda = -0.015 \quad S_N = -0.390 \quad T = 0.030\,. \qquad (12)$$

The doublet spacings for the heavier p-shell hypernuclei consistently require a smaller value for Δ

$$\Delta = 0.330 \quad S_\Lambda = -0.015 \quad S_N = -0.350 \quad T = 0.0239\,. \qquad (13)$$

The matrix elements for the Λ-Σ coupling interaction, based on the G-matrix calculations of (Akaishi *et al.*, 2000) for the NSC97e, f interactions (Rijken *et al.*, 1999), are

$$\overline{V}' = 1.45 \quad \Delta' = 3.04 \quad S'_\Lambda = S'_N = -0.09 \quad T' = 0.16\,. \qquad (14)$$

These parameters are kept fixed throughout the p shell.

We are now in a position to consider the γ-ray data in Fig. 9 in relation to the breakdown of doublet spacings in Table III. First, on a historical note, shell-model analyses of Λ binding energies for p-shell hypernuclei were attempted long ago, and introduced the notation still in use for the ΛN interaction (Gal *et al.*, 1971). These authors also considered a double-one-pion-exchange ΛNN interaction. However, progress on characterizing the ΛN interaction was hampered by a lack of data (Gal. *et al.*, 1972, 1978). Nevertheless, the stage was set for studies of hypernuclear γ-rays (Dalitz and Gal, 1978). The observation of γ-rays in $^{7}_{\Lambda}$Li and $^{9}_{\Lambda}$Be at BNL using the $(K^-,\pi^-\gamma)$ reaction and NaI detectors (May *et al.*, 1983) finally set the stage for a shell-model analysis (Millener *et al.*, 1985) with parameters close to those in Eq. (12), but without the inclusion of Λ-Σ coupling, and inspired other analyses (**?**). Many of the p-shell hypernuclei up to $^{13}_{\Lambda}$C have also been studied in cluster models (**?**).

In the first $(\pi^+, K^+\gamma)$ experiment with the Hyperball at KEK in 1998 (Tamura *et al.*, 2000), four γ-rays in $^{7}_{\Lambda}$Li were seen, namely all except the $7/2^+ \rightarrow 5/2^+$ transiton in Fig. 9. Note that the $3/2^+$ ($L=0, S=3/2$) and $7/2^+$ ($L=2, S=3/2$) require spin-flip and are not strongly populated in the (π^+, K^+) reaction (Hiyama *et al.*, 1999). The high-energy M1 transitions from the $1/2^+; T=1$ level can be seen when the Doppler-shift correction is made and their energy difference matches the 691.7 keV of the transition (peak sharpened by the Doppler correction) between the ground-state doublet members. The lineshape for the 2050-keV $5/2^+ \rightarrow 1/2^+$ transition gives a lifetime for the $5/2^+$ level via the Doppler-shift attenuation method (Tanida *et al.*, 2001). The derived B(E2) is considerably smaller than expected from the known B(E2) for the $3^+ \rightarrow 1^+$ transition in ^{6}Li. The lowest

threshold is for ${}^{5}_{\Lambda}$He+d at 3.94(4) MeV so that the $5/2^+$ state and the $1/2^+$ ground state in ${}^{7}_{\Lambda}$Li are considerably more bound than the core states in ^{6}Li. This entails a shrinkage in the size of the radial wave functions, and a reduction of the B(E2), that is best treated in cluster-model calculations for ${}^{7}_{\Lambda}$Li (Hiyama *et al.*, 1999). The 471-keV M1 γ-ray in the upper doublet was seen via γ-γ coincidence with the $5/2^+ \rightarrow 1/2^+$ transition in a $(K^-, \pi^-\gamma)$ experiment on a ^{10}B target at BNL (Ukai *et al.*, 2006) (following $l=0$ ^{3}He emission from the $s_N^{-1}s_\Lambda$ substitutional state in ${}^{10}_{\Lambda}$B).

From Table III, it can be seen that the ground-state doublet spacing comes mostly from the spin-spin interaction ($3\Delta/2$ in the pure LS limit) with a 10% assistance from Λ-Σ coupling. The situation is similar for the second doublet except that contributions from S_Λ and T reduce the spacing by $\sim$ 100 keV. S_N reduces the excitation energies of the $5/2^+;0$ and $1/2^+;1$ states by 288 keV and 82 keV, respectively (Millener, 2007), making the $1/2^+$ state just bound.

In ${}^{9}_{\Lambda}$Be, the ^{8}Be core states are unbound (by 92 keV for the ground state) but the presence of the Λ raises the α threshold to 3.50 MeV, *viz.*

$$B_\alpha({}^{9}_{\Lambda}\mathrm{Be}) = B_\alpha({}^{8}\mathrm{Be}) + B_\Lambda({}^{9}_{\Lambda}\mathrm{Be}) - B_\Lambda({}^{5}_{\Lambda}\mathrm{He}) \ , \qquad (15)$$

meaning that the γ-rays from the $3/2^+$ and $5/2^+$ states can be observed. This was achieved using the Hyperball in a $(K^-, \pi^-\gamma)$ experiment at BNL (Akikawa *et al.*, 2002). With the Doppler correction, peaks were seen at 3024 and 3067 keV (these are updated energies (**?**)). Only the upper peak is seen following proton emission from ${}^{10}_{\Lambda}$B and strong theoretical arguments (Millener, 2005, 2007) indicate that this γ-ray comes from the $3/2^+$ member of the doublet. Table III shows that the small splitting of the doublet means that S_Λ is small (contributions from Δ, T, and Λ-Σ coupling more or less cancel); the splitting is $-5/2S_\Lambda$ if the ^{8}Be 2^+ state is pure $L=2, S=0$, as it is in the $2\alpha+\Lambda$ cluster model (**?**).

An earlier experiment with NaI detectors at BNL (May *et al.*, 1983) observed a γ-ray at 3079(40) keV and put an upper limit of 100 keV on the doublet splitting. This, and the observation of a 2034(23) keV γ-ray in ${}^{7}_{\Lambda}$Li (May *et al.*, 1983), revived shell-model studies of p-shell hypernuclei (Millener *et al.*, 1985).

The main objective of a 2001 $(K^-, \pi^-\gamma)$ experiment at BNL (Ukai *et al.*, 2004, 2008) was to measure the ground-state doublet spacing of ${}^{16}_{\Lambda}$O which depends strongly on the matrix element of the ΛN tensor interaction T. For a pure $p_{1/2}^{-1}s_\Lambda$ configuration, the spacing is (Dalitz and Gal, 1978)

$$E(1^-_1) - E(0^-) = -\frac{1}{3}\Delta + \frac{4}{3}S_\Lambda + 8\,T \ . \qquad (16)$$

Figure 9 shows that the measured spacing is only 26 keV, derived from the difference in energies of the γ-rays from the 6562-keV 1^- excited state to the members of the ground-state doublet. Table III shows that the small separation is the result of a large cancellation between the contributions of T and the other contributions (mainly Δ). If Δ is known, this doublet spacing fixes T. The major contributor to the increase in the spacing between the two doublets relative to the core spacing of 6.176 MeV is S_N which gives over 500 keV ($\sim 1.5\Delta$).

A weak γ-ray is also seen in the above experiment (Ukai *et al.*, 2008) and is interpreted as a transition from the 2^- member of the upper doublet (the 2^- state requires spin-flip to be populated via the (K^-, π^-) reaction). The ${}^{15}_{\Lambda}$N γ-rays are seen following proton emission from the p_Λ states of ${}^{16}_{\Lambda}$O (see Fig. 3). The 2268-keV γ-ray is sharp without Doppler correction implying a long lifetime (measured at 1.5 ps) while the transitions from the upper doublet are fast and are seen when the Doppler correction is made. It is interesting that the transition from the $1/2^+;1$ level to the $1/2^+$ member of the ground-state doublet is not seen; in the weak-coupling limit, it should be approximately half the strength of the 2268-keV transition. We first note that in ^{14}N the M1 transition from the 3.498-MeV 1^+ level (mainly $L=0, S=1$) to the $0^+;1$ level is strong while the M1 transition from the $0^+;1$ level to the ground-state is weak because this transtion is the analog of ^{14}C β decay and the $< \sigma\tau >$ matrix element essentially vanishes (making the M1 transition mainly orbital). It turns out (Millener, 2007; Ukai *et al.*, 2008) that small admixtures of the $1^+_2;0 \times s_\Lambda$ configuration into the wave functions of the ground-state doublet members produce strong cancellations in the hypernuclear M1 matrix elements giving a predicted lifetime of 0.5 ps for the $0^+;1$ level compared with 0.1 ps for the core transition. The cancellation is more severe for the $1/2^+;1 \rightarrow 1/2^+$ transition but still not quite strong enough and the theoretical γ-ray branch to the $1/2^+$ state is 18% (Ukai *et al.*, 2008). The upper doublet (the lower member is surely$1/2^+$) is based on an $L=0$ core and the splitting is mainly due to the spin-spin interaction (Δ) in complete analogy to the ${}^{7}_{\Lambda}$Li ground-state doublet and, in fact, the excited-state doublet in ${}^{11}_{\Lambda}$B.

In ${}^{12}_{\Lambda}$C, the excitation energies of the excited 1^- states provide a useful check on the energies of the unresolved peaks in the ^{12}C$(e,e'K^+){}^{12}_{\Lambda}$B reaction (Iodice *et al.*, 2007; Tang *et al.*, 2014). The difference in the energies of the transitions from the 1^-_2 level agrees with the 161.5 keV energy measured for the ground-state doublet transition (**?**). This doublet spacing is important because of the failure to observe the corresponding doublet spacing in ${}^{10}_{\Lambda}$B in two $(K^-, \pi^-\gamma)$ experiments at BNL (Chrien *et al.*, 1990; **?**) that both set an upper limit of about 100 keV on the doublet spacing. The core nuclei have similar structures (see Table IV), being essentially particle-hole conjugates in the p shell (a particle or hole in the Nilsson $K=3/2$ orbit). This means that the ΛN contribution to the spacing should be nearly the same. Table IV shows that the ΛN contribution for ${}^{10}_{\Lambda}$B is actually slightly larger than for ${}^{12}_{\Lambda}$C. Table IV also shows that the Λ-Σ coupling increases the doublet separation in ${}^{12}_{\Lambda}$C while decreasing it slightly in ${}^{10}_{\Lambda}$B. This is because the

$< \sigma\tau >$ matrix elements involving the lowest $3/2^-$ and $1/2^-$ states are of opposite sign for the two core nuclei. The coefficients of $\overline{V}'$ and Δ' for matrix elements involving the same core state are of opposite sign for the 1^- and 2^- states and the sign changes between ${}^{10}_{\Lambda}$B and ${}^{12}_{\Lambda}$C. This is a substantial effect but it is lessened by that fact that there is always a push on the 1^- states from the the Σ state with a $1/2^-$ core (with $L=1$). It is certainly possible to reduce the spacing in ${}^{10}_{\Lambda}$B substantially by changing the Λ-Σ coupling interaction (Halderson, 2008; **?**). It has also been suggested that charge-symmetry breaking effects could lower the transition energy in ${}^{10}_{\Lambda}$B (Gal, 2015).

Another way to try to measure the ground-state doublet spacing for the $A = 10$ hypernuclei is to look for γ-rays from the 2^- and 3^- states in ${}^{10}_{\Lambda}$Be based on the 2.43-MeV $5/2^-$ state in ^{9}Be via the ^{10}B$(K^-, \pi^0\gamma)^{10}_{\Lambda}$Be reaction (**?**) (this reference also considers ${}^{8}_{\Lambda}$Li and ${}^{9}_{\Lambda}$Be as possible sources of unassigned p-shell hypernuclear γ rays). Unfortunately, the $2^-_2 \rightarrow 2^-_1$ γ-ray branch is predicted to be only 13% and the $2^-_2 \rightarrow 1^-_1$ and $3^-_1 \rightarrow 2^-_1$ transitions could have very similar energies. There is no chance to see the ground-state doublet transition itself because the B(M1) is proportional to $(g_c - g_\Lambda)^2$ (Dalitz and Gal, 1978) ($g_c = -0.746$, $g_\Lambda = -1.226$) leading to very long electromagnetic lifetime meaning that the 2^- level will undergo weak decay.

In the $(\pi^+, K^+\gamma)$ reaction on ^{11}B, six γ-ray transitions with energies of 264, 458, 505, 570, 1483, and 2477 keV have been identified as transitions in${}^{11}_{\Lambda}$B (**?**) The 1483-keV transition is by far the most intense and is identified as coming from the $1/2^+$ level based on the 718-keV $1^+;0$ level of ^{10}B and acts as a collection point for γ-rays from strongly populated $3/2^+$ and $1/2^+$ levels higher in the spectrum. A $3/2^+;1$ level based on the 5.16-MeV $2^+;1$ level of ^{10}B should be the strongest and the source of the 2477-keV γ-ray seen in the Doppler-corrected spectrum. By making use of the relative intensities and lifetime limits for these γ-rays a plausible decay scheme has been established by comparison with shell-model calculations (**?**). Assignments for the lower part of the spectrum, shown in Fig. 9, have been confirmed from an analysis of the three γ-rays seen following proton emission from ${}^{12}_{\Lambda}$C (**?**). The main failing of the shell-model calculation is not to produce high enough excitation energies for the ${}^{11}_{\Lambda}$B states based on the $1^+;0$ states of ^{10}B at 0.72 and 2.15 MeV (**?**).

The preceding discussion shows that one set of $p_N s_Y$ parameters is quite successful in reproducing data on the doublet spacings in the p shell (with some adjustment for ${}^{7}_{\Lambda}$Li). This statement refers to Δ, S_Λ, T and the Λ-Σ coupling parameters. The parameter S_N augments the nuclear spin-orbit interaction, gives a substantial contribution to B_Λ values in the p shell (**?**), and works in the right direction to reproduce the changes in spacing of doublet centroids from the spacing in the core nucleus. However, a considerably larger value of S_N is required to reproduce the energies of excited-state doublets in ${}^{11}_{\Lambda}$B, ${}^{12}_{\Lambda}$C, and ${}^{13}_{\Lambda}$C. In terms of the ΛN interaction alone, the small value for S_Λ means that the strengths of the symmetric and antisymmetric spin-orbit interactions have to be very nearly equal. This is not the case for effective interactions derived from free-space YN models and nor is the value for S_N large enough (**?**). However, the double one-pion exchange ΛNN interaction (Gal *et al.*, 1971) is independent of the Λ spin and gives, when averaged over the s_Λ wave function, an effective NN interaction that operates in the nuclear core. This interaction contains an antisymmetric spin-orbit component that behaves rather like S_N and has its largest effect beyond the middle of the p shell (Gal *et al.*, 1971). It may, in fact, be responsible for much of the empirical value of S_N and should be re-introduced into p-shell hypernuclear calculations.

In ${}^{13}_{\Lambda}$C, the Λ threshold is the lowest particle-decay channel and the p_Λ orbit is just bound. As noted earlier, the $\sim$ 11-MeV γ-rays from the lowest $3/2^-$ and $1/2^-$ states were measured using an array of NaI detectors and the separation of the states, $152 \pm 54(\text{stat}) \pm 36(\text{syst})$, was determined from the shift in the peak with pion scattering angle (Ajimura *et al.*, 2001; **?**). Figure 10 shows the $p^8 p_\Lambda$ states based on the lowest 0^+ and 2^+ states of the ^{12}C core. From an older BNL experiment (May *et al.*, 1983), the separation between the two $1/2^-$ states was determined to be 6.0 ± 0.4 MeV while that of the $1/2^-_2$ and $5/2^-_2$ states was 1.7 ± 0.4 MeV. The doublets are characterized ly the quantum number $\mathcal{L}$ and split by the spin-dependent interactions where (Auerbach *et al.*, 1981, 1983)

$$\vec{\mathcal{L}} = \vec{J}_c + \vec{l_\Lambda} \quad \text{and} \quad \vec{J} = \vec{\mathcal{L}} + \vec{s_\Lambda} \ . \tag{17}$$

The spectrum, including Λ-Σ coupling, can be calculated from the Gaussian or Yukawa representations of the G-matrices derived from the free YN interaction model. Beause the p_Λ states are only bound by about 0.8 MeV, the calculation is performed using Woods-Saxon wave functions for this binding energy. One can also use an interaction obtained by adjusting the strengths in the various ΛN channels to reproduce the $p_N s_\Lambda$ matrix elements in Eq. (13). There are 20 independent $p_N s p_\Lambda$ matrix elements and pieces of the interactions such as the even-state tensor interaction enter. Furthermore, a $Q_N \cdot Q_\Lambda$ multipole component of the interaction is active as compared to just the spatial monopole for $p_N s_\Lambda$. It is this quadrupole component that splits the $\mathcal{L} = 1, 2, 3$ states of the $2^+ \times p_\Lambda$ multiplet in Fig. 10. This can involve strong mixing of the $p_{1/2}$ and $p_{3/2}$ Λ states to make states with good $\mathcal{L}$ (Auerbach *et al.*, 1983).

For $p_N s_\Lambda$, there is no way to separate the contributions from the even- and odd-state central interactions. However, for $p_N p_\Lambda$ different strengths in the even- and odd-state central interactions give rise to a space-exchange interaction that will separate states with different spatial symmetries. Coupling a p_Λ to the dominantly [44] states of ^{12}C leads to [54] and [441] symmetries for the nine p-shell baryons. These are not very good quantum numbers for the hypernuclear states. Nevertheless, the upper-

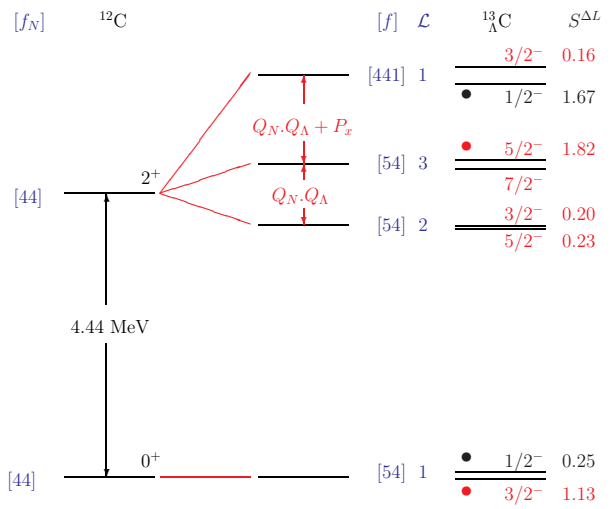

FIG. 10 (color online). p_Λ states in $^{13}_{\Lambda}$C based on the lowest 0^+ and 2^+ states of the ^{12}C core. The spin-doublet structure is explained in the text and Eq.(17. The states of the $2^+\times p_\Lambda$ multiplet are split by the quadrupole-quadrupole component of the $p_N p_\Lambda$ interaction. The states are labelled by their tendency towards a good supermultiplet symmetry [f]. The energy of the uppermost doublet is sensitive to the space-exchange component in the ΛN interaction. The $S^{\Delta L}$ on the right are structure factors governing the relative population of states in the (K^-,π^-) reaction with no spin flip ($\Delta L=0$ for the $1/2^-$ states and $\Delta L=2$ for the others).

most doublet in Fig. 10 tends towards [441] symmetry; note the large structure factor for the substitutional $1/2^-$ state reached via $\Delta L=0, \Delta S=0$ from the ^{13}C ground state in the (K^-,π^-) reaction. The excitation energy of this doublet is indeed sensitive to the space-exchange interaction. For example, The NSC97f interaction has repulsion in both singlet- and triplet-odd states leading to a too large separation of ~ 6.9 MeV from the lower $\mathcal{L}=1$ doublet and a separation of ~ 2.2 MeV from the $\mathcal{L}=3$ doublet. On the other hand, the ESC04 model (Rijken and Yamamoto, 2006a) has repulsion in the singlet-odd channel and attraction in the triplet-odd channel giving 6.0 and 1.2 MeV for the two separations. We note that the ^{12}C ground state has a considerable $L=1, S=1$ component that allows various spin-dependent components of the ΛN interaction to contribute to the spacing of the lowest $1/2^-$ and $3/2^-$ states, in contrast to the situation for the $3\alpha+\Lambda$ model (**?**). The tensor interaction and the Λ-Σ coupling both work to put the $1/2^-$ state below the $3/2^-$ state.

The $p^n p_\Lambda$ shell-model calculations were performed (Auerbach *et al.*, 1983) to understand (K^-,π^-) reaction data coming from CERN and BNL. While these calculations have been updated to include Λ-Σ coupling and the use of realistic radial wave functions, they need to be extended to full $1\hbar\omega$ calculations that include an s_Λ coupled to $1\hbar\omega$ states of the core nucleus. These states are mixed with the $p^n p_\Lambda$ states both by the ΛN interaction and by the requirement that the physical $1\hbar\omega$ states be free from spurious center-of-mass components. The need for such calculations is apparent in the extra structure near the p_Λ peak in Fig. 5 and the fact that a number of p-shell hypernuclear γ-rays are seen in $^{9}_{\Lambda}$Be, $^{11}_{\Lambda}$B, and $^{15}_{\Lambda}$N following proton emission from the primary hypernucleus. In the latter case, the $p^{n-1}(sd)s_\Lambda$ component in the wave function gives the proton spectroscopic factor that controls the relative population of states in the daughter hypernucleus.

The Nijmegen baryon-baryon interactions have continued to evolve with a variety of ESC04 (Rijken and Yamamoto, 2006a) and ESC08 (Nagels *et al.*, 2015b; Rijken *et al.*, 2010) models becoming available. The improvements cover many aspects from strangeness 0 to -4 (**?**). As far as p-shell spectra are concerned, it is found that ESC04a and ESC04b do a reasonable job while ESC04c and ESC04d do not (Halderson, 2008). In addition, the tensor interaction is too weak (wrong ordering of the ground-state doublet in $^{16}_{\Lambda}$O) and the ΛN-ΣN coupling potentials have an unusual radial behavior. For the ESC08 models, the strength of the Λ-spin dependent spin-orbit interaction has been reduced with respect to earlier models (Yamamoto *et al.*, 2010) as demanded by the data. However, the ordering of many doublets in the p-shell hypernuclei are inverted because the combination of attractive triplet-even and triplet-odd central interactions makes the triplet interaction stronger than the singlet ($\Delta<0$). As noted in the section on s-shell hypernuclei, all of the models are missing something. In practice, empirical adjustments to the derived G-matrix interactions are made to fit the available data. Of course, these fits also cover for the missing three-body interactions, the effect of which is likely to be mostly on the absolute binding energies and on vector (LS and ALS) interactions in the core nuclei (represented phenomenologically by S_N).

III. WEAK DECAYS OF Λ HYPERNUCLEI

A. Mesonic decays

Λ hypernuclei are unstable to weak decays of the Λ hyperon. In free space, the Λ weak-interaction lifetime $\tau_\Lambda = \hbar/\Gamma^{\rm free}_\Lambda = 2.632\times10^{-10}$ s is dominated (99.7%) by nonleptonic, mesonic two-body decay (Olive *et al.*, 2014):

$$\Lambda \to p + \pi^- + 38\ \text{MeV} \quad (63.9\pm0.5)\% \ , \qquad (18)$$

$$\Lambda \to n + \pi^0 + 41\ \text{MeV} \quad (35.8\pm0.5)\% \ . \qquad (19)$$

The ratio $\Gamma^{\rm free}_{\Lambda\to p+\pi^-}/\Gamma^{\rm free}_{\Lambda\to n+\pi^0}$ for these branches is close to 2, in agreement with the $\Delta I=1/2$ rule (Boyle *et al.*, 2013) which is also satisfied to a level of a few percent by all other known strangeness-changing nonleptonic weak decays, e.g. in kaon decays. In contrast, a purely $\Delta I=3/2$ rule would give a branching ratio 1/2. The effective $\Lambda\to N\pi$ weak decay Lagrangian is written as

$$\mathcal{L}^W_{\Lambda N\pi} = -iG_F m_\pi^2 \bar\psi_N (A + B\gamma_5)\vec\tau\cdot\vec\phi_\pi\psi_\Lambda \ , \qquad (20)$$

where $G_F m_\pi^2 = 2.211 \times 10^{-7}$, and $A = 1.06,\ B = -7.10$ are fixed by the measured free-space Λ decay parameters. The isospin operator $\vec{\tau}$ imposes the $\Delta I = 1/2$ rule once the Λ hyperon is assigned a fictitious isospin state $(I, I_z) = (1/2, -1/2)$. The nonrelativistic approximation to the free Λ decay width yields

$$\Gamma_\alpha^{\rm free} = c_\alpha (G_F m_\pi^2)^2 \int \frac{d^3\mathbf{q}}{(2\pi)^3 2\omega(\mathbf{q})} 2\pi\delta(m_\Lambda - \omega(\mathbf{q}) - E_N) \\ (S^2 + \frac{P^2}{m_\pi^2}\mathbf{q}^2) \ , \qquad (21)$$

where $c_\alpha = 1, 2$ for $\alpha = \Lambda \to n\pi^0,\ \Lambda \to p\pi^-$, respectively, $S = A,\ P/m_\pi = B/(2m_N)$, and E_N and $\omega(\mathbf{q})$ are the total energies of the emitted nucleon and π meson, respectively. This leads to the following expression for the total free-space decay width:

$$\Gamma_\Lambda^{\rm free} = \frac{3}{2\pi}(G_F m_\pi^2)^2 \frac{m_N q_{\rm cm}}{m_\Lambda}(S^2 + \frac{P^2}{m_\pi^2} q_{\rm cm}^2) \ , \qquad (22)$$

with $q_{\rm cm} \approx 100$ MeV/c for the pion momentum in the center of mass frame.

The empirical $\Delta I = 1/2$ rule (Boyle *et al.*, 2013) is not well understood. However here a key question is whether, and to what extent, it is satisfied by *in medium* Λ weak decays. There has been no unambiguous experimetal test of the validity of this rule in hypernuclei. One reason is the difficulty to resolve two-body exclusive decay channels in the continuum, where a combination of several isospin values for the residual nucleus washes out the effect of the primary $\Delta I = 1/2$ weak decay. For example, the total mesonic decay widths of ${}^{4}_{\Lambda}$He given in Table V naively suggest that the $\Delta I = 3/2$ rule holds. However, realizing the dominance of the *two-body* decay ${}^{4}_{\Lambda}\mathrm{He} \to \pi^0 + {}^{4}\mathrm{He}$, and the impossibility of a $\pi^- + {}^{4}$He two-body final state owing to charge conservation, the reversal of the π^-/π^0 ratio from close to 2 in the free-space decay to close to 1/2 in ${}^{4}_{\Lambda}$He decay only reflects the dominance of the ^{4}He ground-state branch. A similar trend is also seen in the π^-/π^0 ratio of ${}^{12}_{\Lambda}$C total mesonic decay widths listed in the table. On the other hand, the π^-/π^0 ratio for ${}^{5}_{\Lambda}$He is close to the free-space ratio, reflecting the difficulty to divert sufficient kinetic energy to break up the ^{4}He core in the quasi-free decays ${}^{5}_{\Lambda}\mathrm{He} \to {}^{4}\mathrm{He} + N + \pi$. The systematics of the π^-/π^0 ratio, owing to the nuclear structure of p-shell Λ hypernuclei, was discussed by Motoba *et al.* (Motoba *et al.*, 1988).

Another reason for the difficulty of testing the $\Delta I = 1/2$ rule in mesonic decays of hypernuclei is the rapid decrease of the pionic decay width $\Gamma_\pi = \Gamma_{\pi^-} + \Gamma_{\pi^0}$ as a function of hypernuclear mass number A. This is shown in Table V where some of the latest determinations of π^- decay widths in hypernuclei for $A \geq 11$ are listed (Sato *et al.*, 2005). The pionic decay widths fall off from about 0.9 $\Gamma_\Lambda^{\rm free}$ in ${}^{4}_{\Lambda}$He to few percent in ${}_{\Lambda}$Fe. This had been anticipated from the low momentum $q \approx 100$ MeV/c, $q < p_F$, of the nucleon recoil in the pionic decay and was indeed confirmed quantitatively by detailed calculations

TABLE V Measured total pionic decay widths of selected hypernuclei in units of $\Gamma_\Lambda^{\rm free}$.

${}^{A}_{\Lambda}$Z	Γ_{π^-}	Γ_{π^0}	Reference
${}^{4}_{\Lambda}$He	0.289 ± 0.039	0.604 ± 0.073	[a]
${}^{5}_{\Lambda}$He	0.340 ± 0.016	0.201 ± 0.011	[b]
${}^{12}_{\Lambda}$C	0.123 ± 0.015	0.165 ± 0.008	[c]
${}^{28}_{\Lambda}$Si	0.046 ± 0.011	–	[d]
${}_{\Lambda}$Fe	≤ 0.015 (90% CL)	–	[d]

[a] (Parker *et al.*, 2007)
[b] (Kameoka *et al.*, 2005; Okada *et al.*, 2005)
[c] (Okada *et al.*, 2005)
[d] (Sato *et al.*, 2005)

of mesonic decay of Λ hypernuclei. Equation (21) for the free-space decay width is replaced in hypernuclei by

$$\Gamma_\alpha = c_\alpha (G_F m_\pi^2)^2 \textstyle\sum_f \int \frac{d^3\mathbf{q}}{(2\pi)^3 2\omega(\mathbf{q})} 2\pi\delta(E_\Lambda - \omega(\mathbf{q}) - E_N^f) \\ (S^2 \mid \int d^3\mathbf{r}\phi_\Lambda(\mathbf{r})\phi_\pi(\mathbf{r};\mathbf{q})\phi_f^*(\mathbf{r}) \mid^2 + \\ \tfrac{P^2}{m_\pi^2} \mid \int d^3\mathbf{r}\phi_\Lambda(\mathbf{r})\vec{\nabla}\phi_\pi(\mathbf{r};\mathbf{q})\phi_f^*(\mathbf{r}) \mid^2) \ , \qquad (23)$$

where the sum extends over the unoccupied nucleon states f, and the pion wavefunction $\phi_\pi(\mathbf{r};\mathbf{q})$ solves the Klein Gordon equation in the presence of a pion-nuclear optical potential $V_{\rm opt}$:

$$[\nabla^2 - m_\pi^2 - 2\omega(\mathbf{q})V_{\rm opt}(\mathbf{r}) + (\omega - V_c(\mathbf{r}))^2]\phi_\pi(\mathbf{r};\mathbf{q}) = 0 \ . \qquad (24)$$

The free-space Eq. (21) is recovered from Eq. (23) by extending the sum over occupied nucleon states as well, neglecting the pion-nuclear final-state interaction, *i.e.* $\phi_\pi^{\rm free}(\mathbf{r};\mathbf{q}) = \exp(i\mathbf{q}_{\rm cm}\cdot\mathbf{r})$, and using closure. The reduction of the mesonic decay width in hypernuclei by several orders of magnitudes as A increases is due to limiting the sum to unoccupied nucleon states. In realistic calculations, however, the final-state nuclear interaction of the emitted pion plays a significant role, providing *enhancement* of the decay rate in heavy hypernuclei by one to two orders of magnitude over what a PWIA calculation (using $\phi_\pi^{\rm free}(\mathbf{r};\mathbf{q})$) would give (Itonaga *et al.*, 1988; Motoba and Itonaga, 1994; Nieves and Oset, 1993; Oset and Salcedo, 1985).

A weak π^+ decay branch with width of order 0.02 $\Gamma_\Lambda^{\rm free}$ was observed in the decay of ${}^{4}_{\Lambda}$He in emulsion studies (Bohm *et al.*, 1969) and in helium bubble chambers (Fetkovich *et al.*, 1972). Weaker evidence exists for π^+ decay of ${}^{7}_{\Lambda}$Be observed in emulsion. The π^+ *rare* branch was initially studied theoretically by Dalitz and von Hippel (Dalitz and von Hippel, 1964; von Hippel, 1964) who observed that it required an intermediate strong-interaction step to occur through, e.g. (i) $\Lambda \to n + \pi^0$ followed by (π^0, π^+) charge exchange in the final state, or (ii) $\Lambda p \to \Sigma^+ n$, in order to generate a virtual Σ^+ component in the initial Λ hypernuclear wavefunction followed by $\Sigma^+ \to n + \pi^+$. The pion charge-exchange mechanism was recalculated in Ref. (Cieplý and Gal, 1997) where its rate was found larger than in the original calculation

TABLE VI Hypernuclear spin assignments provided by pionic weak decay studies.

${}^{A}_{\Lambda}$Z	J^π	Decay branch	Theory	Experiment
${}^{3}_{\Lambda}$H	$\frac{1}{2}^+$	$\pi^-+{}^3$He	[a]	[b]
${}^{4}_{\Lambda}$H	0^+	$\pi^-+{}^4$He	[a]	[c]
${}^{4}_{\Lambda}$He	0^+	π^0+ all	[a]	[d]
${}^{7}_{\Lambda}$Li	$\frac{1}{2}^+$	$\pi^-+{}^7$Be*(429 keV)	[e]	[f]
${}^{8}_{\Lambda}$Li	1^-	$\pi^-+{}^4$He $+{}^4$He	[g]	[h]
${}^{11}_{\Lambda}$B	$\frac{5}{2}^+$	$\pi^-+{}^{11}$C*(6.48 MeV)	[i]	[j]
${}^{12}_{\Lambda}$B	1^-	$\pi^-+{}^4$He $+{}^4$He $+{}^4$He	[k]	[l]
${}^{15}_{\Lambda}$N	$\frac{3}{2}^+$	$\pi^-+{}^{15}$O$_{\rm g.s.}$	[m]	[n]

[a](Dalitz and Liu, 1959)
[b](Ammar *et al.*, 1962; Bertrand *et al.*, 1970; Block *et al.*, 1964)
[c](Ammar *et al.*, 1961; Bertrand *et al.*, 1970; Block *et al.*, 1962, 1964)
[d](Block *et al.*, 1964; Fetkovich *et al.*, 1972)
[e](Motoba *et al.*, 1988; Motoba and Itonaga, 1994)
[f](Sasao *et al.*, 2004)
[g](Dalitz, 1963a)
[h](Davis *et al.*, 1963)
[i](Ziemińska, 1975)
[j](Jurič *et al.*, 1973)
[k](Kielczewska *et al.*, 1980; Ziemińska and Dalitz, 1975)
[l](Kielczewska *et al.*, 1975)
[m](Gal, 2009)
[n](Agnello *et al.*, 2009)

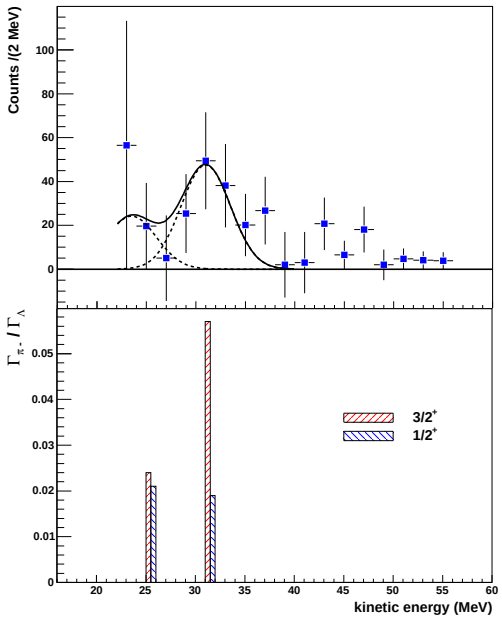

FIG. 11 (color online). Mesonic weak-decay spectrum of ${}^{15}_{\Lambda}$N$\rightarrow \pi^-+{}^{15}$O (upper panel) observed at DAΦNE by the FINUDA Collaboration, compared to calculations (lower panel) for the two possible spin values of the decaying Λ hypernucleus (Gal, 2009) which show preference for a ${}^{15}_{\Lambda}$N g.s. spin $3/2^+$. Figure adapted from (Agnello *et al.*, 2009).

(Dalitz and von Hippel, 1964), but still short by about a factor of two with respect to the observed rate. Gibson and Timmermans (Gibson and Timmermans, 1998) argued that relatively large Σ^+ admixtures were unique to ${}^{4}_{\Lambda}$He and could explain the large π^+ rates observed.

The study of exclusive two-body pionic weak decays of light hypernuclei has yielded valuable information on the ground-state spins of several species, as summarized in Table VI. These pionic weak decays show selectivity to the spin of the hypernuclear ground state owing to the dominance (88%) of the s-wave, parity-violating $\Lambda \rightarrow N\pi$ amplitude (A term in Eq. (20)). This is demonstrated in Fig. 11, taken from a recent FINUDA work (Agnello *et al.*, 2009), showing a π^- weak-decay spectrum for ${}^{15}_{\Lambda}$N, with a preference for a g.s. spin $3/2^+$ for ${}^{15}_{\Lambda}$N (Gal, 2009). In terms of nuclear-core spin J_c values the derived hypernuclear spins J satisfy $J = J_c - \frac{1}{2}$ in the s shell and $p_{\frac{3}{2}}$ subshell, and $J = J_c + \frac{1}{2}$ for ${}^{15}_{\Lambda}$N in the $p_{\frac{1}{2}}$ subshell, all consistent with the ΛN spin-singlet interaction being stronger than the spin-triplet interaction.

B. Nonmesonic decays

Λ hypernuclear total decay widths Γ_Λ are known to remain close to the free-Λ decay width $\Gamma_\Lambda^{\rm free}$, in spite of the rapid decrease as a function of A of the $\Lambda \rightarrow N\pi$ mesonic weak decay (MWD) widths Γ_π, as demonstrated in Table V. A new mode of nonmesonic weak decay (NMWD), predicted by Cheston and Primakoff in 1953 (Cheston and Primakoff, 1953), emerges upon increasing A through the absorption of a weak-decay, virtual pion on one or more nucleons, as illustrated in Fig. 12. Other weak-decay virtual mesons may also mediate these NMWD modes. Historically, Karplus and Ruderman in 1956 (Karplus and Ruderman, 1956) used the observed rates of the nonmesonic weak decay of Λ hypernuclei to argue that the spin of the Λ hyperon was consistent with $J_\Lambda = 1/2$, and that there was no need to ascribe the relatively long lifetimes of strangeness weak decays to an exceptionally large value of J_Λ.

The dominant NMWD modes are believed to involve one nucleon in the initial state:

$$\Lambda + p \rightarrow n + p + 176 \text{ MeV} \quad (\Gamma_p) \ , \tag{25}$$

$$\Lambda + n \rightarrow n + n + 176 \text{ MeV} \quad (\Gamma_n) \ , \tag{26}$$

having a summed width $\Gamma_1 = \Gamma_p + \Gamma_n$. Two-nucleon (2N) modes are also possible (Alberico *et al.*, 1991),

$$\Lambda + N + N \rightarrow n + N + N + 176 \text{ MeV} \quad (\Gamma_2) \ . \tag{27}$$

A conservative estimate given by Alberico *et al.* (Alberico *et al.*, 1991) for these decays is $\Gamma_2/\Gamma_1 \sim 0.2$. The total hypernuclear weak-decay width, $\Gamma_\Lambda = \Gamma_\pi + \Gamma_{\rm nm}$, is a sum of the MWD width Γ_π and the NMWD width, denoted by $\Gamma_{\rm nm} = \Gamma_1 + \Gamma_2 + \cdots$. The dots stand for more involved multinucleon decay modes. Very little is

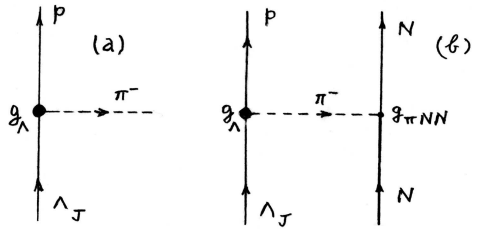

FIG. 12 Graph (a) is for mesonic $\Lambda_J \to p\pi^-$ decay, where Λ_J denotes a Λ hyperon of total spin J. Graph (b) depicts nonmesonic de-excitation for a Λ_J hyperon in nuclear matter. Figure drawn by R.H. Dalitz (Dalitz, 2005).

known about multinucleon decay modes beyond the two-nucleon mode as most experimental and theoretical studies of Λ hypernuclear weak decay have focused on the one-nucleon modes, Eqs. (25,26). The branching ratio of the 2N NMWD contribution to the total ${}^{12}_{\Lambda}$C NMWD width has been determined in KEK (Kim *et al.*, 2009) and in DAϕNE (Agnello *et al.*, 2011b) experiments, with values given by

$$\frac{\Gamma_2}{\Gamma_{\rm nm}} = \quad 0.29 \pm 0.13, \quad 0.21 \pm 0.08\,, \qquad (28)$$

respectively. The latter value was derived from analysis of several NMWD spectra, assuming that this branching ratio is constant in the p shell. The 2N NMWD mode was observed recently through a complete kinematical reconstruction of a three-nucleon final state in two ${}^{7}_{\Lambda}{\rm Li} \to {}^{4}{\rm He} + n + n + p$ decay events at DAΦNE (Agnello *et al.*, 2012), as demonstrated earlier in Fig. **??**.

NMWD dominates the Λ-hypernuclear decay in all but the lightest hypernuclei. This is demonstrated in Fig. 13 where Γ_p, the largest contributor to NMWD, and Γ_{π^-}, the largest contributor to MWD, are shown as a function of A along the p shell as determined by FINUDA and in comparison to various calculations. It is seen clearly that Γ_p rises roughly by a factor of 2, whereas Γ_{π^-} decreases roughly by a factor of 3 from ${}^{5}_{\Lambda}$He to ${}^{15}_{\Lambda}$N, with the ratio Γ_p/Γ_{π^-} reaching a value somewhat larger than 4 at the end of the p shell. NMWD is the only practical way to study the four-fermion, weak-decay interaction. The relatively large momentum transfer, ≈420 MeV/c in free space, could mean that sub-nucleon degrees of freedom are important, but at the present level of experimental data there seems no advantage to invoke explicitly sub-nucleon models. The status of models that consider direct quark (DQ) processes, in addition to meson exchanges, is summarized in Ref. (Sasaki *et al.*, 2005). DQ models offer a natural theoretical framework for departing from the $\Delta I = 1/2$ rule. However, there is no conclusive evidence so far that this rule is not satisfied in Λ hypernuclear NMWD. The models reviewed here are

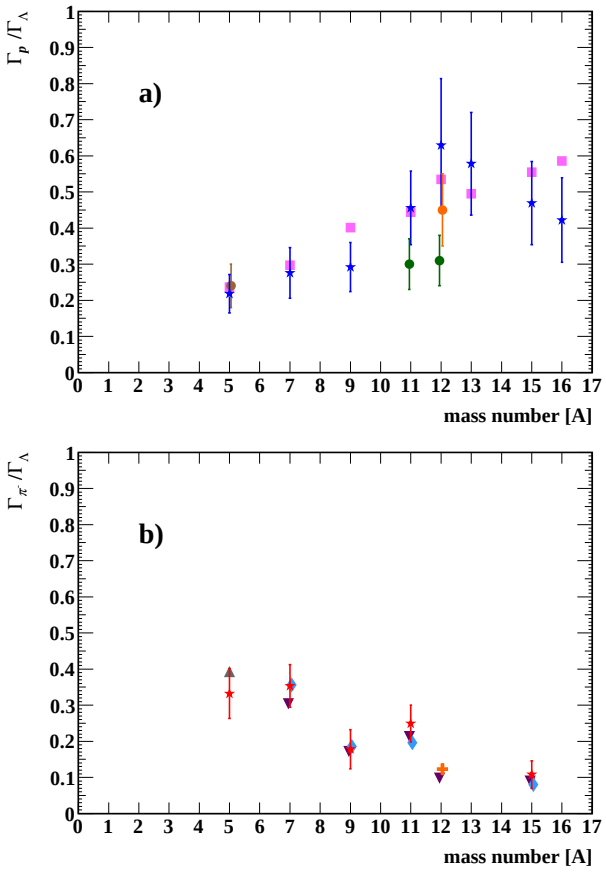

FIG. 13 (Color online). Γ_p (blue stars, upper panel) and Γ_{π^-} (red stars, lower panel), in units of the free Λ decay width, as a function of A from measurements and analysis reported by the FINUDA Collaboration (Agnello *et al.*, 2009, 2014). Other experimental results and theoretical calculations are also marked, see caption to the original Fig. 3 in (Agnello *et al.*, 2014). Courtesy of Elena Botta for the FINUDA Collaboration.

hadronic models that are built upon meson exchanges for which the $\Delta I = 1/2$ rule is assumed to hold. A common approximation is that NMWD occurs dominantly from s-wave ΛN states owing to the short range nature of these decays. The possible $\Lambda + N \to N + N$ transitions are listed in Table VII as taken from (Block and Dalitz, 1963), together with the spin dependence of the corresponding matrix elements. Thus, for capture from ${}^1S_0$ states, parity nonconservation in the weak interactions allows both the parity-conserving (PC) ${}^1S_0 \to {}^1S_0$ as well as the parity-violating (PV) ${}^1S_0 \to {}^3P_0$ transitions. Of the six amplitudes listed, those with a, c, d are PC and those with b, e, f are PV; those with c, d, e, leading to $I = 0$ NN states, are unique to $\Lambda p \to np$ whereas for the a, b, f amplitudes, which lead to $I = 1$ NN states, both nn and np final states are possible with $a_n = \sqrt{2}a_p$, $b_n = \sqrt{2}b_p$, $f_n = \sqrt{2}f_p$ satisfying the $\Delta I = 1/2$ rule.

It is instructive to show the structure of the one-pion-exchange (OPE) transition potential generated by the

TABLE VII $\Lambda + N \to N + N$ amplitudes (Block and Dalitz, 1963). The Pauli spin operator, $\vec{\sigma}_\Lambda$, acts on the initial Λ particle and the final neutron. The final neutron momentum is $\vec{q}/m_N$, and $\vec{Q} \equiv \vec{q}/m_N$.

Transition	Operator	I_{NN}	Rate
$^1S_0 \to {}^1S_0$	$\frac{a}{4}(1 - \vec{\sigma}_\Lambda \cdot \vec{\sigma}_N)$	1	$\mid a \mid^2$
$^1S_0 \to {}^3P_0$	$\frac{b}{8}(\vec{\sigma}_\Lambda - \vec{\sigma}_N) \cdot \vec{Q}\ (1 - \vec{\sigma}_\Lambda \cdot \vec{\sigma}_N)$	1	$\mid b \mid^2 Q^2$
$^3S_1 \to {}^3S_1$	$\frac{c}{4}(3 + \vec{\sigma}_\Lambda \cdot \vec{\sigma}_N)$	0	$\mid c \mid^2$
$^3S_1 \to {}^3D_1$	$\frac{3d}{\sqrt{2}}(\vec{\sigma}_\Lambda \cdot \vec{Q}\ \vec{\sigma}_N \cdot \vec{Q} - \frac{1}{3}\vec{\sigma}_\Lambda \cdot \vec{\sigma}_N\ Q^2)$	0	$\mid d \mid^2 Q^4$
$^3S_1 \to {}^1P_1$	$\frac{e\sqrt{3}}{8}(\vec{\sigma}_\Lambda - \vec{\sigma}_N) \cdot \vec{Q}\ (3 + \vec{\sigma}_\Lambda \cdot \vec{\sigma}_N)$	0	$\mid e \mid^2 Q^2$
$^3S_1 \to {}^3P_1$	$\frac{f\sqrt{6}}{4}(\vec{\sigma}_\Lambda + \vec{\sigma}_N) \cdot \vec{Q}$	1	$\mid f \mid^2 Q^2$

diagram of Fig. 12b. To this end, the weak-interaction Lagrangian Eq. (20) is augmented by a strong-interaction component

$$\mathcal{L}^S_{NN\pi} = -\mathrm{i} g_{NN\pi} \bar{\psi}_N \gamma_5 \vec{\tau} \cdot \vec{\phi}_\pi \psi_N \ , \qquad (29)$$

where $g_{NN\pi} = 13.2$ is the strong-interaction coupling constant. Including the pion propagator between the two vertices given by Eqs. (20) and (29) and applying a non-relativistic reduction, one obtains the OPE momentum-space transition potential

$$V_{\rm OPE}(\vec{q}) = -G_F m_\pi^2 \frac{g_{NN\pi}}{2m_N}(A + \frac{B}{2m_{\rm av}} \vec{\sigma}_\Lambda \cdot \vec{q}) \frac{\vec{\sigma}_N \cdot \vec{q}}{\vec{q}^2 + m_\pi^2} \vec{\tau}_\Lambda \cdot \vec{\tau}_N \ , \qquad (30)$$

where $m_{\rm av} = (m_N + m_\Lambda)/2$. The OPE potential, owing to the sizable momentum transfer involved, is dominated by the tensor component, amplitude d of Table VII. For this amplitude the final NN state has isospin $I = 0$, which is allowed for np but forbidden for nn. Thus, the full OPE transition potential calculations produce a small value for $\Gamma_n/\Gamma_p \leq 0.1$. This is considerably smaller than the range of values, $\Gamma_n/\Gamma_p \sim 0.5$, deduced from old nuclear emulsion work (Montwill *et al.*, 1974) and from the most recent KEK experiments (Kang *et al.*, 2006; Kim *et al.*, 2006), indicating that OPE is insufficient to describe quantitatively NMWD.

In a semiclassical description of the hypernuclear $\Lambda + N \to n + N$ decay, the energy of each one of the two outgoing nucleons should peak at roughly 80 MeV which, assuming equal sharing of the released energy, is about half of the energy available in the decay. A proton-energy spectrum, taken by the FINUDA Collaboration (Agnello *et al.*, 2008) from nonmesonic weak decay of $^5_\Lambda$He produced on thin Li targets, is shown in the upper part of Fig. 14 (circles) in comparison with a proton spectrum taken at KEK (Okada *et al.*, 2004) (triangles). The two spectra were normalized above 35 MeV which is the KEK proton-energy threshold. A peak around 60-90 MeV is clearly observed, with a low-energy rise due to final state interactions (FSI), and perhaps also due to multinucleon induced weak decay. The FINUDA proton spectrum is compared in the lower part of Fig. 14 with the theoretical spectrum calculated by (Garbarino *et al.*, 2004) using an intranuclear cascade (INC) code. The two spectra

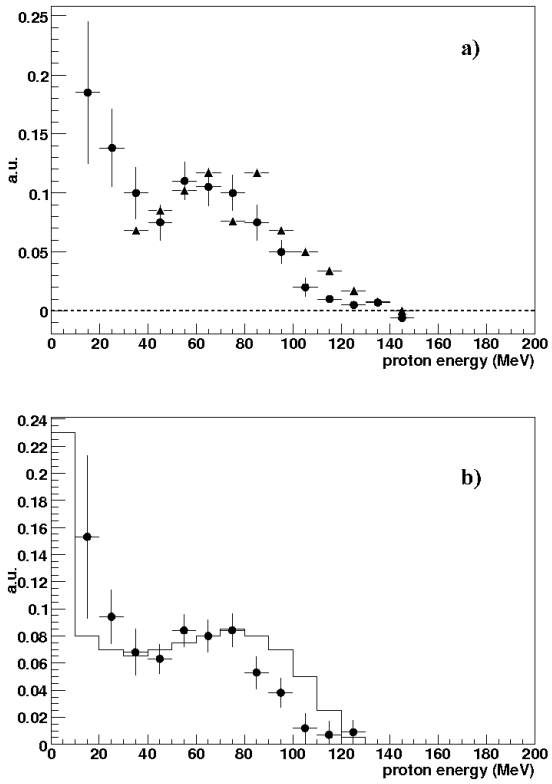

FIG. 14 Upper panel: proton-energy spectrum from $^5_\Lambda$He nonmesonic weak decay measured by FINUDA (circles) and at KEK (triangles). The two spectra were normalized beyond 35 MeV (threshold of the KEK spectrum). Lower panel: comparison between the FINUDA proton-energy spectrum (circles) from the upper panel and the INC calculation (histogram) of (Garbarino *et al.*, 2004). The two spectra were normalized beyond 15 MeV (threshold of the FINUDA spectrum). Figure adapted from (Agnello *et al.*, 2008).

were normalized above 15 MeV which is the FINUDA proton-energy threshold. The agreement between experiment and theory is only qualitative. A more refined methodology to extract NMWD information from the FINUDA measured proton spectra has been presented recently by (Agnello *et al.*, 2014). Neutron-energy spectra were reported by the KEK-PS Experiments 462/508 (Okada *et al.*, 2004), with a shape similar to that of the proton spectrum shown here, and with a similar rise at low energies. We note that the proton and neutron yields, N_p and N_n respectively, when properly normalized are related to the one-nucleon widths by

$$N_p = \Gamma_p \ , \qquad N_n = \Gamma_p + 2\Gamma_n \ . \qquad (31)$$

These expressions disregard FSI and multinucleon stimulated decays.

In the KEK experiments, the number of np pairs, N_{np}, and nn pairs, N_{nn}, corresponding to back-to-back final-state kinematics were identified and determined. Assum-

TABLE VIII Measured and calculated NMWD widths and related entities for selected hypernuclei in units of $\Gamma_\Lambda^{\rm free}$.

Entity	Method	${}^{5}_{\Lambda}$He	${}^{12}_{\Lambda}$C
Γ_n/Γ_p	Emulsion ($_\Lambda$B, $_\Lambda$C, $_\Lambda$N) (Montwill *et al.*, 1974)		0.59 ± 0.15
	KEK-E462/E508 (Kang *et al.*, 2006) (Kim *et al.*, 2006)	$0.45 \pm 0.11 \pm 0.03$	$0.51 \pm 0.13 \pm 0.05$
	OME+$2\pi + 2\pi/\sigma$ (Chumillas *et al.*, 2007)	0.415	0.366
	OME+$2\pi/\sigma + a_1$ (Itonaga and Motoba, 2010; Itonaga *et al.*, 2008)	0.508	0.418
Γ_{nm}	KEK-E462/E508 (Okada *et al.*, 2005)	0.406 ± 0.020	0.953 ± 0.032
	OME+$2\pi + 2\pi/\sigma$ (Chumillas *et al.*, 2007)	0.388	0.722
	OME+$2\pi/\sigma + a_1$ (Itonaga and Motoba, 2010; Itonaga *et al.*, 2008)	0.358	0.758
Γ_Λ	KEK-E462/E508 (Kameoka *et al.*, 2005)	0.947 ± 0.038	1.242 ± 0.042
a_Λ	KEK-E462/E508 (Maruta *et al.*, 2007)	$0.07 \pm 0.08 + 0.08$	$-0.16 \pm 0.28 + 0.18$
	OME (Chumillas *et al.*, 2007, 2008)	-0.590	-0.698
	with final-state interactions	-0.401	-0.340
	OME+$2\pi + 2\pi/\sigma$ (Chumillas *et al.*, 2007, 2008)	$+0.041$	-0.207
	with final-state interactions	$+0.028$	-0.126
	OME+$2\pi/\sigma + a_1$ (Itonaga and Motoba, 2010; Itonaga *et al.*, 2008)	$+0.083$	$+0.044$

ing that FSI has a negligible effect on the ratio N_{nn}/N_{np}, the ratio Γ_n/Γ_p was approximated by N_{nn}/N_{np} and the reported values for ${}^{5}_{\Lambda}$He and ${}^{12}_{\Lambda}$C are listed in Table VIII. For ${}^{12}_{\Lambda}$C the KEK result agrees within error bars with the old emulsion value. A recent re-evaluation of the KEK spectra by (Bauer *et al.*, 2010), accounting also for FSI, leads to a value of $\Gamma_n/\Gamma_p = 0.66 \pm 0.24$, in agreement with the emulsion and KEK values cited in the table. Previous determinations of Γ_n/Γ_p from single-nucleon spectra gave considerably higher values, often in the range $1-2$, but are understood at present to have been subject to strong and unaccounted for FSI effects. This caveat refers, in principle, also to the value cited in the table from emulsion work, which was obtained by matching the experimentally observed fast ($T_p > 30$ MeV) proton spectrum with appropriately weighted spectra from Monte-Carlo INC simulations of both proton and neutron FSI processes (recall that neutrons are not observed directly in emulsion). However, the emulsion estimate of Γ_n/Γ_p appears to agree with the result of the more refined KEK analysis. Finally, two recent calculations using one-meson exchanges (OME) beyond OPE are listed in the table (Chumillas *et al.*, 2007; Itonaga *et al.*, 2008). These calculations reproduce satisfactorily the Γ_n/Γ_p values deduced from the experiments listed in the table. They include also two-pion exchange processes, with or without coupling the ΛN system to ΣN, plus the two-pion $(J^\pi, I)=(0^+, 0)$ resonance known as σ and the axial vector meson a_1 considered as a $\rho - \pi$ resonance. The addition of σ and a_1 exchanges does not effectively change the Γ_n/Γ_p ratio, but proves to be significant in the calculation of the Λ asymmetry parameter as discussed below. Earlier calculations by (Jido *et al.*, 2001), using a chiral-interaction EFT approach, gave a very similar result, $\Gamma_n/\Gamma_p = 0.53$ in ${}^{12}_{\Lambda}$C.

Shown also in Table VIII are experimentally deduced, as well as calculated values of the total NMWD width Γ_{nm} for ${}^{5}_{\Lambda}$He and ${}^{12}_{\Lambda}$C. The deduced NMWD width more than doubles between ${}^{5}_{\Lambda}$He and ${}^{12}_{\Lambda}$C and is already close to saturation for $A = 12$. Both calculations reproduce well the deduced NMWD width in ${}^{5}_{\Lambda}$He, but fall short of it in ${}^{12}_{\Lambda}$C, perhaps due to the increased role of the 2N branch which was not included in the calculation. However, earlier calculations using the same exchanges, but with somewhat different couplings and with different prescriptions for the short-range behavior of the OME exchanges, were able to produce values $\Gamma_{\rm nm}({}^{12}_{\Lambda}{\rm C}) \sim (1.0-1.2)\,\Gamma_\Lambda^{\rm free}$ (Barbero *et al.*, 2003; Itonaga *et al.*, 2002). On the other hand, a more recent calculation by (Bauer and Garbarino, 2010), considering g.s. short-range correlations and including consistently a 2N branch, $\Gamma_2/\Gamma_{\rm nm} = 0.26$, obtained a value $\Gamma_{\rm nm} = 0.98\,\Gamma_\Lambda^{\rm free}$, in very good agreement with the KEK deduced NMWD width. The saturation of the NMWD width for large values of A is demonstrated in Table II where *total* hypernuclear decay lifetimes measured to better than 10% accuracy are displayed. Recall from Table V that for $A = 56$ the mesonic decay width is no more than few percent of the nonmesonic width, hence the total width (lifetime) agrees to this accuracy with the nonmesonic width (lifetime).

In the $\Lambda + N \to n + N$ two-body reactions, each of the final-state nucleons receives a momentum (energy) of order 400 MeV/c (80 MeV), which is well above the Fermi momentum (energy). This large value of momentum transfer justifies the use of semiclassical estimates for inclusive observables, such as the total nonmesonic decay rate of Λ hypernuclei. Denoting a spin-isospin properly averaged nonmesonic decay width on a bound nucleon in nuclear-matter by $\bar{\Gamma}_\Lambda$, the total hypernuclear rate is given in the local density approximation by

$$\frac{\bar{\Gamma}_\Lambda}{\rho_0} \int \rho_\Lambda(r)\rho_N(r){\rm d}^3r, \qquad (32)$$

where $\rho_\Lambda(r)$ and $\rho_N(r)$ are the Λ and the nucleon densities, normalized to 1 and to A, respectively, ρ_0 denotes nuclear-matter density, and zero range was implicitly assumed for the $\Lambda+N \to n+N$ amplitudes. Approximating the nucleon density $\rho_N(r) \approx \rho_0$ over the range of variation of $\rho_\Lambda(r)$ which is of a shorter range than $\rho_N(r)$,

Eq. (32) reduces to $\bar{\Gamma}_\Lambda$, independently of A. For nuclei with $N \neq Z$, the limiting value $\bar{\Gamma}_\Lambda$ is replaced by

$$\bar{\Gamma}^0_\Lambda + \bar{\Gamma}^1_\Lambda \ \frac{N-Z}{A} = \Gamma_n \frac{N}{A} + \Gamma_p \frac{Z}{A} \ , \qquad (33)$$

where $\bar{\Gamma}^0_\Lambda = (\Gamma_n + \Gamma_p)/2$ and $\bar{\Gamma}^1_\Lambda = (\Gamma_n - \Gamma_p)/2$. Eq. (33) provides the leading term in a systematic expansion in powers of the neutron excess parameter $(N-Z)/A$. Finally, accepting that mesonic partial decay widths become negligible in medium- and heavier-weight hypernuclei, and the total decay widths are essentially given by the nonmesonic decay widths, the total nonmesonic decay rate is expected to saturate in heavy hypernuclei, as was demonstrated in Table II.

The last item in Table VIII concerns the Λ intrinsic asymmetry parameter a_Λ in the nonmesonic weak decay Eq. (25) of polarized Λ hypernuclei. The angular distribution of the decay protons is given by

$$W(\theta) = W_0(1 + a_\Lambda \mathcal{P}_\Lambda \cos\theta) \ . \qquad (34)$$

In Eq. (34) $\mathcal{P}_\Lambda$ is the polarization of the Λ spin in the decaying hypernucleus (as produced, e.g. in (π^+, K^+) reactions) and θ is the emission angle of the protons with respect to the polarization axis. The asymmetry arises from the interference between PC and the PV weak-decay amplitudes. The values of a_Λ deduced from experiment and listed in the table are close to zero, in strong disagreement with OME calculations, *e.g.* (Parreño and Ramos, 2001; Parreño *et al.*, 1997). A more recent representative example for such calculations is shown in Table VIII. This long-standing problem was recently resolved with the introduction of a scalar-isoscalar $(0^+, 0)$ exchange which reduces the size of the negative and large asymmetry parameter produced in the OME calculations (Barbero and Mariano, 2006; Sasaki *et al.*, 2005). These studies were motivated by the effective-field-theory (EFT) approach adopted by (Parreño *et al.*, 2004, 2005) where the largest contact term necessary for fitting the weak-decay rates and asymmetries was found to be spin- and isospin-independent; see also the review by (Parreño, 2007). A careful consideration of scalar-isoscalar two-pion exchange, in terms of a dynamically generated σ resonance plus uncorrelated pion exchanges, was shown to resolve the a_Λ puzzle, as listed in Table VIII, without spoiling the agreement with experimental values of $\Gamma_{\rm nm}$ and Γ_n/Γ_p (Chumillas *et al.*, 2007). In contrast, Itonaga *et al.* (Itonaga and Motoba, 2010; Itonaga *et al.*, 2008), using perhaps a less microscopic version of σ-meson degrees of freedom, have claimed that a satisfactory resolution of the a_Λ puzzle requires a consideration of the axial-vector a_1, the chiral partner of the ρ meson, in terms of $\rho - \pi$ and $\sigma - \pi$ correlated exchanges. Their results are also listed in Table VIII. A similarly small and positive value for ${}^{12}_{\Lambda}$C, $a_\Lambda = 0.069$, has also been calculated recently by (Bauer *et al.*, 2012).

IV. Ξ HYPERNUCLEI

The two-body reaction $K^- p \to K^+ \Xi^-$ is the primary method used to produce double strangeness in nuclei. The forward-angle cross section of this reaction peaks for incident K^- momentum around $p_{\rm lab} = 1.8$ GeV/c, with a value close to 50 μb/sr. The usefulness of the *nuclear* (K^-, K^+) reaction in producing Ξ hypernuclei was discussed by Dover and Gal (Dover and Gal, 1983). Missing-mass spectra on ^{12}C from experiments done at KEK (Fukuda *et al.*, 1998) and at BNL (Khaustov *et al.*, 2000a). No conclusive experimental evidence for well defined Ξ hypernuclear levels could be determined because of the limited statistics and detector resolution of ≈10 MeV. However, by fitting to the shape and cross-section yield of the spectra in the Ξ-hypernuclear region, an upper limit of approximately 15 MeV attraction was placed on the Ξ hypernuclear potential strength. The formation of $\Lambda\Lambda$ hypernuclei via a direct (K^-, K^+) reaction without intermediate Ξ production is less favorable, requiring two steps, each on a different proton, *e.g.* $K^- p \to \pi^0 \Lambda$ followed by $\pi^0 p \to K^+ \Lambda$ (Baltz *et al.*, 1983). The expected position of the ${}^{12}_{\Lambda\Lambda}$Be ground state is marked by arrows for the BNL E885 experiment. Given the limited statistics, no firm evidence for the production of ${}^{12}_{\Lambda\Lambda}$Be states was claimed.

A different class of experiments is provided by stopping Ξ^- hyperons in matter, giving rise to two Λs via the two-body reaction $\Xi^- p \to \Lambda\Lambda$ which releases only 23 MeV. Double Λ hypernuclei may then be formed in stopped Ξ^- reactions in a nuclear target, after the Ξ^- hyperons are brought to rest from a (K^-, K^+) reaction (Zhu *et al.*, 1991). Calculations by Yamamoto *et al.*, mostly using double-Λ compound nucleus methodology, provide relative formation rates for $\Lambda\Lambda$ hypernuclei (Sano *et al.*, 1992; Yamamoto *et al.*, 1994b, 1992, 1997). Dedicated experiments with stopped Ξ^- hyperons were proposed in order to produce some of the lightest $\Lambda\Lambda$ hypernuclei, ${}^{6}_{\Lambda\Lambda}$He (Zhu *et al.*, 1991), ${}^{4}_{\Lambda\Lambda}$H (Kumagai-Fuse *et al.*, 1995), and ${}^{12}_{\Lambda\Lambda}$B (Yamada and Ikeda, 1997), by searching for a peak in the outgoing neutron spectrum in the two-body reaction

$$\Xi^- \ + \ {}^{A}Z \ \longrightarrow \ {}^{A}_{\Lambda\Lambda}(Z-1) \ + \ n \, . \qquad (35)$$

These proposals motivated the AGS experiment E885 (Khaustov *et al.*, 2000b) which used a diamond target (${}^{\rm nat}$C) to stop the relatively fast Ξ^- hyperons recoiling from the quasi-free peak of the $p(K^-, K^+)\Xi^-$ reaction in the diamond target. Non-negligible decay losses occur during the stopping time of the Ξ^- hyperon, so that a dense target was used to produce, stop, and capture the Ξ^- hyperons. An upper bound of a few percent was established for the production of the ${}^{12}_{\Lambda\Lambda}$Be hypernucleus. Experimental evidence for ${}^{6}_{\Lambda\Lambda}$He (Takahashi *et al.*, 2001) and ${}^{4}_{\Lambda\Lambda}$H (Ahn *et al.*, 2001b) had to await different techniques, although the evidence for the latter species remains controversial (Randeniya and Hungerford, 2007).

The stopped Ξ^- reaction in deuterium, $(\Xi^- d)_{\rm atom} \to$

Hn, was used in AGS experiment E813 to search for the doubly strange H dibaryon, yielding a negative result (Merrill *et al.*, 2001). An earlier search by the KEK E224 collaboration, stopping Ξ^- on a scintillating fiber active carbon target, also yielded a negative result (Ahn *et al.*, 1996). The (K^-, K^+) reaction was also used, on a ^{3}He target, to establish a stringent upper limit on H-dibaryon production (Stotzer *et al.*, 1997). Theoretically, based on recent lattice QCD calculations by two different groups, NPLQCD (**?**) and HALQCD (**?**), and on extrapolation made to the SU(3)-broken hadronic world (**??**), the H dibaryon is unbound with respect to the $\Lambda\Lambda$ threshold, perhaps surviving in some form near the ΞN threshold.

On the positive side, a double-Λ hypernucleus was discovered in light emulsion nuclei by the KEK stopped Ξ^- experiment E176 (Aoki *et al.*, 1991) and was subsequently interpreted as a ${}^{13}_{\Lambda\Lambda}$B hypernucleus (Dover *et al.*, 1991; Yamamoto *et al.*, 1991). This experiment produced several events, each showing a decay into a pair of known single Λ hypernuclei (Aoki *et al.*, 1993, 1995). Two more events were reported by the KEK-E373 collaboration (Ichikawa *et al.*, 2001; Nakazawa *et al.*, 2015), with the latter event claimed to imply a lightly bound $\Xi^- - {}^{14}$N nuclear state. Using these events, one should be able to deduce the properties of the initial Ξ^- *atomic* states. However, the 100 keV resolution common in emulsion work is three orders of magnitude larger than typical values anticipated for the strong-interaction shifts and widths of Ξ^- atomic levels. This provides a major justification for pursuing a program for the measurement of Ξ^- X rays (Batty *et al.*, 1999), in parallel with strong-interaction reactions involving Ξ hyperons.

If the interaction of Ξ hyperons with nuclei is sufficiently attractive to cause binding as has been repeatedly argued since the original work of (Dover and Gal, 1983), then a rich source of spectroscopic information would become available and the properties of the in-medium ΞN interaction could be extracted. Few-body cluster model calculations using the ESC04d model have been reported recently (Hiyama *et al.*, 2008). Bound states of Ξ hypernuclei would also be useful as a gateway to form double Λ hypernuclei (Dover *et al.*, 1994; Ikeda *et al.*, 1994; Millener *et al.*, 1994; Yamamoto *et al.*, 1994a). Finally, a minimum strength of about 15 MeV for $-V_0^\Xi$ is required to realize the exciting possibility of 'strange hadronic matter' (Schaffner-Bielich and Gal, 2000), where protons, neutrons, Λs and Ξs are held together to form a system which is stable against strong-interaction decay.

Representative values of isoscalar, V_0^Ξ, and isovector, V_1^Ξ, Ξ potential depths and width, Γ_Ξ, from G-matrix calculations at nuclear-matter density ($k_F = 1.35$ fm^{-1}) using the Nijmegen extended soft-core models ESC04d and ESC08c, are listed in Table IX. The isovector (Lane) potential V_1^Ξ is defined by Eq. (**??**) where $\mathbf{t}_\Sigma$ is replaced by $\mathbf{t}_\Xi$. The isoscalar potential comes out repulsive in ESC04a,b and attractive in ESC04c,d, whereas it is attractive in all ESC08 versions. The focus in Table IX on attractive Ξ-nucleus isoscalar potentials, $V_0^\Xi < 0$, is motivated by the experimental hints from KEK (Fukuda *et al.*, 1998) and BNL (Khaustov *et al.*, 2000a) mentioned above. Both ESC04d and ESC08c ΞN potentials are attractive in the isospin $I = 0, 1$ ${}^3S_1 - {}^3D_1$ channels, which might lead to ΞN bound states, while the ${}^1S_0$ channels are repulsive. Both models give rise to a positive isovector potential depth V_1^Ξ. The predictions of spin-flavor SU(6) quark models by (Fujiwara *et al.*, 2007a,b) differ in detail, but the overall picture for the isoscalar Ξ-nuclear potential depths is similar, with a slightly attractive isoscalar potential, $V_0^\Xi < 0$, and a positive isovector potential depth, $V_1^\Xi > 0$. In both approaches, however, the $\Xi - \alpha$ system will not bind, but $3N - \Xi$ bound states are predicted depending on the spin-isospin two-body model dependence.

TABLE IX Isoscalar, V_0^Ξ, and isovector, V_1^Ξ, Ξ nuclear-matter potential depths, and widths Γ_Ξ, all in MeV, in recent extended soft core (ESC) Nijmegen potentials, ESC04 (Rijken and Yamamoto, 2006b) and ESC08 (Nagels *et al.*, 2015a).

Potential	V_0^Ξ	V_1^Ξ	Γ_Ξ
ESC04d	-18.7	$+50.9$	11.4
ESC08c	-7.0	$+21.6$	4.5

V. $\Lambda - \Lambda$ HYPERNUCLEI

Until 2001 only three emulsion events had been considered serious candidates for $\Lambda\Lambda$ hypernuclei: ${}^{10}_{\Lambda\Lambda}$Be (Danysz *et al.*, 1963a,b), ${}^{6}_{\Lambda\Lambda}$He (Prowse, 1966) and ${}^{13}_{\Lambda\Lambda}$B (Aoki *et al.*, 1991). The $\Lambda\Lambda$ binding energies deduced from these emulsion events indicated that the $\Lambda\Lambda$ interaction was quite attractive in the ${}^1S_0$ channel (Dalitz *et al.*, 1989; Dover *et al.*, 1991; Yamamoto *et al.*, 1991), with a $\Lambda\Lambda$ excess binding energy $\Delta B_{\Lambda\Lambda} \sim 4.5$ MeV. However, it was realized that the binding energies of ${}^{10}_{\Lambda\Lambda}$Be and ${}^{6}_{\Lambda\Lambda}$He were inconsistent with each other (Bodmer *et al.*, 1984; Wang *et al.*, 1986). Here, the $\Lambda\Lambda$ excess binding energy is defined by

$$\Delta B_{\Lambda\Lambda}({}^{A}_{\Lambda\Lambda}Z) = B_{\Lambda\Lambda}({}^{A}_{\Lambda\Lambda}Z) - 2\overline{B}_\Lambda({}^{(A-1)}_{\Lambda}Z) \ , \qquad (36)$$

where $B_{\Lambda\Lambda}({}^{A}_{\Lambda\Lambda}Z)$ is the $\Lambda\Lambda$ binding energy of the hypernucleus ${}^{A}_{\Lambda\Lambda}Z$ and $\overline{B}_\Lambda({}^{(A-1)}_{\Lambda}Z)$ is the $(2J+1)$-average of B_Λ values for the ${}^{(A-1)}_{\Lambda}Z$ hypernuclear core levels in the g.s. doublet, as appropriate to a spin-zero $(1s_\Lambda)^2$ configuration of the double-Λ hypernucleus ${}^{A}_{\Lambda\Lambda}Z$. The unambiguous observation of ${}^{6}_{\Lambda\Lambda}$He (Takahashi *et al.*, 2001) by the KEK hybrid-emulsion experiment E373 lowered the accepted $\Delta B_{\Lambda\Lambda}$ value substantially from the value deduced from the older, dubious event (Prowse, 1966), down to $\Delta B_{\Lambda\Lambda}({}^{6}_{\Lambda\Lambda}\mathrm{He}) = 0.67 \pm 0.17$ MeV (Ahn *et al.*, 2013). With this new value of $\Delta B_{\Lambda\Lambda}$, it is natural to inquire where the onset of $\Lambda\Lambda$ binding occurs. From the very beginning it was recognized that the $\Lambda\Lambda$ system (Dalitz, 1963b) and the three-body $\Lambda\Lambda N$ system

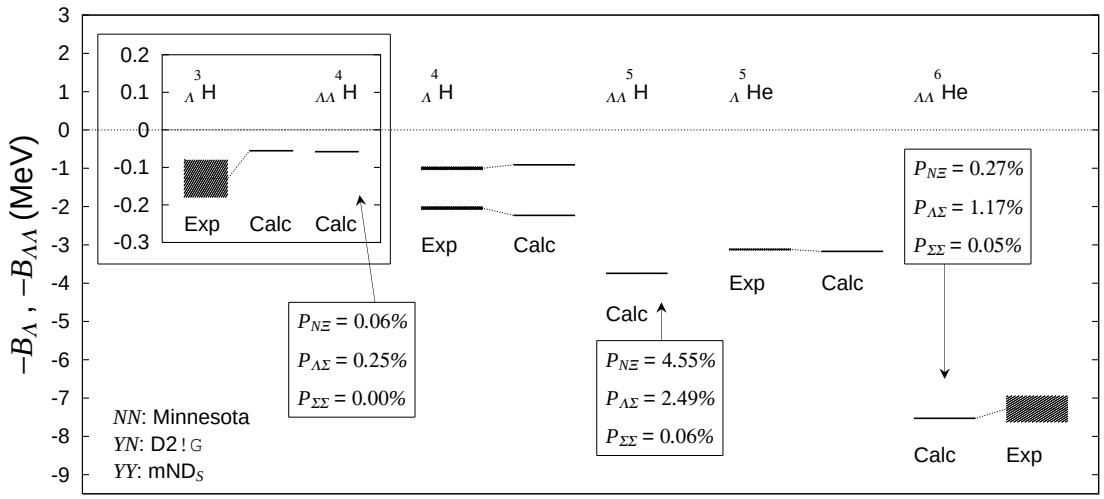

FIG. 15 Calculated Λ and ΛΛ separation energies of s-shell hypernuclei (Nemura *et al.*, 2005).

were unbound (Tang and Herndon, 1965); if $\Lambda\Lambda N$ were bound, the existence of a bound $nn\Lambda$ would follow and $^{6}_{\Lambda\Lambda}$He would most likely become overbound (Gal, 2013a). The existence of a $^{4}_{\Lambda\Lambda}$H bound state was claimed by the AGS experiment E906 (Ahn *et al.*, 2001b), studying correlated weak-decay pions emitted sequentially from ΛΛ hypernuclei apparently produced in a (K^-, K^+) reaction on ^{9}Be, but this interpretation is ambiguous (Randeniya and Hungerford, 2007).

The issue of $^{4}_{\Lambda\Lambda}$H binding was addressed in several subsequent studies. A Faddeev-Yakubovsky (FY) four-body calculation (Filikhin and Gal, 2002b) found no bound state when using an s-wave $V_{\Lambda\Lambda}$ fitted to $B_{\Lambda\Lambda}(^{6}_{\Lambda\Lambda}\mathrm{He})$ and a $V_{\Lambda N}$ partially fitted to $B_\Lambda(^{3}_{\Lambda}\mathrm{H})$. However, when fitting a Λd potential to the low-energy parameters of the s-wave Faddeev calculation for Λpn and solving the s-wave Faddeev equations for a $\Lambda\Lambda d$ model of $^{4}_{\Lambda\Lambda}$H, a 1^+ bound state was obtained. Disregarding spin it can be shown, for essentially an attractive ΛΛ interaction and for a static nuclear core d, that a two-body Λd bound state implies binding for the three-body $\Lambda\Lambda d$ system. Nevertheless, for a *non-static* nuclear core d (made of a pn interacting pair), a Λd bound state does not necessarily imply binding for the $\Lambda\Lambda d$ system.

This $^{4}_{\Lambda\Lambda}$H no-binding conclusion was challenged by (Nemura *et al.*, 2003, 2005) who showed that ΛN-ΣN coupling, which is so important for the quantitative discussion of light Λ hypernuclei, is capable of inducing appreciable ΞN admixures into light ΛΛ hypernuclei via the $\Sigma\Lambda - \Xi N$ coupling. This is shown in Fig. 15 along with all other bound Λ and ΛΛ s-shell hypernuclei. Although in their calculation the second Λ in $^{4}_{\Lambda\Lambda}$H is bound by $0 - 0.07$ MeV, no firm conclusion can be made regarding the particle-stability of this species since in their $^{6}_{\Lambda\Lambda}$He calculation the second Λ is overbound by 0.22 MeV. Thus, the issue of the onset of ΛΛ binding, in particular whether or not $^{4}_{\Lambda\Lambda}$H is particle-stable, is still unresolved.

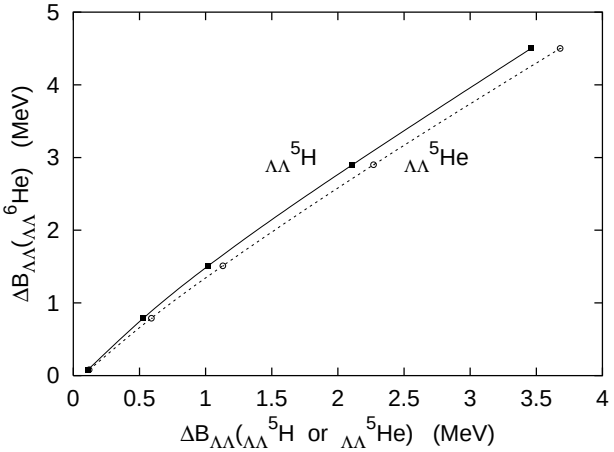

FIG. 16 Faddeev calculations of $\Delta B_{\Lambda\Lambda}$ for $^{6}_{\Lambda\Lambda}$He vs. Faddeev calculations for the mirror ΛΛ hypernuclei $^{5}_{\Lambda\Lambda}$H - $^{5}_{\Lambda\Lambda}$He (Filikhin and Gal, 2002a). The points mark results obtained for various assumptions on $V_{\Lambda\Lambda}$.

Further experimental work is needed to decide whether the events reported in the AGS experiment E906 correspond to $^{4}_{\Lambda\Lambda}$H (Ahn *et al.*, 2001b; Randeniya and Hungerford, 2007), also in view of subsequent conflicting theoretical analyses (Kahana *et al.*, 2003; Kumagai-Fuse and Okabe, 2002).

Regardless of whether $^{4}_{\Lambda\Lambda}$H is particle-stable or not, there is a general consensus that the mirror ΛΛ hypernuclei $^{5}_{\Lambda\Lambda}$H - $^{5}_{\Lambda\Lambda}$He are particle-stable, with $\Delta B_{\Lambda\Lambda} \sim 0.5 - 1$ MeV (Filikhin and Gal, 2002a; Filikhin *et al.*, 2003; Lanskoy and Yamamoto, 2004; Nemura *et al.*, 2005). This is demonstrated in Fig. 16 where calculated $\Delta B_{\Lambda\Lambda}(A = 5)$ values, for several potentials $V_{\Lambda\Lambda}$ with different strengths, are shown to be correlated with calculated $\Delta B_{\Lambda\Lambda}(A = 6)$ values. A minimum value of $\Delta B_{\Lambda\Lambda}(A = 5) \approx 0.1$ is seen to be required for get-

TABLE X $B_{\Lambda\Lambda}$ values (in MeV) from KEK experiments E176 (Aoki *et al.*, 2009) and E373 (Ahn *et al.*, 2013), and as calculated in cluster models (Hiyama *et al.*, 2002, 2010) and in the shell model (Gal and Millener, 2011). $B_{\Lambda\Lambda}({}^{6}_{\Lambda\Lambda}\mathrm{He})$ serves as input in both types of calculations. The E176 entries offer several assignments to the *same* single emulsion event observed.

event	${}^{A}_{\Lambda\Lambda}Z$	$\overline{B}_{\Lambda}({}^{A-1}_{\Lambda}Z)$	$B^{\rm exp}_{\Lambda\Lambda}$	$B^{\rm CM}_{\Lambda\Lambda}$	$B^{\rm SM}_{\Lambda\Lambda}$
E373-Nagara	${}^{6}_{\Lambda\Lambda}$He	3.12 ± 0.02	6.91 ± 0.16	6.91 ± 0.16	6.91 ± 0.16
E373-DemYan	${}^{10}_{\Lambda\Lambda}$Be	6.71 ± 0.04	14.94 ± 0.13	14.74 ± 0.16	14.97 ± 0.22 †
E176-G2	${}^{11}_{\Lambda\Lambda}$Be	8.86 ± 0.11	17.53 ± 0.71	18.23 ± 0.16	18.40 ± 0.28
E373-Hida	${}^{11}_{\Lambda\Lambda}$Be	8.86 ± 0.11	20.83 ± 1.27	18.23 ± 0.16	18.40 ± 0.28
E373-Hida	${}^{12}_{\Lambda\Lambda}$Be	10.02 ± 0.05	22.48 ± 1.21	–	20.72 ± 0.20
E176-E2	${}^{12}_{\Lambda\Lambda}$B	10.09 ± 0.05	20.02 ± 0.78	–	20.85 ± 0.20
E176-E4	${}^{13}_{\Lambda\Lambda}$B	11.27 ± 0.06	23.4 ± 0.7	–	23.21 ± 0.21

† $B^{\rm SM}_{\Lambda\Lambda}({}^{10}_{\Lambda\Lambda}\mathrm{Be}) = 2\,\overline{B}_{\Lambda}({}^{9}_{\Lambda}\mathrm{Be}) + 4\,[\overline{V}({}^{9}_{\Lambda}\mathrm{Be}) - \overline{V}_{\rm average}] + < V_{\Lambda\Lambda} >_{\rm SM}$, see Eq. (38)

ting $\Delta B_{\Lambda\Lambda}(A = 6) > 0$, and for the actual value of $\Delta B_{\Lambda\Lambda}(A = 6) = 0.67 \pm 0.17$ MeV the $A = 5$ $\Lambda\Lambda$ hypernuclei come out safely bound. It was also argued that $\Lambda\Lambda - \Xi N$ coupling is particularly important for the binding of the $A = 5$ $\Lambda\Lambda$ hypernuclei, increasing $\Delta B_{\Lambda\Lambda}$ for these systems above the corresponding value of 1 MeV in ${}^{6}_{\Lambda\Lambda}$He, with the Nijmegen model ESC04d giving as much as 2 MeV (Yamamoto and Rijken, 2008). In addition, substantial charge symmetry breaking effects are expected in these systems, resulting in a higher binding energy of ${}^{5}_{\Lambda\Lambda}$He by up to 0.5 MeV with respect to ${}^{5}_{\Lambda\Lambda}$H (Lanskoy and Yamamoto, 2004; Yamamoto and Rijken, 2008). We note that the Nijmegen soft-core potentials NSC97 (Stoks and Rijken, 1999) and extended soft-core potentials ESC04 (Rijken and Yamamoto, 2006b) provide a quite realistic framework for the relatively weak $\Lambda\Lambda$ interaction. The NSC97 potentials slightly underestimate $\Delta B_{\Lambda\Lambda}({}^{6}_{\Lambda\Lambda}\mathrm{He})$, whereas the ESC04 potentials overestimate it occasionally by about 0.5 MeV and the ESC08 potentials only by up to 0.3 MeV (Yamamoto *et al.*, 2010).

Whereas the assignment of ${}^{6}_{\Lambda\Lambda}$He to the KEK-E373 emulsion event (Takahashi *et al.*, 2001) is unique, because it has no particle-stable excited states to be formed in, and the daughter ${}^{5}_{\Lambda}$He hypernucleus has no particle-stable excited states to be formed in a sequential π^- weak decay, the assignment of other, heavier $\Lambda\Lambda$ hypernuclei to the few emulsion events reported by the KEK-E176 and KEK-E373 experiments is plagued by ambiguities resulting from the presence of particle-stable excited states in which a $\Lambda\Lambda$ hypernucleus may be formed and to which it may weakly decay. In fact, the $B^{\rm exp}_{\Lambda\Lambda}$ value listed in Table X for the KEK-E373 *Demachi-Yanagi* event (Ahn *et al.*, 2001a) assumes that ${}^{10}_{\Lambda\Lambda}$Be was formed in its 2^+ first excited state (Filikhin and Gal, 2002a; Hiyama *et al.*, 2002), whereas the earlier observation of ${}^{10}_{\Lambda\Lambda}$Be (Danysz *et al.*, 1963b) was interpreted as involving the weak decay of ${}^{10}_{\Lambda\Lambda}\mathrm{Be}_{\rm g.s.}$ to the excited doublet levels $(3/2^+, 5/2^+)$ in ${}^{9}_{\Lambda}$Be (Danysz *et al.*, 1963a). The ≈3 MeV unobserved γ-ray de-excitation energy has to be accounted for in each one of these scenarios, and the ≈6 MeV difference between the $B^{\rm exp}_{\Lambda\Lambda}$ values originally claimed for these two events of ${}^{10}_{\Lambda\Lambda}$Be is consistent (6=3+3) with the reinterpretations offered here. Other scenarios, involving production neutrons or decay neutrons which are unobserved in emulsion, have also been considered (Davis, 2005). Similarly, the $B^{\rm exp}_{\Lambda\Lambda}$ value assigned in the table to ${}^{13}_{\Lambda\Lambda}$B also assumes an unobserved γ ray E_γ ≈4.8 MeV from the radiative decay of the excited doublet levels $(3/2^+, 5/2^+)$ in ${}^{13}_{\Lambda}$C formed in the weak decay ${}^{13}_{\Lambda\Lambda}\mathrm{B} \rightarrow {}^{13}_{\Lambda}\mathrm{C}(3/2^+, 5/2^+)$.

Table X provides a comprehensive listing of candidate $\Lambda\Lambda$-hypernuclear emulsion events, along with $\Lambda\Lambda$ binding energy values derived from these events, with caveats explained above for ${}^{10}_{\Lambda\Lambda}$Be and ${}^{13}_{\Lambda\Lambda}$B. The table also lists calculated $\Lambda\Lambda$ binding energies using (i) few-body cluster models (CM) by (Hiyama *et al.*, 2002, 2010), and (ii) shell model evaluations (Gal and Millener, 2011). The table makes it clear that the shell-model (SM) methodology is able to confront any of the reported $\Lambda\Lambda$ species, whereas cluster models have been limited so far to 3-,4- and 5-body calculations. For those $\Lambda\Lambda$ hypernuclei where a comparison between the two models is possible, the calculated binding energies are remarkably close to each other. The SM estimate for $B_{\Lambda\Lambda}$ in the nuclear p shell is given simply by

$$B^{\rm SM}_{\Lambda\Lambda}({}^{A}_{\Lambda\Lambda}Z) = 2\overline{B}_{\Lambda}({}^{A-1}_{\Lambda}Z) + < V_{\Lambda\Lambda} >_{\rm SM}, \qquad (37)$$

where $< V_{\Lambda\Lambda} >_{\rm SM}$ is a $\Lambda\Lambda$ interaction matrix element identified with $\Delta B_{\Lambda\Lambda}({}^{6}_{\Lambda\Lambda}\mathrm{He}) = 0.67 \pm 0.17$ MeV. [In CM calculations (Hiyama *et al.*, 2010), $< V_{\Lambda\Lambda} >_{\rm CM} \equiv B_{\Lambda\Lambda}(V_{\Lambda\Lambda} \neq 0) - B_{\Lambda\Lambda}(V_{\Lambda\Lambda} = 0)$ assumes similar values: 0.54, 0.53 and 056 MeV for ${}^{6}_{\Lambda\Lambda}$He, ${}^{10}_{\Lambda\Lambda}$Be and ${}^{11}_{\Lambda\Lambda}$Be, respectively.] To apply Eq. (37), $\overline{B}_{\Lambda}({}^{A-1}_{\Lambda}Z)$ is derived from the SM calculations outlined in an earlier subsection on p-shell single-Λ hypernuclei. Apart from the spin dependence of the ΛN interaction which is fully constrained by the γ-ray measurements and their SM analyses, the validity of a uniform SM description of hypernuclei throughout the whole p shell depends on the constancy of the ΛN spin-independent matrix element $\overline{V}$ in the mass range considered. Indeed, excluding ${}^{9}_{\Lambda}$Be which deviates substantially from the other species, a common value $\overline{V}^{\rm SM} = -1.06 \pm 0.03$ MeV can be assigned. In ${}^{9}_{\Lambda}$Be the Λ hyperon is attached to a somewhat loose $\alpha - \alpha$ structure, but in ${}^{10}_{\Lambda\Lambda}$Be the second Λ is bound with respect a normal ${}^{5}_{\Lambda}$He–α structure. This suggests to extend

the validity of Eq. (37) also to ${}^{10}_{\Lambda\Lambda}$Be by adding to its r.h.s. a correction term $\delta B^{\rm SM}_{\Lambda\Lambda}$ due to the normally bound second Λ:

$$\delta B^{\rm SM}_{\Lambda\Lambda}({}^{\rm A}_{\Lambda\Lambda}{\rm Z}) = (A-6)\,[\,\overline{V}({}^{\rm A-1}_{\Lambda}{\rm Z}) - \overline{V}^{\rm SM}\,], \qquad (38)$$

where $\Lambda-\Sigma$ contributions $\lesssim 0.1$ MeV were disregarded. Cluster models, on the other hand, are able to treat the ^{8}Be core in terms of $\alpha-\alpha$ loose structure, as well as ${}^{9}_{\Lambda}$Be and ${}^{10}_{\Lambda\Lambda}$Be as $\alpha\alpha n$ and $\alpha\alpha nn$ clusters, respectively, but they encounter difficulties in evaluating consistently spin-dependent ΛN interaction contributions.

Inspection of Table X shows that the binding energies of both ${}^{10}_{\Lambda\Lambda}$Be and ${}^{13}_{\Lambda\Lambda}$B are well reproduced by the shell model, thereby confirming the interpretations of the corresponding emulsion events discussed above. Of the other $\Lambda\Lambda$ hypernuclear candidates, the E373-Hida event (Ahn *et al.*, 2013) does not fit any reasonable assignment as ${}^{11}_{\Lambda\Lambda}$Be or ${}^{12}_{\Lambda\Lambda}$Be. Regarding the species listed in the table as due to E176, they all correspond to different assignments of the *same* event, for which the ${}^{13}_{\Lambda\Lambda}$B assignment is statistically preferable (Aoki *et al.*, 2009).

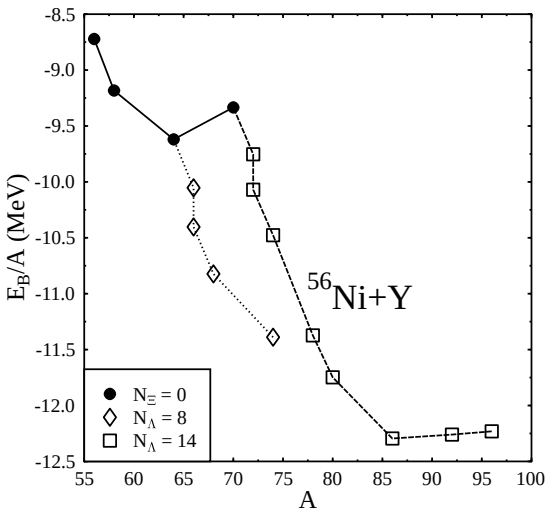

FIG. 17 Calculated binding energy of multistrange nuclei of ^{56}Ni plus Λ and Ξ hyperons, as function of baryon number A. Figure taken from Ref. (Schaffner *et al.*, 1993).

VI. STRANGE DENSE MATTER

A. Strange hadronic matter

Bodmer (Bodmer, 1971), and more specifically Witten (Witten, 1984), suggested that strange quark matter, with roughly equal composition of u, d and s quarks, might provide an absolutely stable form of matter. Metastable strange quark matter was studied by Chin and Kerman (Chin and Kerman, 1984). Jaffe and collaborators (Berger and Jaffe, 1987; Farhi and Jaffe, 1984) subsequently charted the various scenarios possible for the stability of strange quark matter, from absolute stability down to metastability due to weak decays. Finite strange quark systems, so called strangelets, have also been considered (Farhi and Jaffe, 1984; Gilson and Jaffe, 1993).

Less known is the suggestion (Schaffner *et al.*, 1993, 1994) that metastable strange systems with similar properties, i.e. a strangeness fraction $f_S \equiv -S/A \approx 1$ and a charge fraction $f_Q \equiv Z/A \approx 0$, might also exist in hadronic form at moderate values of density, between twice and three times nuclear matter density. These strange systems are made of N, Λ and Ξ baryons. The metastability (i.e. stability with respect to strong interactions, but not to $\Delta S \neq 0$ weak-interaction decays) of these strange hadronic systems was established by extending relativistic mean field (RMF) calculations from ordinary nuclei ($f_S = 0$) to multi-strange nuclei with $f_S \neq 0$. Although the detailed pattern of metastability, as well as the actual values of the binding energy, depend specifically on the partly unknown hyperon potentials in dense matter, the predicted phenomenon of metastability turned out to be robust in these calculations (Balberg *et al.*, 1994). A conservative example is given in Fig. 17, assuming a relatively weak hyperon-hyperon attractive interaction. The figure shows the calculated binding energy of ^{56}Ni + $N_\Lambda\Lambda$ multi-Λ hypernuclei for $N_\Lambda = 0, 2, 8, 14$ and how it becomes energetically favorable to add Ξ hyperons when N_Λ exceeds some fairly small threshold value. As soon as the Λ p-shell is filled, Ξ hyperons may be placed in their s-shell owing to Pauli blocking of the strong-interaction conversion process $\Xi N \to \Lambda\Lambda$ which in free space releases about 25 MeV.

A less conservative example is provided by applying the Nijmegen soft-core model NSC97 (Stoks and Rijken, 1999) which predicts strongly attractive $\Xi\Xi$, $\Sigma\Sigma$ and $\Sigma\Xi$ interactions, but fairly weak $\Lambda\Lambda$ and $N\Xi$ interactions that roughly agree with existing phenomenology. It was found (Schaffner-Bielich and Gal, 2000) that strange hadronic matter (SHM) is comfortably metastable for any allowed value of $f_S > 0$. However for $f_S \geq 1$, Σs replace Λs due to the exceptionally strong $\Sigma\Sigma$ and $\Sigma\Xi$ interactions in this model. A first-order phase transition occurs from $N\Lambda\Xi$ dominated matter for $f_S \leq 1$ to $N\Sigma\Xi$ dominated matter for $f_S \geq 1$, as shown in Fig. 18 where the binding energy is drawn versus the baryon density for several representative fixed values of f_S. At $f_S \approx 1.0$ a secondary minimum at higher baryon density becomes energetically favored. The system then undergoes a first-order phase transition from the low density state to the high density state.

Fig. 19 demonstrates explicitly that the phase transition involves transformation from $N\Lambda\Xi$ dominated matter to $N\Sigma\Xi$ dominated matter, by showing the calculated composition of SHM for this model (denoted N for Ni-

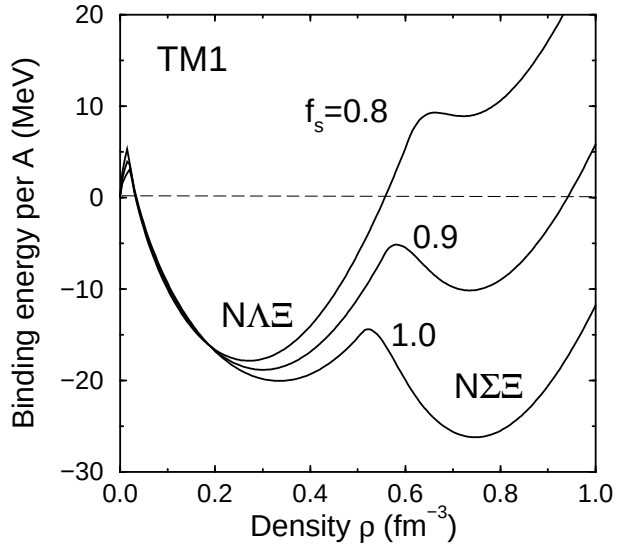

FIG. 18 Transition from $N\Lambda\Xi$ to $N\Sigma\Xi$ matter upon increasing the strangeness fraction f_S (Schaffner-Bielich and Gal, 2000).

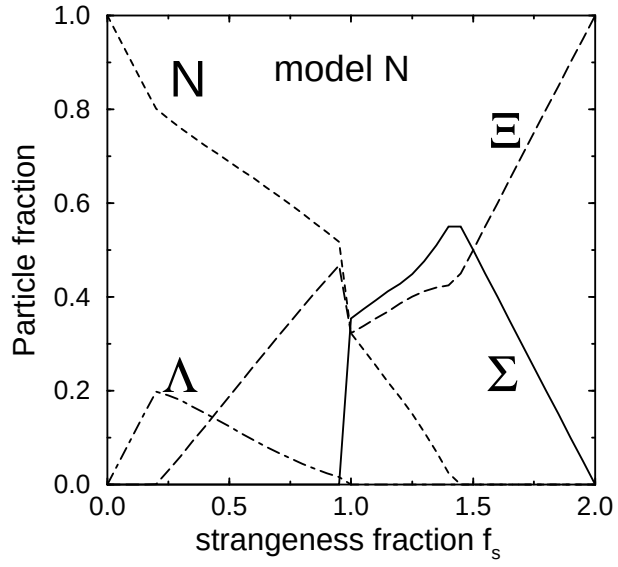

FIG. 19 Strange hadronic matter composition as function of strangeness fraction f_S (Schaffner-Bielich and Gal, 2000).

jmegen) as function of the strangeness fraction f_S. The particle fractions for each baryon species change as function of f_S. At $f_S = 0$, one has pure nuclear matter, whereas at $f_S = 2$ one has pure Ξ matter. In between, matter is composed of baryons as dictated by chemical equilibrium. A change in the particle fraction may occur quite drastically when new particles appear, or existing ones disappear. A sudden change in the composition is seen in Fig. 19 for $f_S = 0.2$ when Ξs (long-dashed line) emerge in the medium, or at $f_S = 1.45$ when nucleons (short-dashed line) disappear. The situation at $f_S = 0.95$ is a special one, as Σs (solid line) appear in the medium, marking the first-order phase transition observed in the previous figure. The baryon composition alters completely at that point, from $N\Xi$ baryons plus a rapidly vanishing fraction of Λs (dot-dashed line) into $\Sigma\Xi$ hyperons plus a decreasing fraction of nucleons. At the very deep minimum of the binding energy curve (not shown here) SHM is composed mainly of Σs and Ξs with a very small admixture of nucleons. The phase transition demonstrated above has been discussed by the Frankfurt group (Schaffner *et al.*, 2002) in the context of a phase transition to hyperon matter in neutron stars. Unfortunately, it will be difficult to devise an experiment to determine the depth of the $\Lambda\Xi$, $\Xi\Xi$, $\Xi\Sigma$, $\Sigma\Sigma$ interaction potentials, which are so crucial to verify these results.

B. Neutron stars

Neutron stars are gravitationally held massive objects in β-equilibrium with radii of about 12 km and masses of about $(1-2)M_\odot$, perhaps up to $2.5M_\odot$. Here $M_\odot$ stands for a solar mass (Leahy *et al.*, 2011). Although their composition at low density is dominated by neutrons, transmutation to hyperons, beginning at 2 to 3 times normal nuclear matter density $\rho_0 = 0.17$ fm^{-3}, would act to alleviate the Pauli pressure of nucleons and leptons. Matter in the core of neutron stars is further compressed to about $(5-6)\rho_0$. At these high densities strange hadronic matter, which may already be self bound at densities $(2-3)\rho_0$, could become stable even to weak decay (Schaffner *et al.*, 2002). Such matter may perhaps form kaon condensates (Kaplan and Nelson, 1986) and even deconfine to quarks (Baym and Chin, 1976), forming strange quark matter. However, it is also possible that a star having a mixed phase of hyperons and quarks in its interior is produced. Because the star rapidly rotates, losing energy via radiation, the rotational inertia of the star changes, and the rotational frequency depends on its composition which is coupled to the rotational frequency. Obviously while more astrophysical observations are needed, the only terrestrial handle on this physics comes from hypernuclei, particularly multi-strange hypernuclei. The physics of neutron stars was reviewed recently by Lattimer (Lattimer, 2012).

It is important to recognize that hypernuclei, and in particular multi-strange hypernuclei which were reviewed in Sect. VI.A, are a low-density manifestation of strange hadronic matter. As such, studies of their interactions at normal nuclear density impact the construction of models of density dependent interactions for use at higher densities. Thus, hyperon potentials in dense matter control the composition of dense neutron star matter, as shown by a recent RMF calculation in Fig. 20. As a function of density, the first hyperon to appear is the lightest one, the Λ at about $2\rho_0$, by converting protons and electrons directly to Λs instead of neutrons, thereby decreasing the neutron Pauli pressure. It is reasonable to assume that this composition varies radially, perhaps having a

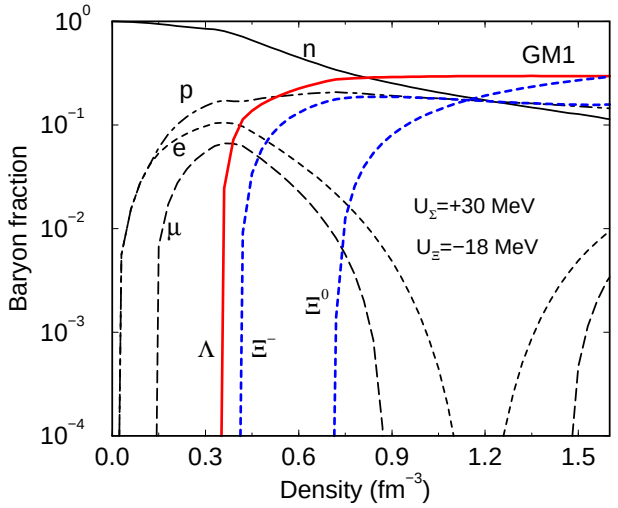

FIG. 20 Neutron star matter fractions of baryons and leptons, calculated as a function of density (Schaffner-Bielich, 2008).

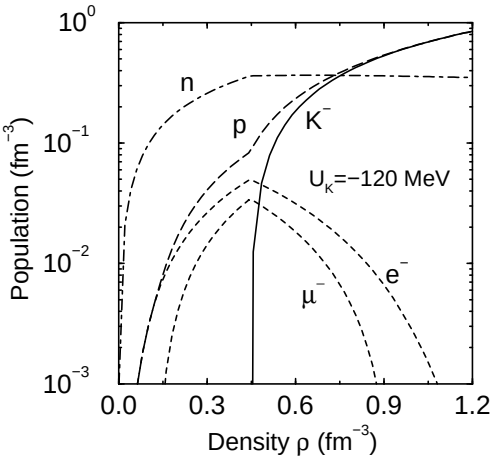

FIG. 21 Population of neutron star matter, allowing for kaon condensation, calculated as a function of nucleon density (Glendenning and Schaffner-Bielich, 1999).

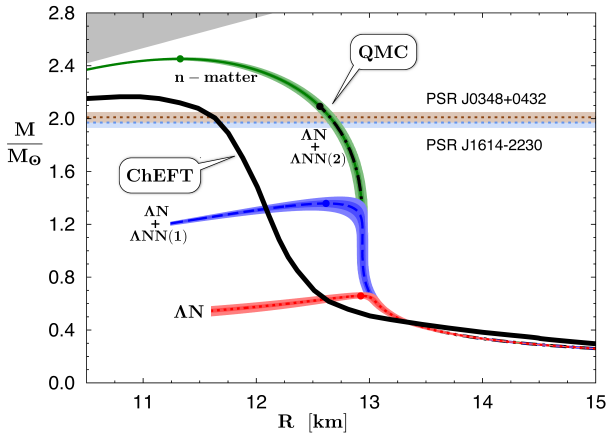

FIG. 22 Mass-radius relationship for various EoS scenarios of neutron stars, including nucleons and leptons only (Hell and Weise, 2014) as well as upon including Λ hyperons (Lonardoni *et al.*, 2015). Figure adapted from (Weise, 2015).

crust and an atmosphere composed of neutrons. Among the negatively charged hyperons the lightest one, Σ^-, does not appear at all over the wide range of densities shown owing to its repulsion in nuclear matter, and most likely also in neutron matter (Balberg and Gal, 1997). Its potential role in reducing the Pauli pressure of the leptons (e^- and μ^-) could be replaced by the heavier Ξ^- hyperon, assuming overall Ξ-nuclear attraction. The specific calculation sketched by Fig. 20 predicts that the hyperon population takes over the nucleon population for densities larger than about $6\rho_0$, where the inner core of a neutron star may be viewed as a giant hypernucleus (Glendenning, 1985).

Negative strangeness may also be injected into neutron star matter by agents other than hyperons. Thus, a robust consequence of the sizable $\bar{K}$-nucleus attraction, as discussed in the next section, is that K^- condensation is expected to occur in neutron stars at a density about $3\rho_0$ in the absence of hyperons, as shown in Fig. 21 for a RMF calculation using a strongly attractive K^- nuclear potential $U_{\bar{K}}(\rho_0) = -120$ MeV. Since it is more favorable to produce kaons in association with protons, the neutron density shown in the figure stays nearly constant once kaons start to condense, while the lepton populations decrease as the K^- meson provides a new neutralizing agent via the weak processes $\ell^- \to K^- + \nu_\ell$. However, including negatively charged hyperons in the equation of state (EoS) of neutron star matter defers K^- condensation to higher densities (Glendenning, 2001; Knorren *et al.*, 1995) where the neutron-star maximum mass $M_{\rm max}$ is lowered by only $\approx 0.01 M_\odot$ below the value reached through the inclusion of hyperons (Knorren *et al.*, 1995).

Given the high matter density expected in a neutron star, a phase transition from ordinary nuclear matter to some exotic mixtures cannot be ruled out. Whether a stable neutron star is composed dominantly of hyperons, quarks, or some mixture thereof, and just how this occurs, is not clear as both the strong and weak interactions, which operate on inherently different time scales, are in play. The EoS of any possible composition constrains the mass-radius ($M-R$) relationship for a rotating neutron star. Thus, the maximum mass $M_{\rm max}$ for a relativistic free neutron gas is given by $M_{\rm max} \approx 0.7 M_\odot$ (Oppenheimer and Volkoff, 1939; Tolman, 1939), whereas higher mass limits are obtained under more realistic EoS assumptions. Without strangeness, but for interacting nucleons (plus leptons) $M_{\rm max}$ comes out invariably above $2M_\odot$, as shown by the curves marked n-matter from Quantum Monte Carlo (QMC) calculations (Lonardoni *et al.*, 2015) and ChEFT (Hell and Weise, 2014) in Fig. 22. $M_{\rm max}$ values of up to $2M_\odot$ are within the reach of hybrid (nuclear plus quark matter) star calculations in

which strangeness materializes via non-hadronic degrees of freedom (Alford *et al.*, 2005). In the hadronic basis, adding hyperons softens the EoS, thereby lowering $M_{\rm max}$ in RMF calculations to the range $(1.4-1.8)M_\odot$ (Glendenning, 2001; Knorren *et al.*, 1995), also if/when a phase transition occurs to SHM (Schaffner *et al.*, 2002). More recent HF and BHF calculations using NSC97, ESC08 and χEFT YN interactions find values of $M_{\rm max}$ lower than $1.4M_\odot$ (Djapo *et al.*, 2010; Schulze *et al.*, 2006; Schulze and Rijken, 2011), while the inclusion of several of the YY interactions from the Nijmegen ESC08 model appears to increase $M_{\rm max}$ by $0.3M_\odot$ to about $1.65M_\odot$ (Rijken and Schulze, 2016).

Until recently, the neutron star mass distribution for radio binary pulsars was given by a narrow Gaussian with mean & width values $(1.35\pm0.04)M_\odot$ (Thorsett and Chakrabarty, 1999), somewhat below the Chandrasekhar limit of $1.4M_\odot$ for white dwarfs, above which these objects become gravitationally unstable. However, there is now some good evidence from X-ray binaries classified as neutron stars for masses about and greater than $2M_\odot$ (Barret *et al.*, 2006). The highest *accepted* value of neutron star mass is provided at present by the precise mass measurements of the pulsars PSR J1614-2230 (Demorest *et al.*, 2010) and PSR J0348+0432 (Antoniadis *et al.*, 2013), marked by horizontal lines in Fig. 22. These yield nearly $2M_\odot$ and thereby exclude several 'soft' EoS scenarios for dense matter (Freire *et al.*, 2009; Lattimer, 2012). The figure demonstrates how the gradual introduction of repulsive ΛNN interactions (Lonardoni *et al.*, 2015), from version 1 to version 2, leads to a corresponding increase of the calculated $M_{\rm max}$ value by increasing the matter density $\rho_{\rm min}$ at which Λ hyperons appear first in neutron-star matter to higher values, until this $\rho_{\rm min}$ exceeds the value $\rho_{\rm max}$ corresponding to $M_{\rm max}$. When this happens, for version 2, the mass-radius dotted curve overlaps with the purely 'n-matter' green curve below the point marked in the figure for the value of $M_{\rm max}$ reached. This scenario in which hyperons are excluded from the EoS of neutron stars exclusively by strongly repulsive YNN forces, thereby resolving the 'hyperon puzzle', requires further study.

In this context, Fig. 23 shows how the introduction of repulsive ΛNN interactions within QMC calculations relieves the over-binding of Λ hypernuclei which arises progressively with increasing the mass number A (corresponding to smaller values of $A^{-2/3}$ in the figure) upon using microsocopically constructed purely two-body ΛN interactions dominated by attraction. In particular, the same version 'ΛN+ΛNN (II)' that according to Fig. 22 resolves the 'hyperon puzzle', also resolves according to Fig. 23 the 'B_Λ over-binding' problem. It is worth noting, however, that the purely two-body ΛN interaction of version 'ΛN' overbinds heavy Λ hypernuclei substantially beyond the ΛN two-body contribution $D_\Lambda^{(2)} \sim 60$ MeV to the Λ-nucleus potential well-depth derived from the A dependence of the (π^+, K^+)-measured Λ binding energies (Millener *et al.*, 1988). This excessive overbinding is then

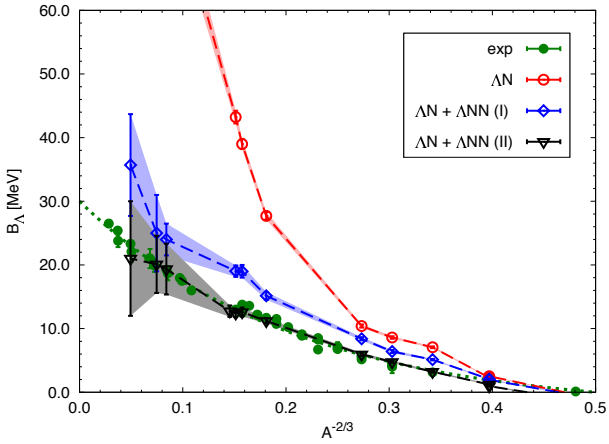

FIG. 23 QMC calculations (Lonardoni *et al.*, 2014) of Λ hypernuclear binding energies for purely two-body ΛN interactions and for two versions of adding repulsive ΛNN interactions. Figure adapted from (Lonardoni *et al.*, 2014).

compensated in (Lonardoni *et al.*, 2014) by a similarly excessive ΛNN repulsion which makes the neutron-star matter EoS as stiff as to exclude hyperons from appearing in neutron-star matter. In other, phenomenological models that introduce softer repulsive ΛNN interactions in a more controlled way, values of $M_{\rm max}$ in the range $(1.6-1.7)M_\odot$ are obtained (Balberg and Gal, 1997; Vidana *et al.*, 2011), short however of resolving the 'hyperon puzzle'. Nevertheless, it is possible to reach values of $M_{\rm max} \geq 2M_\odot$ by introducing in addition to moderately repulsive ΛNN interactions also phenomenological repulsive NNN interactions that have not been tested yet in nuclear structure calculations (Yamamoto *et al.*, 2013, 2014, 2016). Obviously, more work is required in this direction to make sure whether or not the 'hyperon puzzle' is indeed resolved, see (Chatterjee and Vidana, 2015) for a comprehensive review of related works.

VII. $\bar{K}$-NUCLEAR INTERACTIONS AND BOUND STATES

The $\bar{K}N$ interaction near and below threshold is attractive in models which dynamically generate the $\Lambda(1405)$ subthreshold resonance. This motivates a search for K^- quasi-bound states in nuclei (Gal, 2013b; Hyodo, 2013). The $\Lambda(1405)$ was predicted as early as 1959 (Dalitz and Tuan, 1959) by analyzing the available data on the strong interactions of K^- mesons with protons above threshold, and was discovered two years later in the Berkeley hydrogen bubble chamber (Alston *et al.*, 1961) as an $I=0$ $\pi\Sigma$ resonance by studying the reaction $K^-p \to \Sigma+3\pi$ for several charge states. The proximity of this $\pi\Sigma$ resonance to the $\bar{K}N$ threshold, at 1432 MeV for K^-p, suggested that it can be dynamically generated by $\bar{K}N-\pi\Sigma$ inter-hadron forces. This was subsequently shown (Dalitz *et al.*, 1967) to be possible within a dynamical model of SU(3)-octet vector-meson exchange. The

model provides a concrete physical mechanism for the Tomozawa-Weinberg leading term in the chiral expansion of the meson-baryon Lagrangian (Tomozawa, 1966; Weinberg, 1966).

A next-to-leading-order (NLO) chiral-model calculation of the K^-p center-of-mass (cm) scattering amplitude f_{K^-p} is shown in Fig. 24. This NLO amplitude agrees qualitatively with leading-order K^-p amplitudes derived in the mid 1990s, *e.g.* (Kaiser *et al.*, 1995; Oset and Ramos, 1998), the main quantitative improvement arising from the threshold value constraint provided by the SIDDHARTA measurement of kaonic hydrogen $1s$ level shift and width (Bazzi *et al.*, 2011, 2012). The large positive values of Re f_{K^-p}, which exceed 1 fm in the subthreshold region, indicate a strong attraction. Although all NLO models agree above threshold, because of fitting to the same K^-N low-energy scattering and reaction data, a nonnegligible model dependence below threshold can be deduced by comparing to other NLO chiral calculations, *e.g.* (Guo and Oller, 2013). However, it is the subthreshold region that is needed in bound state calculations, which is also true for kaonic atoms where the kaon energy is essentially at threshold (Gal *et al.*, 2014). Fortunately, the two K^-N scattering amplitudes used in the most recent atomic and nuclear quasi-bound state calculations, IHW (Ikeda *et al.*, 2011, 2012) of Fig. 24 and NLO30 (Cieplý and Smejkal, 2012) shown in a later figure, are also similar in the subthreshold region despite the different methodologies involved in their derivations.

The lightest $\bar{K}$-nuclear quasi-bound state is expected to be K^-pp. Such a $\bar{K}NN$ state would have isospin $I = \frac{1}{2}$ and spin-parity $J^\pi = 0^-$, dominated by $I_{NN} = 1$ and s waves. A representative compilation of recent few-body calculations of this system is given in Table XI. These calculations suggest robust binding for K^-pp, but the calculated widths are all large (of order 50 MeV). The table shows that chiral-model calculations using energy dependent $\bar{K}N$ interactions give weaker binding than those calculated when disregarding the energy dependence away from the $\bar{K}N$ threshold. Since the K^-pp quasi-bound state may be regarded as $\Lambda(1405)N$ bound state (Uchino *et al.*, 2011), this difference partly reflects the higher $\Lambda(1405)$ mass obtained in chiral models (see caption to Fig. 24 for the $\Lambda(1405)$ pole position in that calculation).

While several experiments have suggested evidence for a K^-pp quasi-bound state with somewhat conflicting binding energy, there seems to be no consensus on this matter and it awaits further experimentation. A brief listing of past searches, culminating with two ongoing J-PARC experiments, is deferred to Sect. VIII.G. Here we only show in Fig. 25 a missing-mass spectrum is shown for the $d(\pi^+, K^+)$ reaction at 1.69 GeV/c taken at J-PARC (Ichikawa *et al.*, 2014). The main features of this spectrum are the quasi-free Λ, Σ and Y^* components. The latter rests on a broad phase-space structure. As for dynamical structures aside from the expected ΣN cusp structure around 2.13 GeV/c^2, one observes (in red) a

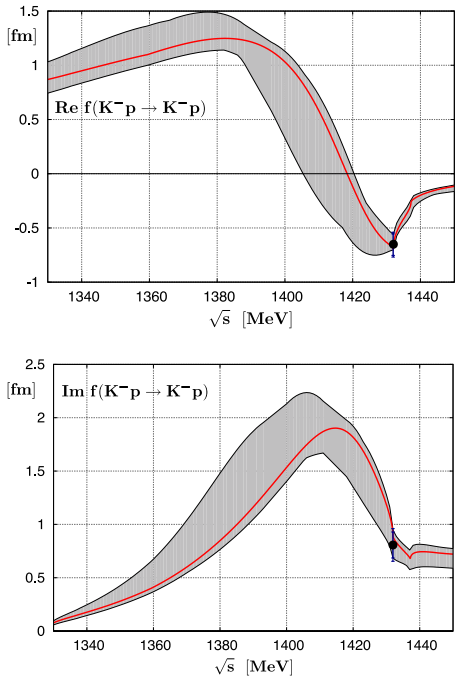

FIG. 24 NLO chiral-model calculation of the real and imaginary parts of the K^-p cm scattering amplitude, denoted IHW in the text (Ikeda *et al.*, 2012). The pole position of the $\Lambda(1405)$ resonance is at 1424−i26 MeV. The K^-p threshold values marked by solid dots follow from the SIDDHARTA measurement of kaonic hydrogen $1s$ level shift and width (Bazzi *et al.*, 2011, 2012).

TABLE XI Calculated K^-pp binding energies B & widths Γ. DHW stands for (Doté *et al.*, 2008, 2009), BGL for (Barnea *et al.*, 2012), IKS for (Ikeda *et al.*, 2010), RS for (Révai and Shevchenko, 2014), YA for (Yamazaki and Akaishi, 2002), WG for (Wycech and Green, 2009), SGM for (Shevchenko *et al.*, 2007a,b) and IS for (Ikeda and Sato, 2007, 2009).

Energy dependent meson-baryon interactions

	Variational		Faddeev	
(MeV)	DHW	BGL	IKS	RS
B	17–23	16	9–16	32
Γ	40–70	41	34–46	49

Energy independent meson-baryon interactions

	Variational		Faddeev	
(MeV)	YA	WG	SGM	IS
B	48	40–80	50–70	60–95
Γ	61	40–85	90–110	45–80

20–30 MeV downward shift of the broad bump representing the Y^* component. This indicates attraction for the Y^*N system. Unfortunately, in this kinematical region the contributions of $\Sigma(1385)$ and $\Lambda(1405)$ overlap and are indistinguishable. A $\Sigma(1385)N$ quasi-bound realization of such a structure was previously discussed by (Gal and Garcilazo, 2013) as a possible $I = \frac{3}{2}$, $J^\pi = 2^+$ πYN resonance near the $\pi\Sigma N$ threshold (about 100 MeV below the $\bar{K}NN$ threshold). The main attraction in this 'pion-

assisted dibaryon' comes from the $p_{3/2}$-wave pion-baryon interactions, where $\bar{K}NN$ admixtures play a negligible role.

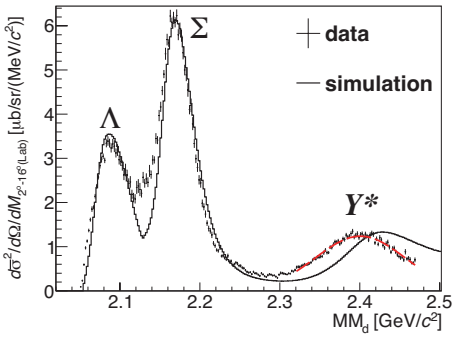

FIG. 25 Missing-mas spectrum ($\mathrm{MM_d}$) of the $d(\pi^+, K^+)$ reaction in the J-PARC E27 experiment at forward angles. A phase-space simulated spectrum is shown by a solid line (Ichikawa *et al.*, 2014).

Of the K^-pp calculations listed in Table XI, we chose to review the hyperspherical-basis variational calculations including also four-body bound states (Barnea *et al.*, 2012). The energy dependence of the $\bar{K}N$ interaction in this calculation is treated self consistently. The binding energies are shown in Fig. 26 for three- and four-body kaonic bound states. $\Gamma(\bar{K}N \to \pi Y)$ width estimates are plotted as vertical bars, given by

$$\frac{\Gamma}{2} \approx \langle\, \Psi_{\mathrm{g.s.}} |\, -\mathrm{Im}\, \mathcal{V}_{\bar{K}N} \,|\, \Psi_{\mathrm{g.s.}} \,\rangle\ , \qquad (39)$$

where $\mathcal{V}_{\bar{K}N}$ consists of all pairwise $\bar{K}N$ interactions. This expression provides a good approximation because $|\mathrm{Im}\, \mathcal{V}_{\bar{K}N}| \ll |\mathrm{Re}\, \mathcal{V}_{\bar{K}N}|$ (Hyodo and Weise, 2008). The calculated binding energies (widths) typically are found to be 10 (10 to 40) MeV lower than when one uses threshold values as input, due to the self-consistency requirement which results in weaker $\bar{K}N$ interactions below threshold. In particular, the $I = \frac{1}{2}$ $\bar{K}NN$ g.s. (K^-pp) lies only 4.3 MeV below the 11.4 MeV centroid of the $I = 0$ $\bar{K}N$ quasi-bound state. The latter value differs substantially from the 27 MeV binding energy traditionally assigned to the $\Lambda(1405)$ resonance used in non-chiral calculations. The $\bar{K}N \to \pi Y$ widths are of order 40 MeV for single-$\bar{K}$ clusters and twice that for double-$\bar{K}$ clusters. Additional $\bar{K}NN \to YN$ contributions of up to ∼10 MeV in K^-pp (Doté *et al.*, 2009) and ∼20 MeV in the four-body systems (Barnea *et al.*, 2012) are likely.

For calculations of heavier $\bar{K}$ nuclear systems one needs in-medium $\bar{K}N$ scattering amplitudes. The in-medium K^-N isoscalar amplitudes obtained from the chirally motivated coupled-channel model of (Cieplý and Smejkal, 2012), and denoted NLO30 in the text, are shown in Fig. 27 above and below threshold. The real part of the subthreshold amplitude, which is relevant to K^- atomic and nuclear states, is strongly attractive (∼1 fm) and similar to that of the IHW subthreshold

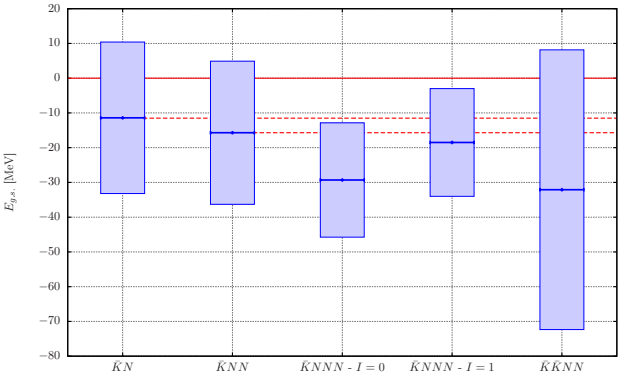

FIG. 26 Binding energies and widths, $\Gamma(\bar{K}N \to \pi Y)$, of $\bar{K}$ and $\bar{K}\bar{K}$ few-body quasi-bound states (in MeV) calculated by (Barnea *et al.*, 2012). Horizontal lines denote particle-stability thresholds. Widths are represented by vertical bars. Not shown in the figure is a possible $I = \frac{1}{2}$, $J^\pi = \frac{1}{2}^+$ $\bar{K}\bar{K}N$ quasi-bound state (Shevchenko and Haidenbauer, 2015).

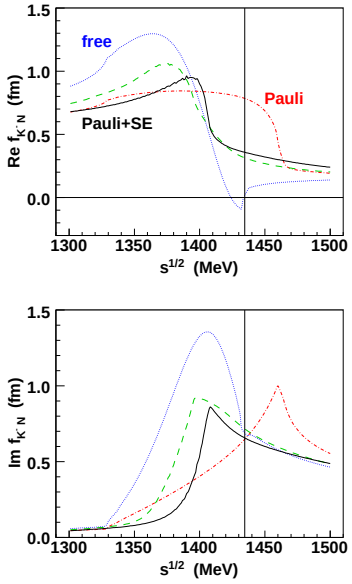

FIG. 27 Near-threshold energy dependence of K^-N cm scattering amplitudes in model NLO30 (Cieplý and Smejkal, 2012) for free-space (dotted) and Pauli-blocked amplitudes at $\rho = \rho_0$ with (solid) and without (dot-dashed) meson and baryon self-energies (SE). The dashed curves show Pauli-blocked amplitudes with SE at $\rho = 0.5\rho_0$. The K^-N threshold is marked by a thin vertical line.

amplitude. This implies that K^- quasi-bound states are likely to exist. Note that the attraction as well as absorption (expressed by the imaginary part of the amplitude) become moderately weaker for $\rho \geq 0.5\rho_0$, as demonstrated by comparing the solid ($\rho = \rho_0$) and dashed curves ($\rho = 0.5\rho_0$).

The NLO30 in-medium $\bar{K}N$ s-wave scattering amplitudes shown in Fig. 27 were used by (Gazda and Mareš,

TABLE XII Self-consistently calculated (Gazda and Mareš, 2012) binding energies B_K and widths Γ_K (in MeV) of K^- quasi-bound states in Ca using a static RMF Ca density and NLO30 in-medium K^-N subthreshold amplitudes (Cieplý and Smejkal, 2012).

	NLO30		+ p wave		+ $2N$ abs.	
	B_K	Γ_K	B_K	Γ_K	B_K	Γ_K
$1s_K$	70.5	14.9	73.0	14.8	68.9	58.9
$1p_K$	50.6	18.0	53.1	17.9	49.2	53.6
$1d_K$	28.8	30.3	32.1	29.3	27.7	59.7
$2s_K$	23.9	33.8	26.3	34.2	21.6	67.1

2012) to evaluate self-consistently K^- quasi-bound states using RMF nuclear-core densities across the periodic table. Calculated K^- binding energies, B_K, and widths, Γ_K, in Ca are listed in Table XII for several choices of input interactions. Listed in the table are also values of B_K and Γ_K derived by adding a $\Sigma(1385)$-motivated p-wave K^-N interaction from (Weise and Haertle, 2008). This marginally increases B_K by a few MeV and modifies Γ_K by less than 1 MeV. By adding a two-nucleon (2N) $K^-NN \to YN$ absorption term estimated from fitting to kaonic atoms, a $\lesssim$2 MeV decrease of B_K results, but the width substantially increases to $\Gamma_K \sim (50-70)$ MeV. Given these large widths, it is unlikely that distinct quasi-bound states can be uniquely resolved, except perhaps in very light K^- nuclei.

The hierarchy of widths listed in Table XII is also worth noting. One expects a maximal width in the lowest, most localized $1s_K$ states for energy-independent potentials, which gradually decreases in excited states since these are less localized within the nucleus. The reverse is observed here, particularly when excluding 2N absorption. This is a corollary of the required self consistency; the more excited a K^- quasi-bound state, the lower nuclear density it feels and thus a smaller subthreshold downward shift it experiences. Since $\mathrm{Im}\, f_{K^-N}(\rho)$ decreases strongly below threshold, see Fig. 27, the contribution to the calculated width gets larger as the excitation energy of the quasi-bound state increases.

K^- nucleus optical potential fits to kaonic atom data across the periodic table reveal that the in-medium IHW-based, or NLO30-based one-nucleon (1N) amplitude input to V_{K^-} fails to reproduce, even qualitatively, the K^- atomic level shifts and widths. This is demonstrated in Fig. 28 by the considerably stronger component, attributed to multi-nucleon (mN) processes with m=2,3,$\cdots$, of the fitted V_{K^-}. The composition of the imaginary part of the potential is of particular interest. It indicates that the mN component, which is sizable in the nuclear interior, becomes negligible about half a fermi outside the half-density radius. This has implications for optimally choosing the kaonic-atom candidates where widths of two atomic levels can be measured (Friedman and Okada, 2013) to substantiate the 1N vs mN pattern observed in global fits (Friedman and Gal, 2013). Finally,

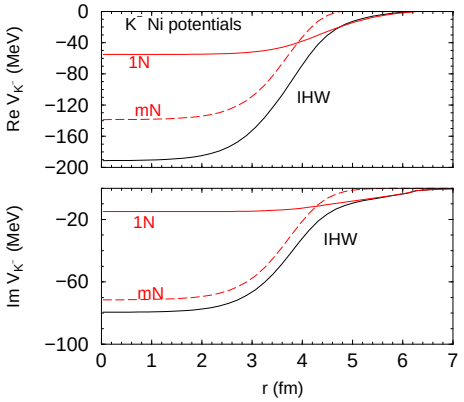

FIG. 28 A self-consistent K^- nuclear potential V_{K^-} for K^- atoms of Ni derived from global fits (Friedman and Gal, 2013) based on in-medium IHW one-nucleon (1N) amplitudes, together with its 1N and multi-nucleon (mN) components.

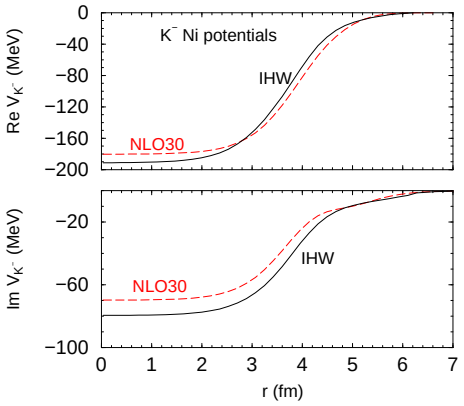

FIG. 29 Self-consistent K^- nuclear potentials V_{K^-} for K^- atoms of Ni derived from global fits (Friedman and Gal, 2012) based on the in-medium IHW 1N amplitudes (solid curves), see Fig. 28 above, and (in dashed curves) as based on the in-medium NLO30 1N amplitudes.

Fig. 29 demonstrates that both IHW and NLO30 energy-dependent in-medium amplitude inputs to V_{K^-} lead to practically the same strongly attractive and absorptive nuclear-matter potential $V_{K^-}(\rho_0)$.

It is worth noting that the strong K^- nuclear attraction forces the atomic K^- wavefunction to overlap appreciably with the nuclear density down to almost 90% of the central nuclear density ρ_0 (Friedman and Gal, 2007; Gal, 2013b). This does not hold for the shallower optical potentials V_{K^-} based on 1N energy-independent f_{K^-N} input consisting of threshold values (Baca *et al.*, 2000). Such potentials do not penetrate significantly beyond 10% of ρ_0 and also do not provide equally good atomic fits as shown in Fig. 22 of (Friedman and Gal, 2007). In this context, a reaction that discriminates between deep and shallow attractive K^- nuclear potentials is the formation of Λ hypernuclear states localized within the nuclear in-

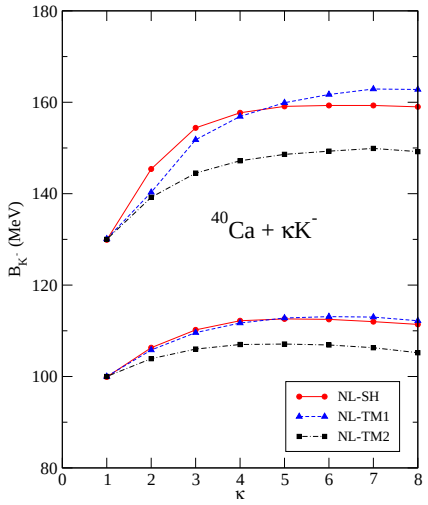

FIG. 30 Saturation of $1s_{K^-}$ separation energies B_{K^-} as calculated in multi-K^- (^{40}Ca+κK^-) nuclei (Gazda *et al.*, 2008) for several versions of RMF input marked in the inset. The lower (upper) group of curves was constrained to produce $B_{K^-} = 100$ (130) MeV for $\kappa = 1$.

terior in K^- capture at rest. The calculated formation rates show sensitivity to how far the relevant K^- atomic wavefunctions penetrate into the nucleus (Cieplý *et al.*, 2011). Formation rates of several p-shell hypernuclear ground states, available from FINUDA experiments (Agnello *et al.*, 2011a) and analyzed by (Cieplý *et al.*, 2011) favor deep K^- nuclear potentials to shallow ones.

One might expect increased binding in multi K^- nuclei when calculated using strongly attractive K^- nuclear potentials, which are fitted to K^- atom data, since the bosonic nature of kaons allows them to occupy the same high-density central region of nuclei. This turns out not to be the case, as demonstrated by the RMF calculations of (Gazda *et al.*, 2008) shown in Fig. 30. The difference between the various curves representing a given starting value of B_{K^-}, originates from the balance of the RMF inputs between the vector fields which generate $\bar{K}\bar{K}$ repulsion and the σ scalar field which generates overall attraction. The separation energies, B_{K^-}, saturate as a function of the number of K^- mesons, κ, such that $B_{K^-}(\kappa \to \infty) \ll (m_K + M_N - M_\Lambda) \approx 320$ MeV. This implies that anti-kaons do not replace Λ hyperons in the g.s. realization of multi-strange hadronic systems. Stated differently, anti-kaons do not condense in a finite self-bound hadronic system.

VIII. FUTURE EXPERIMENTS AND DIRECTIONS

Even though SU(3)$_{\rm f}$ symmetry is badly broken, it is a useful way to organize the discussion of strangeness within a nucleus. Thus techniques in, and knowledge of, traditional nuclear physics may readily be applied. As examples, spectroscopy which resolves the spin structure, and the weak decay mechanisms which operate within the nuclear interior illuminate new features of the hadronic many body problem.

Because the ΛN interaction is weak, hypernuclear spectroscopy can be represented by a superposition of particle-hole states resulting in 5-10 MeV spaced $\hbar\omega$ structures, and these can be resolved, as previously discussed, by experiments with 1–2 MeV resolution. However, it is more difficult to extract levels which involve nuclear-core excitations, or to resolve Λ spin-flip excitations within the enclosing $\hbar\omega$ structures. Indeed, direct observation of Λ spin doublet structure in many instances requires resolutions approaching 100 keV or better, and thus well beyond the capabilities of present magnetic spectroscopy. Still, resolution of nuclear core excitations at the $\leq$ 500 keV level carry substantial physics interest, and are accessible with modern, continuous-beam electron accelerators (Nakamura, 2013), and perhaps meson beams at the J-PARC (Japan Proton Accelerator Research Complex) 50 GeV proton synchrotron (Takahashi, 2013).

In addition to spectroscopy, non-mesonic weak decays provide information on the local nuclear environment, including for example NN correlations. Also by comparing energy shifts between charge symmetric hypernuclei, information on the dynamical behavior of the nuclear core and the admixture of other hyperons in the ground state wave function can be obtained. Finally, multi-hyperon states provide information on hyperon-hyperon interactions, which are needed to extend SU(3)$_{\rm f}$ symmetry, and develop a better understanding of nuclear matter at high density in astrophysical objects.

Future programs will be driven by the new proton accelerator at J-PARC, the continuous electron accelerators at Jlab and Mainz, and the antiproton facility at FAIR. Not only do these facilities have infrastructure designed for hypernuclear research, but the experiments will be able to take advantage of new, innovative detectors and electronics which will allow higher rates, better energy resolution, and better particle and signal identification. It is anticipated that this field will remain interesting and fertile to new exploration.

A. Spectroscopy using meson beams

1. Hyperon production and hyperon-nucleon interactions

As discussed in the preceding sections, the mainstay of hypernuclear research used the (K^-, π^-) and (π^+, K^+) mesonic reactions. On the other hand, studies of heavy hypernuclear systems may prove difficult. Therefore, it is important to undertake better measurements of elementary hyperon production cross sections and, in particular, polarization observables may prove useful. Polarization is small at the forward angles where the *e.g.* Λ production amplitude is sufficient to be experimentally useful. However, polarization is crucial in experiments attempting to

measure the weak decay asymmetry. Although the residual polarization after hypernuclear production appears consistent with zero, polarization due to the large spin-flip amplitudes in the (K^-, π^-) reaction at 1.1 and 1.5 GeV/c has not been explored systematically. This may be more accessible with the intense kaon beams available at J-PARC, as indeed proved in the E13 experiment by populating the ${}^{4}_{\Lambda}\mathrm{He}(1^+)$ level in the (K^-, π^-) reaction on ${}^{4}\mathrm{He}$ at $p_K = 1.5$ GeV/c (Yamamoto *et al.*, 2015).

Most importantly, there should be a plan to systematically study the elementary hyperon-nucleon (YN) interaction. To date only approximately 40 data points of YN scattering cross sections are available from mostly old experiments that studied hyperon post-production secondary interactions. Some of the more recent ΣN data were obtained using the SCIFI (SCIntillator FIber) active detector system of the 1990s. One approved experiment at J-PARC, E40 (Takahashi, 2013), will extend these measurements. Such new and improved data are particularly important from a theoretical standpoint in constructing YN potential models for use in hypernuclear structure applications. We note that successive Nijmegen extended soft core (ESC) potentials, the latest of which is ESC08 (Nagels *et al.*, 2015a), have led to increasingly repulsive Σ-nucleus G-matrix potentials, in agreement with deductions made from Σ hypernuclear production experiments. Therefore, it would be useful to enhance the YN data base of these models by new and more precise ΣN cross section data in order to confirm the validity of these nuclear-matter deductions. Similarly, it would be useful to enhance the $S = -2$ baryon-baryon data base by new and more precise ΞN cross section data, particularly by remeasuring and extending the poorly measured $\Xi^- p \to \Lambda\Lambda$ reaction cross sections. This input is crucial for confirming that the $S = -2$ baryon-baryon interactions are fairly weak, as suggested by the absence of a particle-stable H dibaryon and by the accurately known $B_{\Lambda\Lambda}({}^{6}_{\Lambda\Lambda}\mathrm{He})$ value, and in agreement with a recent NLO χEFT study (Haidenbauer *et al.*, 2016).

2. Reaction spectroscopy with mesons

The absence of a modern hadron accelerator, providing intense beams of energetic kaons and pions, has hindered the exploration of hypernuclear experiments, particularly those involving the study of doubly strange nuclear systems. This impediment is being resolved with the introduction of experiments at J-PARC (Takahashi, 2013). The 30 GeV proton beam at J-PARC is operative, producing various high-intensity beams of secondary pions and kaons. Two beamlines are initially available, with high resolution magnetic spectrometers that are able to reach missing-mass resolution of somewhat less than 2 MeV at best. A proposed high-resolution (π^+, K^+) spectrometer for use in a future extension of the hadron facility should achieve missing mass resolutions for hypernuclear spectroscopy of ≤ 500 keV. So far, the spectroscopy of single Λ hypernuclei has been addressed in brief running periods of experiments E10, search for ${}^{6}_{\Lambda}\mathrm{H}$ (Sugimura *et al.*, 2014), and E13, γ-ray studies in the s, p, and sd shells (Tamura *et al.*, 2013), with the latter observing a 1.41 MeV $1^+ \to 0^+$ γ transition in ${}^{4}_{\Lambda}\mathrm{He}$ (Yamamoto *et al.*, 2015). Also high on the hypernuclear agenda is experiment E05 which is a search for the ${}^{12}_{\Xi}\mathrm{Be}$ hypernucleus via ${}^{12}\mathrm{C}(K^-, K^+){}^{12}_{\Xi}\mathrm{Be}$ (Nagae, 2013). In this experiment, the overall energy resolution in the Ξ^- bound-state region is expected to be in the range of 1.5–3 MeV at FWHM.

3. Experiments using emulsion detectors

As described earlier, nuclear emulsion was the first detection system used to investigate hypernuclear events. The advantage of emulsion is its excellent position and energy resolution, which allows detailed investigation of any scanned event production and decay products. Coupling counters with emulsion, although somewhat clumsy, can still provide needed information under certain experimental conditions. Indeed this technique was crucial in the KEX-E373 determination of the binding energy of ${}^{6}_{\Lambda\Lambda}\mathrm{He}$ (Ahn *et al.*, 2013; Takahashi *et al.*, 2001). A coupled counter-emulsion detector is proposed for the study of $\Lambda\Lambda$ systems at J-PARC. In this experiment, E07, Ξ^- are produced in a diamond target upstream of the emulsion and are tracked as they recoil into, and stop in the emulsion (Takahashi, 2013). Particle emission from the stopping vertex is then analyzed for various reactions, including the production of $S = -2$ systems.

4. Spectroscopy using electromagnetic transitions

While the energy resolution using direct spectroscopy to specific states with magnetic spectrometers and meson beams is presently limited to no better than a few hundred keV, the energy of electromagnetic transitions between states can be measured to a few keV. Thus, measurement of electromagnetic transitions is a powerful tool for hypernuclear spectroscopy. This requires a dedicated beam line to tag the formation of a specific hypernucleus, and large acceptance, high resolution Ge detectors. The photon detectors to be used have high photo-peak efficiency and rate handling capabilities. The system at J-PARC is called HYPERBALL-J (Tamura *et al.*, 2013) and consists of 28 mechanically-cooled Ge detectors having 60% relative efficiency. Each Ge crystal is enclosed by 2 cm thick PWO counters to suppress Compton scattering and gammas from π^0 decays. The readout requires special electronics for high counting rate and large dynamic range of the signals.

J-PARC has tested and mounted equipment to undertake a study of gamma emission from excited levels in ${}^{4}_{\Lambda}\mathrm{He}$, ${}^{10}_{\Lambda}\mathrm{Be}$, ${}^{11}_{\Lambda}\mathrm{Be}$, and ${}^{19}_{\Lambda}\mathrm{F}$ (Tamura *et al.*, 2013). A first result for ${}^{4}_{\Lambda}\mathrm{He}$ has been obtained (Yamamoto *et al.*,

2015). Lifetimes can be measured using the Doppler Shift Attenuation Method (DSAM) which has already been used to extract the lifetime of the $5/2^+$ state of ${}^{7}_{\Lambda}$Li, and thus its electromagnetic E2 transition strength $B(E2)$ value (Tanida *et al.*, 2001). Also, the lifetime of the lowest $1/2^+;T=1$ state in ${}^{15}_{\Lambda}$N has been measured (Ukai *et al.*, 2008). Perhaps with the higher intensities provided at J-PARC, the Λ magnetic moment in the nuclear medium might also be inferred from measuring the lifetime of M1 transitions between ground-state hypernuclear doublet levels, such as the $(3/2^+ \rightarrow 1/2^+)$ γ ray in ${}^{7}_{\Lambda}$He (Tamura *et al.*, 2013). In the weak-coupling limit the strength of the electromagnetic M1 transition $B(M1)$ is proportional to $(g_c - g_\Lambda)^2$, where g_c is the core g-factor and g_Λ is the Λ g-factor (for the $0s_\Lambda$ orbit in this example). For the simple Λ hypernuclear configurations considered here, the in-medium Λ g-factors could deviate from their corresponding free-space s.p. Schmidt values by 10% at most (Dover *et al.*, 1995; Saito *et al.*, 1997). The lifetime measurement accuracy required to test a few-percent departure of g_Λ from its Schmidt value can be reached at J-PARC (Tamura *et al.*, 2013).

As the target mass increases to heavier systems the number of both nuclear and hypernuclear gammas increases while the yield to specific hypernuclear states decreases. Although the Doppler shift of in-flight hypernuclear transitions can discriminate between at-rest nuclear transitions, it still becomes more difficult to assign observed gammas in a particular hypernuclear level scheme. Thus, coincident gamma decays, as well as better resolution of the tagging spectrometer, becomes more important.

The first $\gamma\gamma$ coincidence observation was reported (Ukai *et al.*, 2006), but gamma coincidences cannot be a useful tool until production rates are substantially improved. Note that an increase in yield involves more than increasing beam flux, because gamma detectors are sensitive to backgrounds of all types, and resolution is degraded by rate-dependent, electronic pileup.

In addition to $\gamma\gamma$ coincidence measurements, a coincidence between a γ and a weak decay can be used to extract information about hypernuclear structure. For hypernuclei with masses up to the middle of the $1p$ shell, mesonic, as opposed to non-mesonic, weak decay is sufficiently probable that detection of mono-energetic π^- emission can be used as a coincidence to tag a specific hypernucleus. If the hypernucleus can be uniquely identified from its mesonic decay, then detection and missing mass analysis of the production reaction would not be necessary, and the observation of gammas from hyperfragments in coincidence with their π^- decay would increase the efficiency of a gamma-ray experiment. The technique also gives access to hypernuclei which could only be produced by fragmentation or nucleon emission; see also the discussion of the Mainz program in section VIII.B.1 below.

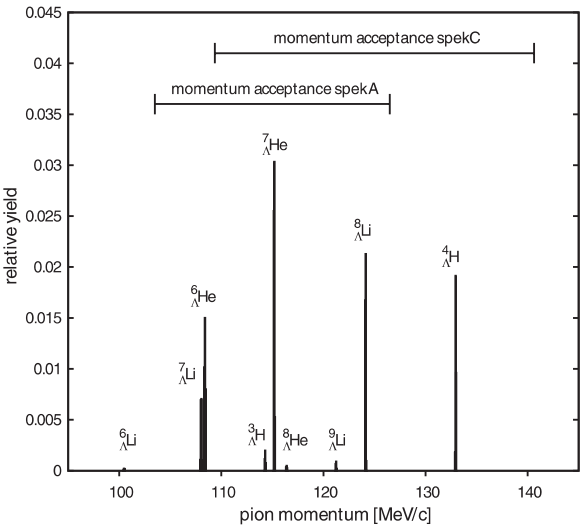

FIG. 31 Pion-decay momentum lines expected from weak decay of hypernuclei produced in the fragmentation of ${}^{9}_{\Lambda}$Li* (Esser *et al.*, 2013).

B. Spectroscopy with electron accelerators

1. Electroproduction at Mainz (MAMI)

An ongoing program at the Mainz microtron (MAMI) involves studying the mesonic weak decay of light hypernuclei formed by fragmentation of excited hypernuclear levels reached in electroproduction. This interesting, unexplored technique uses counters, not emulsion. The microtron energy of 1.5 GeV allows experiments to determine ground state masses of light hypernuclei by measuring the pion weak decays following the fragmentation of heavier hypernuclear systems reached in kaon electro-production, *e.g.* ^{9}Be$(e;e',K^+)^{9}_{\Lambda}$Li*. The hypernucleus (${}^{9}_{\Lambda}$Li* in this example) fragments into various lighter hypernuclei which decay and the emitted pions observed. This process is illustrated in Fig. 31 which simulates the mesonic-decay pion energies associated with a specific hypernucleus. The ${}^{4}_{\Lambda}$H line at $p_\pi = 133$ MeV/c resulting from the weak decay ${}^{4}_{\Lambda}\mathrm{H}\rightarrow{}^{4}\mathrm{He}+\pi^-$ has been seen recently (Esser *et al.*, 2015) and used to obtain a binding energy value of $B_\Lambda({}^{4}_{\Lambda}\mathrm{H})$=2.12±0.01±0.09 MeV, consistent with the old emulsion value 2.04±0.04 MeV (cf Table I). Figure 32 shows the beamline geometry for the planned MAMI experiments. The KAOS spectrometer detects kaon production with the kaons identified by time-of-flight (TOF) and an aerogel Cherenkov detector. Spectrometers A and C detect the decay pions. Problems certainly exist in assigning the observed pion decay spectrum to specific hypernuclear states. Nevertheless, because the decay of these hypernuclei can be determined by 2-body kinematics, the assignment of masses and binding energies is potentially possible. However, note that mesonic decays from hypernuclear ground states do not necessarily end up in the corresponding

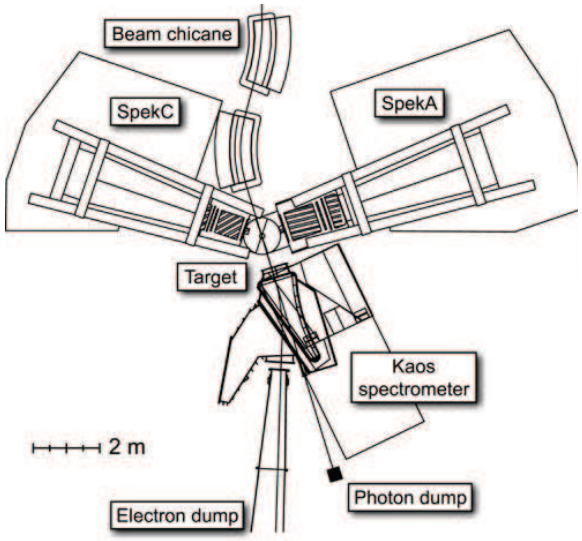

FIG. 32 The spectrometer system at the Mainz microtron designed to observe the pion decay of light hypernuclei formed by fragmentation of heavier hypernuclear systems formed in kaon electro-production. The KAOS spectrometer detects the kaons emitted in the $(e; e', K^+)$ reaction, and spectrometers A and C detect the decay pions (Esser *et al.*, 2013).

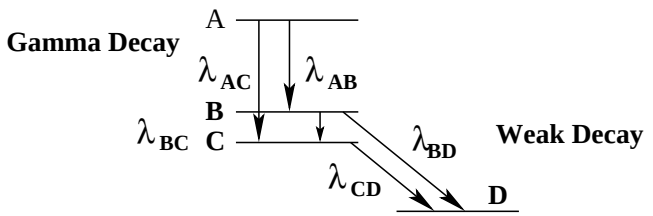

FIG. 33 A schematic illustration of gamma and weak decay between hypernuclear levels with a ground state doublet (B,C) having energy spacing $\leq$ 100 keV.

daughter-nuclei ground states (Gal, 2009; Motoba *et al.*, 1994; Randeniya and Hungerford, 2007) as represented in Fig. 31.

The use of a gamma-weak decay coincidence has also been proposed to obtain the lifetime of hypernuclear levels which have gamma lifetimes comparable to those of weak decay (200 ps). This could be used, for example, to measure the gamma lifetime of the upper level of a hypernuclear ground state doublet, where the lifetime of the upper level competes with weak decay. This generally occurs for high multipolarity transitions of low transition energy, $\leq$ 100 keV. A simultaneous fit to the coincidence times between the weak decays of the doublet levels and the gamma transitions from A to B and B to C as shown in the level diagram of Fig. 33 would provide the lifetimes of the B and C levels. Such a program fits into a potential program at Mainz, but the hypernuclei are electro-produced which will have significant gamma backgrounds, and this may preclude gamma-pion coincidnece experiments.

2. Electroproduction at Jlab

There is substantial, new electro-produced hyperon data from the CLAS detector Collaboration at JLab, particularly polarization and spin transfer data (Carman and Raue, 2009; Dey *et al.*, 2010; McCracken *et al.*, 2010), providing a consistent data base for partial-wave YN amplitude analysis. The electro-production of hyperons is a complicated process involving a number of overlapping strange and non-strange resonances (Bydžovský and Skoupil, 2013). Whereas s-channel diagrams are found to be most important at low energy, t-channel/Reggeon exchange dominates when $W > 2$ GeV (*i.e.* above the resonance region). More data is expected from CLAS and and also from LEPS at SPring-8 (Niiyama, 2013).

Jlab will be upgraded to a higher energy with more intense beams. The new large solid-angle spectrometers drawn in Fig. **??**, HKS (High-resolution Kaon Spectrometer) and HES (High-resolution Electron Spectrometer), with a new splitting magnet (SPL), will be available. Previously $(e, e'K^+)$ hypernuclear programs were undertaken in both Hall A and Hall C. When Jlab transitions to 12 GeV electron beams, hypernuclear experiments will take place in only one Hall. If this is Hall A, a plan exists to design two new septum magnets and move the HKS and the HES from Hall C into Hall A behind the target station. A waterfall target (H_2O) will be retained and could be used to further study the elementary electro-production amplitude at forward angles and for spectrometer calibrations. By carefully selecting the scattering geometry, bremsstrahlung and Möller backgrounds can be reduced and the luminosity increased to obtain rates of several 10's per hour to specific states. This allows electromagnetic production of hypernuclei through the *sd* shell with perhaps resolutions approaching 300 keV. Proposals have been made for improved energy resolution experiments, after the 12 GeV upgrade, aiming at the electro-production of Λ hypernuclei beyond the p-shell hypernuclei explored so far in Halls A and C (Garibaldi *et al.*, 2013; Tang *et al.*, 2014)

C. Experiments at PANDA

The PANDA collaboration using anti-protons at the FAIR future facility in Darmstadt, proposes to produce double-Λ hypernuclei, followed by high-resolution γ-spectroscopy study, in order to provide for the first time precise information on their bound-state spectra (Esser *et al.*, 2013). The PANDA detector is to be set up at the High Energy Storage Ring (HESR) which produces high-intensity phase-space cooled antiprotons with momenta between 1.5 and 15 GeV/c. The antiprotons from the storage ring are extracted and allowed to interact on a nuclear target at $p_{\rm lab} \approx$3 GeV/c (Pochodzalla, 2005),

$$\bar{p} + p \rightarrow \Xi^- + \bar{\Xi}^+, \quad \bar{p} + n \rightarrow \Xi^- + \bar{\Xi}^0. \quad (40)$$

The trigger for these reactions will be based on the detection of high-momentum $\bar{\Xi}$ anti-hyperons at small angles or on K^+ mesons produced by the absorption of anti-hyperons in the primary target nuclei. Produced Ξ^-, with typical momenta between 0.5 to 1 GeV/c, are decelerated in a secondary target. The slow Ξ^- are then either directly absorbed by the nucleus or are captured into an atomic orbit, cascading downward through the Ξ^- atom levels until absorbed in the $\Xi^- p \to \Lambda\Lambda$ reaction, thereby partially forming a double-Λ hypernucleus. X-ray de-excitation between Ξ atomic states, and gamma de-excitation between states in the $\Lambda\Lambda$ hypernuclei which may be formed, are to be studied with an array of Ge detectors (Esser *et al.*, 2013; Pochodzalla, 2005). One expects to identify approximately 3000 stopped Ξ^- hyperons per day, see the simulation by (Ferro *et al.*, 2007). Ξ^- capture yields, associated fragmentation mass spectra and production cross sections of double-Λ hypernuclei have been estimated in two recent works (Gaitanos *et al.*, 2014, 2012) using transport in-medium calculations.

D. Weak decay of hypernuclei

1. mesonic decays

Mesonic decays of hypernuclei have been studied since the beginning of hypernuclear experimentation, first in emulsion and more recently in counter experiments at BNL, KEK and by the FINUDA Collaboration at DAΦNE, Frascati (Botta *et al.*, 2012). A wealth of binding energies and spin-parity values of light Λ hypernuclei were deduced in these studies. The well understood mesonic decay of the Λ can be used as a tool to explore nuclear structure when strangeness is injected into the nuclear medium. The pion decay spectroscopy program at Mainz (Esser *et al.*, 2013) which was reviewed in a preceding subsection is poised to develop this tool, primarily by improving the momentum resolution in detecting the emitted pion.

The limitation of mesonic decay studies to light hypernuclei is due to the low momentum of the recoiling nucleon in the $\Lambda \to N + \pi$ decay, which is well below the nuclear Fermi momentum p_F for $A \geq 6$. However, the Λ mesonic decay rate in the nuclear medium is extremely sensitive to pion distortion effects from in-medium nuclear and electromagnetic interactions. The inclusion of pion-nuclear distortion allows the recoiling nucleon to assume momentum values greater than p_F, enhancing both π^0 and π^- emission, while Coulomb distortion is expected to raise the π^- decay rates to measurable levels for the heaviest hypernuclei. Indeed, the prediction is that the ratio of the in-medium to free rate saturates at about 10^{-2} (Motoba and Itonaga, 1994). However, another calculation, which predicts somewhat similar behavior, results in a rate about a factor of 10 lower in the case of ^{208}Pb (Oset *et al.*, 1994). There are no available experimental data.

Hypernuclei generally de-excite by gamma emission to the ground state where they undergo weak decay . In situations where the ground state belongs to a spin doublet based on the nuclear core g.s., weak decay from the upper level can successfully compete with the M1 interdoublet electromagnetic transition when the transition energy is lower than typically 100 keV, see Fig. 33. This may occur in the case of the $(1^-_{\rm g.s.}, 2^-_{\rm exc.})$ doublet in $^{10}_{\Lambda}$B where no gamma ray between these two levels has been seen (Chrien *et al.*, 1990; Tamura *et al.*, 2005). Of the two levels, only the 2^- is expected to have been populated in the non-spin-flip production reactions of these experiments. Therefore, in $^{10}_{\Lambda}$B either the doublet splitting is less than 100 keV, thereby hindering the gamma transition with respect to weak decay, or the level ordering of the spin-doublet members is reversed.

Furthermore, the π^- decay spectrum is substantially different for weak decays from each member of the doublet (Gal, 2009), providing a way to identify the decay sequence. However, in general one might expect a mixture of weak decays from the doublet levels, and a more detailed analysis would be required to extract the decay ratios and determine the ordering. Note that an energy resolution of $\leq$ 100 keV is required to measure the π^- transition energy shifts in the decays. This may be possible if excellent resolution and sufficient statistics are available. Nevertheless, comparison of the observed pion decay to one calculated for various spin possibilities should allow the level order to be determined.

2. nonmesonic decays

Of the various observables studied so far, data on non-mesonic weak-decay asymmetry are scarce. Asymmetry and coincident weak-decay experiments are difficult, requiring thick targets, with low yields. A definitive asymmetry experiment would require a substantial increase in intensity and/or polarization, as well as the determination of the polarization of the hypernuclear ground state from which the decay occurs. Better missing-mass resolution to tag ground state production and the use of a polarizing reaction such as (π^+, K^+) at an angle $> 10^\circ$ would help, but this requires higher beam intensity.

It would also be important to measure the neutron and proton simulated decays from $^{4}_{\Lambda}$H compared to the same decays from $^{4}_{\Lambda}$He. This comparison would significantly help to resolve the question as to whether the $\Delta I = 1/2$ rule applies in non-mesonic weak decay $\Lambda + N \to N + N$ transitions. However, the production of $^{4}_{\Lambda}$H requires a charge exchange as well as a strangeness exchange reaction when using a ^{4}He target. Photoproduction is a possibility as well as the (K^-, π^0) reaction. High beam intensity and large solid angle detectors would be required. A test of the $\Delta I = 1/2$ rule requires that the final NN states have isospin $I_f(NN) = 1$, which is reached by the a, b, f amplitudes defined in Table VII. This practically leads to the requirement that the initial ΛN state is a

purely $^1S_0$. In this case the $\Delta I = 1/2$ rule predicts that

$$\Gamma_n(^4_\Lambda\mathrm{He}) \;=\; 2\,\Gamma_p(^4_\Lambda\mathrm{H})\;, \tag{41}$$

which may be tested in the non-mesonic decays of the $A = 4$ hypernuclei. The value of the left-hand side $\Gamma_n(^4_\Lambda\mathrm{He})$ has been determined to be very small, $\Gamma_n(^4_\Lambda\mathrm{He})/\Gamma_\Lambda^{\mathrm{free}} \leq 0.035$ (Parker *et al.*, 2007), whereas the value of $\Gamma_p(^4_\Lambda\mathrm{H})$ is unknown. This will be studied in the J-PARC E22 Experiment.

Another area of interest for nonmesonic weak decays would be to study exclusive decay modes, in analogy to the exclusive, two-body mesonic decay modes of Λ hypernuclei which have provided valuable information on spins of Λ hypernuclear levels, Table VI. The study of exclusive decay modes in *nonmesonic* weak decays could yield valuable information on the $\Lambda + N \to N + N$ amplitudes of Table VII. Examples of such modes in light nuclei are

$$^5_\Lambda\mathrm{He} \to n^4\mathrm{He},\; ddn,\; nn^3\mathrm{He},\; pn^3\mathrm{H}, \tag{42}$$

$$^4_\Lambda\mathrm{He} \to p^3\mathrm{H},\; n^3\mathrm{He},\; dd,\; dpn, \tag{43}$$

Rates for some of these decays were measured in bubble chambers and emulsion (Coremans *et al.*, 1970). In passing we mention that the Λ hypernuclear program at J-PARC also includes a search for multi-nucleon emission in the weak decay of hypernuclei, experiment E18 (Takahashi, 2013).

3. Λ hypernuclear lifetimes

Accurate measurements of Λ hypernuclear lifetimes in heavy systems beyond $A = 56$, as listed in Table II, could confirm the saturation of the nonmesonic decay width, Eq. (33), as well as provide a check on the Γ_n/Γ_p ratio systematics as a function of A. Previously, lifetime measurements in delayed fission triggered by proton and antiproton reactions on heavy nuclei, were interpreted as due to the production of Λ hypernuclei and their subsequent weak decay. The latest and most accurate measurements of this kind yielded lifetimes [(Cassing *et al.*, 2003), (Kulessa *et al.*, 1998) and (Armstrong *et al.*, 1993), respectively],

$$\tau_\Lambda(p + \mathrm{Au}) = (145 \pm 11)\ \mathrm{ps}\,, \tag{44}$$

$$\tau_\Lambda(p + \mathrm{Bi}) = (161 \pm 7 \pm 14)\ \mathrm{ps}\,, \tag{45}$$

$$\tau_\Lambda(\bar{p} + \mathrm{U}) = (125 \pm 15)\ \mathrm{ps}\,. \tag{46}$$

These are considerably shorter than values extrapolated from Table II, and taken at face value, imply unreasonably large values for Γ_n/Γ_p for heavy hypernuclei.

Finally, we would like to focus attention again to recent measurements of the $^3_\Lambda$H lifetime in heavy-ion experiments. As reviewed in Sect. I.B.5, the $^3_\Lambda$H lifetime was measured in several heavy-ion facilities using the time dilation of a Lorentz boost to a recoiling hypernucleus produced in a heavy ion reaction. Lifetimes deduced by the STAR Collaboration at BNL-RHIC, by the HypHI Collaboration at GSI and very recently by the ALICE Collaboration at CERN-LHC (see Fig. 7 in Sect. I.B.5) are listed in Table XIII together with a $^3_\Lambda$H lifetime derived in bubble-chamber (BC) studies (Keyes *et al.*, 1973, 1970). The $^3_\Lambda$H lifetime values deduced from measurements done in the heavy-ion facilities are about 25% shorter than the free Λ lifetime, and about 20% shorter than the value measured in a bubble chamber. Note that the BC measurement does not suffer from the uncertainty incurred in emulsion by a possible in-flight Coulomb dissociation of $^3_\Lambda$H (Bohm and Wysotzki, 1970). A recent statistical analysis of all the reported $^3_\Lambda$H lifetime measurements gives an average value $\tau(^3_\Lambda\mathrm{H})$=$(216^{+19}_{-16})$ ps (Rappold *et al.*, 2014). A realistic calculation of the lifetime (Kamada *et al.*, 1998) derives a lifetime shorter by only 3% than the free Λ lifetime τ_Λ=(263±2) ps, in agreement with (Rayet and Dalitz, 1966) which marks the first correct calculation of $\tau(^3_\Lambda\mathrm{H})$. The discrepancy between the lifetimes measured in heavy-ion collisions and the lifetime prescribed by theory is disturbing, posing a major problem for the understanding of $^3_\Lambda$H, the lightest and hardly bound hypernucleus. More work is necessary to understand the heavy-ion lifetime results. We note that $\tau(^4_\Lambda\mathrm{H})$ is also considerably shorter than τ_Λ, with a world average of $\tau(^4_\Lambda\mathrm{H})$=$192^{+20}_{-18}$ ps (Rappold *et al.*, 2014), but this is theoretically anticipated and well understood.

TABLE XIII $^3_\Lambda$H lifetime (in ps): measurements vs. theory. The free Λ lifetime is (263 ± 2) ps (Olive *et al.*, 2014). The first marked error is statistical, the second one is systematic.

BC[a]	STAR[b]	HypHI[c]	ALICE[d]	Theory[e]
246^{+62}_{-41}	$182^{+89}_{-45} \pm 27$	$183^{+42}_{-32} \pm 37$	$181^{+54}_{-39} \pm 33$	256

[a] (Keyes *et al.*, 1973) [b] (Abelev *et al.*, 2010) [c] (Rappold *et al.*, 2013) [d] (Adam *et al.*, 2016a) [e] (Kamada *et al.*, 1998)

E. Multi-strange systems

Nuclear systems with $S = -2$ are essential to experimentally access the hyperon-hyperon interaction. While several light double Λ hypernuclei have been observed, and their phenomenology is fairly well understood (Gal and Millener, 2011), bound Ξ hypernuclei have yet to be observed. Light Ξ hypernuclear systems are predicted to be bound by several MeV, and with sufficiently narrow widths to provide spectroscopy (Hiyama *et al.*, 2008). Intense K^- beams are required for their investigation. The E05 experiment searching for the $^{12}_{\Xi}$Be hypernucleus (Nagae, 2007) is high on the agenda of J-PARC. It proposes to use the ^{12}C(K^-, K^+) reaction to obtain 1.5 MeV (FWHM) resolution (Takahashi, 2013) which should be sufficient to observe any quasibound structure.

A similar experimental setup is also capable of producing $\Lambda\Lambda$ hypernuclei, either directly or by the conversion $\Xi N \rightarrow \Lambda\Lambda$. Identification of a $\Lambda\Lambda$ hypernucleus could occur either through direct production or by observation of the decay products. In direct production, one would observe the missing mass in a (K^-, K^+) reaction. In this case, cross sections are small due to the fact that the reaction requires a multi-step interaction on two nucleons. On the other hand, detection in light hypernuclei could occur by observing sequential mono-energetic π^- decays of the embedded Λs. In either case, good energy resolution and tracking is important. All experiments will be difficult because production rates are not expected to be high. A particularly important task would be to settle the question as to whether ${}^{4}_{\Lambda\Lambda}$H is bound (Filikhin and Gal, 2002c; Nemura *et al.*, 2003). Interest in the ${}^{4}_{\Lambda\Lambda}$H arises as it may be the least bound double $\Lambda\Lambda$ system. A previous experimental claim for the observation of ${}^{4}_{\Lambda\Lambda}$H (Ahn *et al.*, 2001b) is probably incorrect, as shown by a re-analysis of the data (Randeniya and Hungerford, 2007).

A possibly strong $\Lambda-\Xi$ attraction in the NSC97 model was pointed out by (Filikhin and Gal, 2002c). Here the $S = -3$ hypernucleus ${}^{6}_{\Lambda\Xi}$He, or ${}^{7}_{\Lambda\Lambda\Xi}$He, may provide the onset of Ξ stability in nuclear mater. This observation, and the repulsive nature of the Σ-nucleus potential, are relevant to the composition of neutron stars, as discussed in Sect. VI.B.

F. Experiments at heavy-ion facilities

Collisions between heavy nuclei ($A \gg 1$) at relativistic energies produce copiously hadrons and anti-hadrons, including hyperons and strange mesons. The formation of exotic nuclear systems and their study in relativistic heavy ion collisions was suggested by (Kerman and Weiss, 1973). This was further developed by more quantitative evaluations using a variety of production mechanisms, *e.g.* (Andronic *et al.*, 2011; Baltz *et al.*, 1994; Pop and Gupta, 2010; Steinheimer *et al.*, 2012). Following collision, the local hadron density produced in the "fireball" stabilizes in times of order 60 fm/c, resulting in the formation of hadronic clusters. These clusters potentially include strange dibaryons, hypernuclei, and other multi-strange hadrons. Predictions of production rates use two types of models: (i) thermal models in which entropy conservation governs the resulting production yields, following chemical freeze-out at a limiting temperature $T \approx$160 MeV (Andronic *et al.*, 2011), and (ii) coalescense models which apply inter-nuclear cascade simulations of particle collisions and captures, based on particle overlaps in both coordinate and momentum phase space (Steinheimer *et al.*, 2012).

Somewhat surprisingly, the predicted production yields of hypernuclei are model independent above an approximate collision energy of 10 A GeV, and both types of models predict saturation of the yield at beam energies

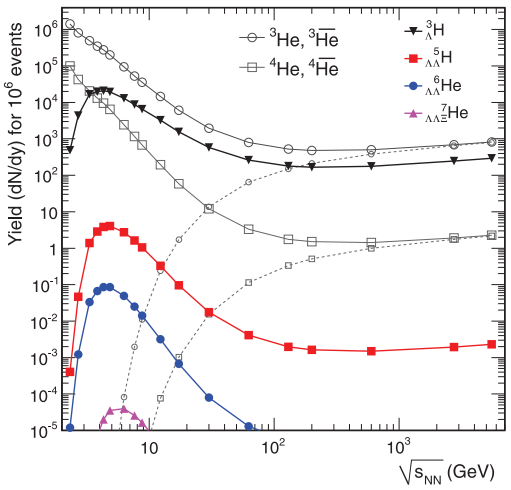

FIG. 34 Energy dependence of predicted yields for several multi-strange isotopes of hydrogen and helium at mid-rapidity for 10^6 heavy-ion central collisions. Predicted yields for two non-strange helium isotopes and their anti-isotopes are also plotted for comparison (Andronic *et al.*, 2011).

$\approx$15 A GeV (Andronic *et al.*, 2011; Botvina *et al.*, 2013). Dibaryon production, however, is found to be strongly model dependent. These simulation studies demonstrate that 10–20 A GeV is the optimal energy for hypernuclear production. Observation of hypernuclear production in relativistic heavy ion collisions is difficult, and except for light systems, present-day detectors are not really designed to identify and investigate hypernuclear systems of unknown mass and binding energies. The development of an hypernuclear research program using ion beams of lower mass, *e.g.* C, with energies of approximately 10–20 A GeV would seem appropriate, and can be pursued at the FAIR and NICA facilities (Botvina *et al.*, 2015). Fig. 34 illustrates yield predictions for light multi-strange hypernuclei production at mid-rapidity per 10^6 central collisions. These thermal-model predictions were constrained by fitting to RHIC hadron production yields at 200 GeV.

Focusing on the lightest $A = 3, 4$ hypernuclei, which are essentially the only ones studied so far in relativistic heavy-ion collisions, the BNL-AGS E864 Collaboration (Armstrong *et al.*, 2004) reported the observation of ${}^{3}_{\Lambda}$H in central Au+Pt collisions at energy per NN collision of $\sqrt{s_{NN}} = 11.5$ GeV. Subsequent work by the STAR Collaboration at the BNL-RHIC collider (Abelev *et al.*, 2010) identified both ${}^{3}_{\Lambda}$H and its anti-hypernucleus, $\overline{{}^{3}_{\Lambda}\mathrm{H}}$, in Au+Au collisions at $\sqrt{s_{NN}} = 200$ GeV. This was followed recently at the CERN-LHC facility by the ALICE Collaboration (Adam *et al.*, 2016a) in Pb+Pb collisions at $\sqrt{s_{NN}} = 2.76$ TeV. The ${}^{3}_{\Lambda}$H lifetime measurements reported by these heavy-ion experiments were listed and discussed in Table XIII above and in the related text.

Searches for exotic nuclear states such as $\Lambda\Lambda$ and $\overline{\Lambda n}$ bound states were also undertaken by the ALICE Collaboration (Adam *et al.*, 2016b), thereby placing up-

per limits which are typically smaller by one order of magnitude than yields anticipated from thermal models for the production of such states. Another ALICE Collaboration experiment studied the low energy Λ-Λ interaction, producing useful constraints on the scattering length and effective range: $a_{\Lambda\Lambda} = -1.10 \pm 0.37^{+0.68}_{-0.08}$ fm and $r_{\Lambda\Lambda} = 8.52 \pm 2.56^{+2.09}_{-0.74}$ fm (Adamczyk *et al.*, 2015). This result suggests a relatively weak Λ-Λ interaction, in accord with other existing experimental and theoretical estimates summarized recently by (Morita *et al.*, 2015).

A program somewhat similar to that of the HypHI Collaboration at GSI (Rappold *et al.*, 2015) was proposed for the under-construction Nuclotron-based Ion Collider fAcility (NICA) at Dubna, using an approximate 3 GeV/nucleon ^{6}Li beam incident on a $^{\rm nat}$C target. A more sophisticated trigger would be based on identifying the recoiling hypernuclei by using a new magnetic spectrometer to measure the momentum of their two-body pionic decays. The pions and residual particles from the decays would be detected with multi-wire proportional chambers placed behind the spectrometer magnet to reconstruct the hypernuclei from their decay products, which were presumed to be ${}^{A}_{\Lambda}{\rm H} \rightarrow {}^{A}{\rm He} + \pi^-$ or ${}^{A}_{\Lambda}{\rm He} \rightarrow {}^{A}{\rm Li} + \pi^-$ (Averyanov *et al.*, 2008). The main interest in this program would be the potential production of light, neutron-rich hypernuclei inaccessible by other reactions. However, obtaining lifetimes of heavy hypernuclei, where mesonic decay is suppressed and essentially unobservable, is more compelling at present.

G. $\overline{K}$-nucleus bound-state searches

The topic of K^--nuclear bound states has generated much heat and perhaps a little illumination. Experimental searches for these states using stopped kaon reactions with outgoing neutrons, at KEK, or protons, at DAΦNE, at first suggested bound-state structure at more than 100 MeV below threshold. However, the KEK observation (Suzuki *et al.*, 2004, 2005) of a $\bar{K}NNN$ structure is now believed to be an experimental artifact, and at least a large part of the FINUDA Collaboration observation of a K^-pp structure at DAΦNE (Agnello *et al.*, 2005a) must be due to final state interactions (Magas *et al.*, 2006). Yet the theoretical prediction of a K^-pp bound state is reasonably robust, with microscopic preference for shallow binding of few tens of MeV (Gal, 2013a). Recent searches by the HADES Collaboration using the $pp \rightarrow \Lambda p K^+$ reaction at GSI and performing a complete background evaluation (Epple and Fabbietti, 2015) have refuted earlier claims for a deeply bound K^-pp state based on a DISTO Collaboration analysis of older proton-beam data (Yamazaki *et al.*, 2010). In addition, the LEPS Collaboration at SPring-8 also published upper limits, although less significant than with meson beams, for the production of a K^-pp bound state via the $d(\gamma, K^+\pi^-)$ reaction at $E_\gamma = 1.5 - 2.4$ GeV (Tokiyasu *et al.*, 2014).

Ongoing experiments in J-PARC using meson beams reach contradictory results. E27 claims to have observed a deeply bound "K^-pp-like" structure in the $d(\pi^+, K^+)$ reaction at $p_\pi = 1.69$ GeV/c (Ichikawa *et al.*, 2015), whereas E15 presented upper limits in the ^{3}He(K^-, n) reaction at $p_K = 1$ GeV/c (Hashimoto *et al.*, 2015) that appear to rule out a K^-pp bound state with binding energy similar to that claimed by E27. However, E15, by focusing on the detection of Λp pairs, now suggests a broad K^-pp bound-state structure at just 15 MeV below threshold (Sada *et al.*, 2016). This ambiguity in identifying broad $\bar{K}$-nuclear bound-state structures reflects an experimental difficulty to directly access the formation and decay of such kaonic bound states. In particular, the detector used in such experiments must have good resolution, particle identification, and large angular acceptance. Further, improved experimentation searching for $\bar{K}$-nucleus bound-state structures is required to settle this issue.

IX. SUMMARY

Strangeness nuclear physics has been invesitgated since the first hyperon, Λ, was observed in cosmic rays. Progress in this field has not been rapid but continuous, with its development critically dependent on both the experimental and theoretical tools to fully exploit the physics. The previous sections reviewed the production mechanisms with which Λ and Σ hyperons are injected into the nuclear medium. In addition, multistrangeness and the 'hyperon puzzle' in neutron stars were reviewed, along with the strong interaction of $\bar{K}$ mesons in and with nuclei, including the possibility to form $\bar{K}$-nuclear quasi-bound states. The non-mesonic weak decay of hypernuclei offers the unique opportunity to study the four-fermion weak interaction, and in particular, the fundamental origin (if any) of the empirical $\Delta{\rm I} = 1/2$ rule. A number of potential experimental areas which seem critical for further advances in this field were pointed out.

To highlight obvious achievements in strangeness nuclear physics and outstanding problems facing this field of research for the coming years, a brief, perhaps subjective list follows:

- ΛN hypernuclear spin dependence deciphered.
- How small is Λ spin-orbit splitting and why?
- Role of 3-body ΛNN interactions in hypernuclei and at neutron-star densities?
- Repulsive Σ-nuclear interaction; how repulsive?
- Onset of ΛΛ binding: ${}^{\ \ 4}_{\Lambda\Lambda}{\rm H}$ or ${}^{\ \ 5}_{\Lambda\Lambda}{\rm H}$ & ${}^{\ \ 5}_{\Lambda\Lambda}{\rm He}$?
- Do Ξ hyperons quasi-bind in nuclei and how broad are they against $\Xi N \rightarrow \Lambda\Lambda$? recall that no quasi-bound Ξ state has been observed yet.
- Onset of Ξ stability: ${}^{\ \ 6}_{\Lambda\Xi}{\rm He}$ or ${}^{\ \ 7}_{\Lambda\Lambda\Xi}{\rm He}$?

TABLE XIV J-PARC scheduled experiments related to strangeness nuclear physics.

Exp.	title	status
E03	X rays from Ξ^- atoms	
E05	${}^{12}\mathrm{C}(K^-,K^+){}^{12}_{\Xi}\mathrm{Be}$	day-1 experiment
E07	S=-2 emulsion-counter studies	
E10	DCX studies of neutron-rich ${}^{A}_{\Lambda}Z$	negative result for ${}^{6}_{\Lambda}\mathrm{H}$
E13	γ-ray spectroscopy of Λ hypernuclei	day-1 experiment, ${}^{4}_{\Lambda}\mathrm{He}$ γ ray observed
E15	search for K^-pp in ${}^3\mathrm{He}(K^-,n)$	day-1 experiment, shallow K^-pp bound state suggested
E18	${}^{12}_{\Lambda}\mathrm{C}$ weak decays	
E19	search for Θ^+ pentaquark in $\pi^-p\to K^-X$	day-1 experiment, upper bound established
E22	weak interactions in ${}^{4}_{\Lambda}\mathrm{H}-{}^{4}_{\Lambda}\mathrm{He}$	
E27	search for K^-pp in $d(\pi^+,K^+)$	deeply-bound "K^-pp-like" state claimed
E31	study of $\Lambda(1405)$ by in-flight $d(K^-,n)$	
E40	measurement of Σp scattering	
E42	search for H-dibaryon in (K^-,K^+) nuclear reactions	
E62	precision spectroscopy of X-rays from kaonic atoms with TES	supersedes old day-1 experiment E17

- No $\bar{K}$ condensation occurs in self-bound stable matter, but search vigorously for K^-pp in spite of the large width, $\Gamma \geq 50$ MeV, anticipated.
- Is strange hadronic matter, made of roughly equal amounts of nucleons, Λ and Ξ hyperons, likely to provide the g.s. of strange matter?

The field is now poised to begin exploiting the new programs proposed at J-PARC, MAMI, FAIR, and at the upgraded JLab. These programs take advantage of new detection and electronic technologies which allow higher rates and coincidence experiments. To demonstrate the richness of the experimental programs we list in Table XIV the J-PARC scheduled experiments which, obviously, are limited to meson beams but still cover a broad spectrum of strangeness nuclear physics topical issues.

Acknowledgments

This work was supported by the U.S. DOE under Contract No. DE-AC02-98-CH10886.

References

Abelev, B. I., *et al.*, 2010, Science **328**, 58, sTAR Collaboration.
Adam, J., *et al.*, 2016a, Phys. Lett. B **754**, 360, aLICE Collaboration.
Adam, J., *et al.*, 2016b, Phys. Lett. B **752**, 267, aLICE Collaboration.
Adamczyk, L., *et al.*, 2015, Phys. Rev. Lett. **114**, 022301.
Agnello, M., *et al.*, 2005a, Phys. Rev. Lett. **94**, 212303.
Agnello, M., *et al.*, 2005b, Phys. Lett. B **622**, 35.
Agnello, M., *et al.*, 2008, Nucl. Phys. A **804**, 151.
Agnello, M., *et al.*, 2009, Phys. Lett. B **681**, 139, fINUDA Collaboration and A. Gal.
Agnello, M., *et al.*, 2011a, Phys. Lett. B **698**, 219.
Agnello, M., *et al.*, 2011b, Phys. Lett. B **701**, 556.
Agnello, M., *et al.*, 2012, Nucl. Phys. A **881**, 322.
Agnello, M., *et al.*, 2014, Phys. Lett. B **738**, 499.
Ahn, J. K., *et al.*, 1996, Phys. Lett. B **378**, 53.
Ahn, J. K., *et al.*, 2001a, in *Hadrons and Nuclei: First International Symposium, Seoul, Korea*, edited by S.-W. Hong, I.-T. Cheon, T. Choi, and S. H. Lee (AIP Conference Proceedings No. 594), p. 180.
Ahn, J. K., *et al.*, 2001b, Phys. Rev. Lett. **87**, 132504.
Ahn, J. K., *et al.*, 2013, Phys. Rev. C **88**, 014003.
Ajimura, S., *et al.*, 2001, Phys. Rev. Lett. **86**, 4255.
Akaishi, Y., T. Harada, S. Shinmura, and K. S. Myint, 2000, Phys. Rev. Lett. **84**, 3539.
Akikawa, H., *et al.*, 2002, Phys. Rev. Lett. **88**, 082501.
Alberico, W. M., A. D. Pace, M. Ericson, and A. Molinari, 1991, Phys. Lett. B **256**, 134.
Alford, M., M. Braby, M. Paris, and S. Reddy, 2005, Astrophys. J. **629**, 969.
Alston, M., *et al.*, 1961, Phys. Rev. Lett. **6**, 698.
Ammar, R., W. Dunn, and M. Holland, 1962, Nuovo Cimento **26**, 840.
Ammar, R., R. L. Setti, W. Slater, S. Limentani, P. Schlein, and P. Steinberg, 1961, Nuovo Cimento **19**, 20.
Andronic, A., P. Braun-Munzinger, J. Stachel, and H. Stöcker, 2011, Phys. Lett. B **697**, 203.
Antoniadis, J., *et al.*, 2013, Science **340**, 6131.
Aoki, S., *et al.*, 1991, Prog. Theor. Phys. **85**, 1287.
Aoki, S., *et al.*, 1993, Prog. Theor. Phys. **89**, 493.
Aoki, S., *et al.*, 1995, Phys. Lett. B **355**, 45.
Aoki, S., *et al.*, 2009, Nucl. Phys. A **828**, 191.
Armstrong, T. A., *et al.*, 1993, Phys. Rev. C **47**, 1957.
Armstrong, T. A., *et al.*, 2004, Phys. Rev. C **70**, 024902, e864 Collaboration.
Auerbach, E. H., A. J. Baltz, C. B. Dover, A. Gal., S. H. Kahana, L. Ludeking, and D. J. Millener, 1981, Phys. Rev. Lett. **47**, 1110.
Auerbach, E. H., A. J. Baltz, C. B. Dover, A. Gal., S. H. Kahana, L. Ludeking, and D. J. Millener, 1983, Ann. Phys. (N.Y.) **148**, 381.
Averyanov, A. V., *et al.*, 2008, Phys. At. Nucl. **71**, 2101.
Baca, A., C. Garcia-Recio, and J. Nieves, 2000, Nucl. Phys. A **673**, 335.
Balberg, S., and A. Gal, 1997, Nucl. Phys. A **625**, 435.
Balberg, S., A. Gal, and J. Schaffner, 1994, Prog. Theor.

Phys. Suppl. **117**, 325.
Baltz, A. J., C. B. Dover, S. H. Kahana, Y. Pang, T. J. Schlagel, and E. Schnedermann, 1994, Phys. Lett. B **325**, 7.
Baltz, A. J., C. B. Dover, and D. J. Millener, 1983, Phys. Lett. B **123**, 9.
Barbero, C., C. D. Conti, A. P. G. ao, and F. Krmpotić, 2003, Nucl. Phys. A **726**, 267.
Barbero, C., and A. Mariano, 2006, Phys. Rev. C **73**, 024309.
Barnea, N., A. Gal, and E. Liverts, 2012, Phys. Lett. B **712**, 132.
Barret, D., J.-F. Olive, and M. C. Miller, 2006, Mon. Not. Roy. Astron. Soc. **370**, 1140.
Batty, C. J., E. Friedman, and A. Gal, 1999, Phys. Rev. C **59**, 295.
Bauer, E., and G. Garbarino, 2010, Phys. Rev. C **81**, 064315.
Bauer, E., G. Garbarino, A. Parreno, and A. Ramos, 2010, Nucl. Phys. A **836**, 199.
Bauer, E., G. Garbarino, A. Parreño, and A. Ramos, 2012, Phys. Rev. C **85**, 024321.
Baym, G. A., and S. A. Chin, 1976, Phys. Lett. B **62**, 241.
Bazzi, M., *et al.*, 2011, Phys. Lett. B **704**, 113.
Bazzi, M., *et al.*, 2012, Nucl. Phys. A **881**, 88.
Berger, M. S., and R. L. Jaffe, 1987, Phys. Rev. C **35**, 213.
Bertrand, D., *et al.*, 1970, Nucl. Phys. B **16**, 77.
Bhang, H., *et al.*, 1998, Phys. Rev. Lett. **81**, 4321.
Block, M. M., and R. H. Dalitz, 1963, Phys. Rev. Lett. **11**, 96.
Block, M. M., L. Lendinara, and L. Monari, 1962, in *Proc. Int. Conf. High-Energy Phys., CERN, 1962*, edited by J. Prentki (CERN, Geneva), p. 371.
Block, M. M., *et al.*, 1964, in *Proc. Int. Conf. Hyperfragments, St. Cergue, 1963*, edited by W. Lock (CERN 64-1, Geneva), p. 63.
Bocquet, J. P., *et al.*, 1987, Phys. Lett. B **192**, 312.
Bodmer, A. R., 1971, Phys. Rev. D **4**, 1601.
Bodmer, A. R., Q. N. Usmani, and J. Carlson, 1984, Nucl. Phys. A **422**, 510.
Bohm, G., and F. Wysotzki, 1970, Nucl. Phys. B **15**, 628.
Bohm, G., *et al.*, 1969, Nucl. Phys. B **9**, 1, and references cited therein.
Bohm, G., *et al.*, 1970a, Nucl. Phys. B **16**, 46.
Bohm, G., *et al.*, 1970b, Nucl. Phys. B **23**, 93.
Botta, E., T. Bressani, and G. Garbarino, 2012, Eur. Phys. J. A **48**, 41.
Botvina, A. S., K. K. Gudima, and J. Pochodzalla, 2013, Phys. Rev. C **88**, 054605.
Botvina, A. S., J. Steinheimer, E. Bratkovskaya, M. Bleicher, and J. Pochodzalla, 2015, Phys. Lett. B **742**, 7.
Boyle, P. A., *et al.*, 2013, Phys. Rev. Lett. **110**, 152001.
Bydžovský, P., and D. Skoupil, 2013, Nucl. Phys. A **914**, 14.
Cantwell, T., *et al.*, 1974, Nucl. Phys. A **236**, 445.
Carman, D. S., and B. A. Raue, 2009, Phys. Rev. C **79**, 065205, for the CLAS Collaboration.
Cassing, W., *et al.*, 2003, Eur. Phys. J. A **16**, 549.
Chatterjee, D., and I. Vidana, 2015, Eur. Phys. J. A **in press**, arXiv:1510.06306.
Cheston, W. B., and H. Primakoff, 1953, Phys. Rev. **92**, 1537.
Chin, S. A., and A. K. Kerman, 1984, Phys. Rev. Lett. **43**, 1292.
Chrien, R. E., *et al.*, 1990, Phys. Rev. C **41**, 1062.
Chumillas, C., G. Garbarino, A. Parreño, and A. Ramos, 2007, Phys. Lett. B **657**, 180.
Chumillas, C., G. Garbarino, A. Parreño, and A. Ramos, 2008, Nucl. Phys. A **804**, 162.
Cieplý, A., E. Friedman, A. Gal, and V. Krejčiřík, 2011, Phys. Lett. B **698**, 226.
Cieplý, A., and A. Gal, 1997, Phys. Rev. C **55**, 2715.
Cieplý, A., and J. Smejkal, 2012, Nucl. Phys. A **881**, 115.
Clayton, E. F., *et al.*, 1975, Nucl. Phys. B **95**, 130.
Coremans, G., J. Sacton, D. O'Sullivan, F. Esmael, D. H. Davis, M. A. Shaukat, T. Pniewski, and J. E. Allen, 1970, Nucl. Phys. B **16**, 209.
Dalitz, R. H., 1963a, Nucl. Phys. **41**, 78.
Dalitz, R. H., 1963b, Phys. Lett. **5**, 53.
Dalitz, R. H., 2005, Nucl. Phys. A **754**, 14c.
Dalitz, R. H., D. H. Davis, P. H. Fowler, A. Montwill, J. Pniewski, and J. Zakrzewski, 1989, Proc. Roy. Soc. London A **426**, 1.
Dalitz, R. H., D. H. Davis, and D. N. Tovee, 1986, Nucl. Phys. A **450**, 311c.
Dalitz, R. H., and A. Gal, 1978, Ann. Phys. (N.Y.) **116**, 167.
Dalitz, R. H., and A. Gal, 1981, Ann. Phys. (N.Y.) **131**, 314.
Dalitz, R. H., and F. von Hippel, 1964, Nuovo Cimento **34**, 799.
Dalitz, R. H., and L. Liu, 1959, Phys. Rev. **116**, 1312.
Dalitz, R. H., and F. S. Tuan, 1959, Phys. Rev. Lett. **2**, 425.
Dalitz, R. H., T. C. Wong, and G. Rajasekaran, 1967, Phys. Rev. **153**, 1617.
Danysz, M., and J. Pniewski, 1953, Phil. Mag. **44**, 348.
Danysz, M., *et al.*, 1963a, Nucl. Phys. **49**, 121.
Danysz, M., *et al.*, 1963b, Phys. Rev. Lett. **11**, 29.
Davis, D. H., 1991, in *LAMPF Workshop on* (π, K) *Physics*, edited by B. F. Gibson, W. R. Gibbs, and M. B. Johnson (AIP Conference Proceedings No. 224), p. 38.
Davis, D. H., 2005, Nucl. Phys. A **754**, 3c.
Davis, D. H., and J. Pniewski, 1986, Contemp. Phys. **27**, 91.
Davis, D. H., R. L. Setti, and M. Raymund, 1963, Nucl. Phys. **41**, 73.
Demorest, P., *et al.*, 2010, Nature **467**, 1081.
Dey, B., C. A. Meyer, M. Bellis, M. E. McCracken, and M. Williams, 2010, Phys. Rev. C **82**, 025202, for the CLAS Collaboration.
Djapo, H., *et al.*, 2010, Phys. Rev. C **81**, 035803.
Dłuzewski, P., K. Garbowska-Pniewska, J. Pniewski, Y. Tymieniecka, P. Cook, and D. H. Davis, 1988, Nucl. Phys. A **484**, 520.
Doté, A., T. Hyodo, and W. Weise, 2008, Nucl. Phys. A **804**, 197.
Doté, A., T. Hyodo, and W. Weise, 2009, Phys. Rev. C **79**, 014003.
Dover, C. B., H. Feshbach, and A. Gal, 1995, Phys. Rev. C **51**, 541.
Dover, C. B., and A. Gal, 1983, Ann. Phys. (NY) **146**, 309.
Dover, C. B., A. Gal, and D. J. Millener, 1994, Nucl. Phys. A **572**, 85.
Dover, C. B., L. Ludeking, and G. E. Walker, 1980, Phys. Rev. C **22**, 2073.
Dover, C. B., D. J. Millener, A. Gal, and D. H. Davis, 1991, Phys. Rev. C **44**, 1905.
Epple, E., and L. Fabbietti, 2015, Phys. Rev. C **92**, 044002.
Esser, A., *et al.*, 2013, Nucl. Phys. A **914**, 519.
Esser, A., *et al.*, 2015, Phys. Rev. Lett. **114**, 232501.
Farhi, E., and R. L. Jaffe, 1984, Phys. Rev. D **30**, 2379.
Ferro, F., M. Agnello, F. Iazzi, and K. Szymańska, 2007, Nucl. Phys. A **789**, 209.
Fetkovich, J. G., *et al.*, 1972, Phys. Rev. D **6**, 3069, and references cited therein.

Filikhin, I. N., and A. Gal, 2002a, Nucl. Phys. A **707**, 491.
Filikhin, I. N., and A. Gal, 2002b, Phys. Rev. Lett. **89**, 172502.
Filikhin, I. N., and A. Gal, 2002c, Phys. Rev. C **65**, 041001.
Filikhin, I. N., A. Gal, and V. M. Suslov, 2003, Phys. Rev. C **68**, 024002.
Freire, P. C., *et al.*, 2009, arXiv:0902.2891 .
Friedman, E., and A. Gal, 2007, Phys. Rep. **452**, 89.
Friedman, E., and A. Gal, 2012, Nucl. Phys. A **881**, 150.
Friedman, E., and A. Gal, 2013, Nucl. Phys. A **899**, 60.
Friedman, E., and S. Okada, 2013, Nucl. Phys. A **915**, 170.
Fujiwara, Y., M. Kohno, and Y. Suzuki, 2007a, Nucl. Phys. A **784**, 161.
Fujiwara, Y., Y. Suzuki, and C. Nakamoto, 2007b, Prog. Part. Nucl. Phys. **58**, 439, and refereces cited therein.
Fukuda, T., *et al.*, 1995, Nucl. Intrum. Methods A **361**, 485.
Fukuda, T., *et al.*, 1998, Phys. Rev. C **58**, 1306.
Gaitanos, T., , and H. Lenske, 2014, Phys. Lett. B **737**, 256.
Gaitanos, T., A. B. Larionov, H. Lenske, and U. Mosel, 2012, Nucl. Phys. A **881**, 240.
Gal, A., 2009, Nucl. Phys. A **828**, 72.
Gal, A., 2013a, Phys. Rev. Lett. **110**, 179201.
Gal, A., 2013b, Nucl. Phys. A **914**, 270.
Gal, A., 2015, Phys. Lett. B **744**, 352.
Gal, A., E. Friedman, N. Barnea, A. Cieplý, J. Mareš, and D. Gazda, 2014, Acta Phys. Polon. B **45**, 673.
Gal, A., and H. Garcilazo, 2013, Nucl. Phys. A **897**, 167.
Gal, A., and D. J. Millener, 2011, Phys. Lett. B **701**, 342.
Gal, A., J. M. Soper, and R. H. Dalitz, 1971, Ann. Phys. (N.Y.) **63**, 53.
Gal., A., J. M. Soper, and R. H. Dalitz, 1972, Ann. Phys. (N.Y.) **72**, 445.
Gal., A., J. M. Soper, and R. H. Dalitz, 1978, Ann. Phys. (N.Y.) **113**, 79.
Garbarino, G., A. Parreño, and A. Ramos, 2004, Phys. Rev. C **69**, 054603.
Garibaldi, F., *et al.*, 2013, Nucl. Phys. A **914**, 34.
Gazda, D., E. Friedman, A. Gal, and J. Mareš, 2008, Phys. Rev. C **77**, 045206.
Gazda, D., and J. Mareš, 2012, Nucl. Phys. A **881**, 159.
Gell-Mann, M., 1953, Phys. Rev. **92**, 833.
Gibson, B. F., and D. R. Lehman, 1988, Phys. Rev. C **37**, 679.
Gibson, B. F., and R. G. E. Timmermans, 1998, Nucl. Phys. A **628**, 417.
Gilson, E. P., and R. L. Jaffe, 1993, Phys. Rev. Lett. **71**, 332.
Glendenning, N. K., 1985, Astrophys. J. **293**, 470.
Glendenning, N. K., 2001, Phys. Rev. C **64**, 025801.
Glendenning, N. K., and J. Schaffner-Bielich, 1999, Phys. Rev. C **60**, 025803.
Guo, Z. H., and J. A. Oller, 2013, Phys. Rev. C **87**, 035202.
Haidenbauer, J., U.-G. Meißner, and S. Petschauer, 2016, Nucl. Phys. A **in press**, arXiv:1511.05859.
Halderson, D., 2008, Phys. Rev. C **77**, 034304.
Hasegawa, T., *et al.*, 1996, Phys. Rev. C **53**, 1210.
Hashimoto, O., and H. Tamura, 2006, Prog. Part. Nucl. Phys. **57**, 564.
Hashimoto, T., *et al.*, 2015, Prog. Theor. Exp. Phys. **2015**, 061D01.
Hell, T., and W. Weise, 2014, Phys. Rev. C **90**, 045801.
von Hippel, F., 1964, Phys. Rev. **136**, B455.
Hiyama, E., M. Kamimura, K. Miyazaki, and T. Motoba, 1999, Phys. Rev. C **59**, 2351.
Hiyama, E., M. Kamimura, T. Motoba, T. Yamada, and Y. Yamamoto, 2002, Phys. Rev. C **66**, 024007, and earlier work cited therein.
Hiyama, E., M. Kamimura, Y. Yamamoto, and T. Motoba, 2010, Phys. Rev. Lett. **104**, 212502.
Hiyama, E., Y. Yamamoto, T. Motoba, T. A. Rijken, and M. Kamimura, 2008, Phys. Rev. C **78**, 054316.
Hotchi, H., *et al.*, 2001, Phys. Rev. C **64**, 044302.
Hungerford, E. V., 1994, Prog. Theor. Phys. Suppl. **117**, 135.
Hyodo, T., 2013, Nucl. Phys. A **914**, 260.
Hyodo, T., and W. Weise, 2008, Phys. Rev. C **77**, 035204.
Ichikawa, A., *et al.*, 2001, Phys. Lett. B **500**, 37.
Ichikawa, Y., *et al.*, 2014, Prog. Theor. Exp. Phys. **2014**, 101D03.
Ichikawa, Y., *et al.*, 2015, Prog. Theor. Exp. Phys. **2015**, 021D01.
Ikeda, K., T. Fukuda, T. Motoba, M. Takahashi, and Y. Yamamoto, 1994, Prog. Theor. Phys. **91**, 747.
Ikeda, Y., T. Hyodo, and W. Weise, 2011, Phys. Lett. B **706**, 63.
Ikeda, Y., T. Hyodo, and W. Weise, 2012, Nucl. Phys. A **881**, 98.
Ikeda, Y., H. Kamano, and T. Sato, 2010, Prog. Theor. Phys. **124**, 533.
Ikeda, Y., and T. Sato, 2007, Phys. Rev. C **76**, 035203.
Ikeda, Y., and T. Sato, 2009, Phys. Rev. C **79**, 035201.
Iodice, M., *et al.*, 2007, Phys. Rev. Lett. **99**, 052501, jLab Hall A experiment E94-107.
Itonaga, K., and T. Motoba, 2010, Prog. Theor. Phys. Suppl. **185**, 252.
Itonaga, K., T. Motoba, and H. Bandō, 1988, Z. Phys. A **330**, 209.
Itonaga, K., T. Motoba, T. Ueda, and T. A. Rijken, 2008, Phys. Rev. C **77**, 044605.
Itonaga, K., T. Ueda, and T. Motoba, 2002, Phys. Rev. C **65**, 034617.
Jido, D., E. Oset, and J. E. Palomar, 2001, Nucl. Phys. A **694**, 525.
Jurič, M., *et al.*, 1972, Nucl. Phys. B **47**, 36.
Jurič, M., *et al.*, 1973, Nucl. Phys. B **52**, 1.
Kahana, D. E., S. H. Kahana, and D. J. Millener, 2003, Phys. Rev. C **68**, 037302.
Kaiser, N., P. B. Siegel, and W. Weise, 1995, Nucl. Phys. A **594**, 325.
Kamada, H., J. Golak, K. Miyagawa, H. Witala, and W. Glöckle, 1998, Phys. Rev. C **57**, 1595.
Kameoka, S., *et al.*, 2005, Nucl. Phys. A **754**, 173c.
Kang, B. H., *et al.*, 2006, Phys. Rev. Lett. **96**, 062301.
Kaplan, D. B., and A. E. Nelson, 1986, Phys. Lett. B **175**, 57.
Karplus, R., and M. Ruderman, 1956, Phys. Rev. **102**, 247.
Kerman, A. K., and M. S. Weiss, 1973, Phys. Rev. C **8**, 408.
Keyes, G., J. Sacton, J. H. Wickens, and M. M. Block, 1973, Nucl. Phys. B **67**, 269.
Keyes, G., *et al.*, 1970, Phys. Rev. D **1**, 66.
Khaustov, P., *et al.*, 2000a, Phys. Rev. C **61**, 054603.
Khaustov, P., *et al.*, 2000b, Phys. Rev. C **61**, 027601.
Kielczewska, D., D. Ziemińska, and R. Dalitz, 1980, Nucl. Phys. A **333**, 367.
Kielczewska, D., *et al.*, 1975, Nucl. Phys. A **238**, 437.
Kim, M., *et al.*, 2009, Phys. Rev. Lett. **103**, 182502.
Kim, M. J., *et al.*, 2006, Phys. Lett. B **641**, 28.
Knorren, R., M. Prakash, and P. J. Ellis, 1995, Phys. Rev. C **52**, 3470.
Kulessa, P., *et al.*, 1998, Phys. Lett. B **427**, 403.

Kumagai-Fuse, I., T. Koike, and Y. Akaishi, 1995, Nucl. Phys. A **585**, 367c.

Kumagai-Fuse, I., and S. Okabe, 2002, Phys. Rev. C **66**, 014003.

Lanskoy, D. E., and Y. Yamamoto, 2004, Phys. Rev. C **69**, 014303.

Lattimer, J. M., 2012, Annu. Rev. Nucl. Part. Sci. **62**, 485.

Leahy, D. A., *et al.*, 2011, Astrophys. J. **742**, 17.

Lonardoni, D., A. Lovato, S. Gandolfi, and F. Pederiva, 2015, Phys. Rev. Lett. **114**, 092301.

Lonardoni, D., F. Pederiva, and S. Gandolfi, 2014, Phys. Rev. C **89**, 014314.

Magas, V. K., E. Oset, A. Ramos, and H. Toki, 2006, Phys. Rev. C **74**, 025206.

Maruta, T., *et al.*, 2007, Eur. Phys. J. A **33**, 255.

May, M., *et al.*, 1981, Phys. Rev. Lett. **47**, 1106.

May, M., *et al.*, 1983, Phys. Rev. Lett. **51**, 2085.

McCracken, M. E., M. Bellis, C. A. Meyer, and M. Williams, 2010, Phys. Rev. C **81**, 025201, for the CLAS Collaboration.

Merrill, F., *et al.*, 2001, Phys. Rev. C **63**, 035206.

Millener, D. J., 2005, Nucl. Phys. A **754**, 48c.

Millener, D. J., 2007, 31.

Millener, D. J., C. B. Dover, and A. Gal, 1988, Phys. Rev. C **38**, 2700.

Millener, D. J., C. B. Dover, and A. Gal, 1994, Prog. Theor. Phys. Suppl. **117**, 307.

Millener, D. J., A. Gal, C. B. Dover, and R. H. Dalitz, 1985, Phys. Rev. C **31**, 499.

Milner, C., *et al.*, 1985, Phys. Rev. Lett. **54**, 1237.

Montwill, A., *et al.*, 1974, Nucl. Phys. A **234**, 413.

Morita, K., T. Furumoto, and A. Ohnishi, 2015, Phys. Rev. C **91**, 024916.

Motoba, T., H. Bandō, R. Wünsch, and J. Žofka, 1988, Phys. Rev. C **38**, 1322.

Motoba, T., and K. Itonaga, 1994, Prog. Theor. Phys. Suppl. **117**, 477.

Motoba, T., D. Lanskoy, D. Millener, and Y. Yamamoto, 2008, Nucl. Phys. A **804**, 99.

Motoba, T., M. Sotona, and K. Itonaga, 1994, Prog. Theor. Phys. Suppl. **117**, 123.

Nagae, T., 2001, Nucl. Phys. A **691**, 76c.

Nagae, T., 2007, in *Topics in Strangeness Nuclear Physics*, edited by P. Bydžovský, A. Gal, and J. Mareš (Springer, Berlin Heidelberg), Lecture Notes in Physics, Vol. 724, p. 81.

Nagae, T., 2013, Few-Body Syst. **54**, 785.

Nagels, M. M., T. A. Rijken, and Y. Yamamoto, 2015a, arXiv **1504**, 02634.

Nagels, M. M., T. A. Rijken, and Y. Yamamoto, 2015b, arXiv **1501**, 06636.

Nakamura, S. N., 2013, Nucl. Phys. A **914**, 3.

Nakazawa, K., *et al.*, 2015, Prog. Theor. Exp. Phys. **2015**, 033D02.

Nemura, H., Y. Akaishi, and K. S. Myint, 2003, Phys. Rev. C **67**, 051001(R).

Nemura, H., Y. Akaishi, and Y. Suzuki, 2002, Phys. Rev. Lett. **89**, 142504.

Nemura, H., S. Shinmura, Y. Akaishi, and K. S. Myint, 2005, Phys. Rev. Lett. **94**, 202502.

Nield, K. J., *et al.*, 1976, Phys. Rev. C **13**, 1263.

Nieves, J., and E. Oset, 1993, Phys. Rev. C **47**, 1478.

Niiyama, M., 2013, Nucl. Phys. A **914**, 543.

Noga, V. I., 1986, Sov. J. Nucl. Phys. **43**, 856.

Nogga, A., 2013, Nucl. Phys. A **914**, 140.

Nogga, A., H. Kamada, and W. Glöckle, 2002, Phys. Rev. Lett. **88**, 172501.

Okada, S., *et al.*, 2004, Nucl. Phys. A **754**, 178c.

Okada, S., *et al.*, 2005, Phys. Lett. B **597**, 249.

Olive, K. A., *et al.*, 2014, Chin. Phys. C **38**, 090001, particle Data Group.

Oppenheimer, J. R., and G. M. Volkoff, 1939, Phys. Rev. **55**, 374.

Oset, E., P. Fernández de Córdoba, J. Nieves, A. Ramos, and L. L. Salcedo, 1994, Prog. Theor. Phys. Suppl. **117**, 461.

Oset, E., and A. Ramos, 1998, Nucl. Phys. A **635**, 99.

Oset, E., and L. L. Salcedo, 1985, Nucl. Phys. A **443**, 704.

Park, H., *et al.*, 2000, Phys. Rev. C **61**, 054004.

Parker, J. D., *et al.*, 2007, Phys. Rev. C **76**, 035501.

Parreño, A., 2007, Lect. Notes Phys. **724**, 141.

Parreño, A., C. Bennhold, and B. R. Holstein, 2004, Phys. Rev. C **70**, 051601(R).

Parreño, A., C. Bennhold, and B. R. Holstein, 2005, Nucl. Phys. A **754**, 127c.

Parreño, A., and A. Ramos, 2001, Phys. Rev. C **65**, 015204.

Parreño, A., A. Ramos, and C. Bennhold, 1997, Phys. Rev. C **56**, 339.

Pile, P., *et al.*, 1991, Phys. Rev. Lett. **66**, 2585.

Pochodzalla, J., 2005, Nucl. Phys. A **754**, 430c.

Pop, T., and S. D. Gupta, 2010, Phys. Rev. C **81**, 054911.

Poulard, G., A. Givernaud, and A. Borg, 1973, Phys. Lett. B **46**, 135.

Povh, B., 1980, Nucl. Phys. A **335**, 233.

Prem, R. J., and P. H. Steinberg, 1964, Phys. Rev. **136**, B1803.

Prowse, D. J., 1966, Phys. Rev. Lett. **17**, 782.

Pysz, K., *et al.*, 1999, Nucl. Inst. Meth. Phys. Res. A **420**, 356.

Randeniya, S. D., and E. V. Hungerford, 2007, Phys. Rev. C **76**, 064308.

Rappold, C., *et al.*, 2013, Nucl. Phys. A **913**, 170.

Rappold, C., *et al.*, 2014, Phys. Lett. B **728**, 543.

Rappold, C., *et al.*, 2015, Phys. Lett. B **747**, 129.

Rayet, M., and R. H. Dalitz, 1966, Nuovo Cim. A **46**, 786.

Révai, J., and N. Shevchenko, 2014, Phys. Rev. C **90**, 034004.

Rijken, T. A., M. M. Nagels, and Y. Yamamoto, 2010, Nucl. Phys. A **835**, 160.

Rijken, T. A., and H.-J. Schulze, 2016, Eur. Phys. J. A **52**, 21.

Rijken, T. A., V. J. G. Stoks, and Y. Yamamoto, 1999, Phys. Rev. C **59**, 21.

Rijken, T. A., and Y. Yamamoto, 2006a, Phys. Rev. C **73**, 044008.

Rijken, T. A., and Y. Yamamoto, 2006b, arXiv:nucl-th/0608074 .

Rosenthal, A. S., D. Halderson, K. Hodgkinson, and F. Tabakin, 1988, Ann. Phys. (N.Y.) **184**, 33.

Sada, Y., *et al.*, 2016, Prog. Theor. Exp. Phys. **2016**, arXiv:1601.06876, j-PARC E15 Experiment.

Saito, K., M. Oka, and T. Suzuki, 1997, Nucl. Phys. A **625**, 95.

Sakata, S., 1956, Prog. Theor. Phys. **16**, 686.

Sano, M., M. Wakai, and Y. Yamamoto, 1992, Prog. Theor. Phys. **87**, 957.

Sasaki, K., M. Izaki, and M. Oka, 2005, Phys. Rev. C **71**, 035502.

Sasao, J., *et al.*, 2004, Phys. Lett. B **579**, 258.

Sato, Y., *et al.*, 2005, Phys. Rev. C **71**, 025203.

Schaffner, J., C. B. Dover, A. Gal, C. Greiner, and H. Stöcker, 1993, Phys. Rev. Lett. **71**, 1328.
Schaffner, J., C. B. Dover, A. Gal, D. J. Millener, C. Greiner, and H. Stöcker, 1994, Ann. Phys. (N.Y.) **235**, 35.
Schaffner, J., M. Hanauske, H. Stöcker, and W. Greiner, 2002, Phys. Rev. Lett. **89**, 171101.
Schaffner-Bielich, J., 2008, Nucl. Phys. A **804**, 309.
Schaffner-Bielich, J., and A. Gal, 2000, Phys. Rev. C **62**, 034311, and references cited therein.
Schulze, H.-J., A. Polls, A. Ramos, and I. Vidana, 2006, Phys. Rev. C **73**, 058801.
Schulze, H.-J., and T. A. Rijken, 2011, Phys. Rev. C **84**, 035801.
Shevchenko, N., A. Gal, and J. Mareš, 2007a, Phys. Rev. Lett. **98**, 082301.
Shevchenko, N., A. Gal, J. Mareš, and J. Révai, 2007b, Phys. Rev. C **76**, 044004.
Shevchenko, N. V., and J. Haidenbauer, 2015, Phys. Rev. C **92**, 044001.
Steinheimer, J., K. Gudima, A. Botvina, I. Mishustin, M. Bleicher, and H. Stöcker, 2012, Phys. Lett. B **714**, 85.
Stoks, V. G. J., and T. A. Rijken, 1999, Phys. Rev. C **59**, 3009.
Stotzer, R. W., *et al.*, 1997, Phys. Rev. Lett. **78**, 3646.
Sugimura, H., *et al.*, 2014, Phys. Lett. B **729**, 39.
Suzuki, T., *et al.*, 2004, Phys. Lett. B **597**, 263.
Suzuki, T., *et al.*, 2005, Nucl. Phys. A **754**, 375c.
Takahashi, H., *et al.*, 2001, Phys. Rev. Lett. **87**, 212502.
Takahashi, T., 2013, Nucl. Phys. A **914**, 530.
Tamura, H., *et al.*, 2000, Phys. Rev. Lett. **84**, 5963.
Tamura, H., *et al.*, 2005, Nucl. Phys. A **754**, 58c.
Tamura, H., *et al.*, 2013, Nucl. Phys. A **914**, 99.
Tang, L., *et al.*, 2014, Phys. Rev. C **90**, 034320.
Tang, Y. C., and R. C. Herndon, 1965, Phys. Rev. Lett. **14**, 991.
Tanida, K., *et al.*, 2001, Phys. Rev. Lett. **86**, 1982.
Thiessen, H. A., *et al.*, 1980, *AGS Proposal # 738*, Brookhaven National Laboratory.
Thorsett, S. E., and D. Chakrabarty, 1999, Astrophys. J. **512**, 288.
Tokiyasu, A. O., *et al.*, 2014, Phys. Lett. B **728**, 616, lEPS Collaboration.
Tolman, R. C., 1939, Phys. Rev. **55**, 364.
Tomozawa, Y., 1966, Nuovo Cimento **46**, 707.
Uchino, T., T. Hyodo, and M. Oka, 2011, Nucl. Phys. A **868-869**, 53.
Ukai, M., *et al.*, 2004, Phys. Rev. Lett. **93**, 232501.
Ukai, M., *et al.*, 2006, Phys. Rev. C **73**, 012501(R).
Ukai, M., *et al.*, 2008, Phys. Rev. C **77**, 054315.
Vidana, I., D. Logoteta, C. Providencia, A. Polls, and I. Bombaci, 2011, Eur. Phys. Lett. **94**, 11002.
Wang, X. C., H. Takaki, and H. Bandō, 1986, Prog. Theor. Phys. **76**, 865.
Weinberg, S., 1966, Phys. Rev. Lett. **17**, 616.
Weise, W., 2015, Hyp. Int. **233**, 131.
Weise, W., and R. Haertle, 2008, Nucl. Phys. A **804**, 173.
Witten, E., 1984, Phys. Rev. D **30**, 272.
Wycech, S., and A. Green, 2009, Phys. Rev. C **79**, 014001.
Yamada, T., and K. Ikeda, 1997, Phys. Rev. C **56**, 3216.
Yamamoto, T. O., *et al.*, 2015, Phys. Rev. Lett. **115**, 222501, j-PARC E13 Collaboration.
Yamamoto, Y., H. Bandō, and J. Žofka, 1988, Prog. Theor. Phys. **80**, 757.
Yamamoto, Y., T. Furumoto, N. Yasutake, and T. A. Rijken, 2013, Phys. Rev. C **88**, 022801.
Yamamoto, Y., T. Furumoto, N. Yasutake, and T. A. Rijken, 2014, Phys. Rev. C **90**, 045805.
Yamamoto, Y., T. Furumoto, N. Yasutake, and T. A. Rijken, 2016, Eur. Phys. J. A **52**, 19.
Yamamoto, Y., T. Motoba, H. Himeno, K. Ikeda, and S. Nagata, 1994a, Prog. Theor. Phys. Suppl. **117**, 361.
Yamamoto, Y., T. Motoba, and T. A. Rijken, 2010, Prog. Theor. Phys. Suppl. **185**, 72.
Yamamoto, Y., and T. A. Rijken, 2008, Nucl. Phys. A **804**, 139.
Yamamoto, Y., M. Sano, and M. Wakai, 1994b, Prog. Theor. Phys. Suppl. **117**, 265.
Yamamoto, Y., H. Takaki, and K. Ikeda, 1991, Prog. Theor. Phys. **86**, 867.
Yamamoto, Y., M. Wakai, T. Fukuda, and M. Sano, 1992, Prog. Theor. Phys. **88**, 1163.
Yamamoto, Y., M. Wakai, T. Motoba, and T. Fukuda, 1997, Nucl. Phys. A **625**, 107.
Yamazaki, T., and Y. Akaishi, 2002, Phys. Lett. B **535**, 70.
Yamazaki, T., *et al.*, 2010, Phys. Rev. Lett. **104**, 132502.
Zech, G., *et al.*, 1977, Nucl. Phys. B. **124**, 413.
Zhu, D., C. Dover, A. Gal, and M. May, 1991, Phys. Rev. Lett. **67**, 2268.
Ziemińska, D., 1975, Nucl. Phys. A **242**, 461.
Ziemińska, D., and R. H. Dalitz, 1975, Nucl. Phys. A **238**, 453.